Published November 24, 2014

MicroRNA-214 controls skin and hair follicle development by modulating the activity of the Wnt pathway

Mohammed I. Ahmed,[1]* Majid Alam,[1]* Vladimir U. Emelianov,[2] Krzysztof Poterlowicz,[1] Ankit Patel,[1] Andrey A. Sharov,[2] Andrei N. Mardaryev,[1] and Natalia V. Botchkareva[1]

[1]Centre for Skin Sciences, School of Life Sciences, University of Bradford, Bradford BD7 1DP, England, UK
[2]Department of Dermatology, Boston University, Boston, MA 02118

Skin development is governed by complex programs of gene activation and silencing, including microRNA-dependent modulation of gene expression. Here, we show that miR-214 regulates skin morphogenesis and hair follicle (HF) cycling by targeting β-catenin, a key component of the Wnt signaling pathway. miR-214 exhibits differential expression patterns in the skin epithelium, and its inducible overexpression in keratinocytes inhibited proliferation, which resulted in formation of fewer HFs with decreased hair bulb size and thinner hair production. The inhibitory effects of miR-214 on HF development and cycling were associated with altered activities of multiple signaling pathways, including decreased expression of key Wnt signaling mediators β-catenin and Lef-1, and were rescued by treatment with pharmacological Wnt activators. Finally, we identify β-catenin as one of the conserved miR-214 targets in keratinocytes. These data provide an important foundation for further analyses of miR-214 as a key regulator of Wnt pathway activity and stem cell functions during normal tissue homeostasis, regeneration, and aging.

Introduction

Skin development is a complex dynamic process that results in formation of the epidermis, a stratified self-renewed epithelium, and several skin appendages including hair follicles (HFs), nails, and glands (Blanpain and Fuchs, 2009). HF morphogenesis is driven by bidirectional ectodermal–mesenchymal interactions between epidermal keratinocytes and a specialized population of dermal fibroblasts, and results in formation of the hair bulb, in which epithelial progenitor cells proliferate and differentiate into six distinct cell lineages to form the hair shaft and its supporting layers of the inner root sheath (Millar, 2002; Schmidt-Ullrich and Paus, 2005; Blanpain and Fuchs, 2009). HF morphogenesis is governed by a well-balanced interplay between cell proliferation, differentiation, and apoptosis, which are controlled at several levels including signaling/transcription factor-mediated and epigenetic regulatory mechanisms (Millar, 2002; Schmidt-Ullrich and Paus, 2005; Blanpain and Fuchs, 2009; Botchkarev et al., 2012; Frye and Benitah, 2012).

During postnatal life, HFs undergo cyclic regeneration with periods of active growth (anagen), regression (catagen), and relative resting (telogen; Stenn and Paus, 2001; Schneider et al., 2009). Initiation of a new growth phase in resting HFs occurs as a result of signaling exchange between epithelial stem cells residing in the bulge/secondary hair germ and dermal papilla fibroblasts, and is driven by the growth stimulatory molecules (Wnt ligands, BMP inhibitors, Shh, TGF-β2, FGF7, FGF10), the effects of which predominate over the growth inhibitory signals generated by the BMP ligands or FGF18 (Hsu and Fuchs, 2012).

In addition to signaling/transcription factor–mediated and epigenetic regulatory mechanisms, programs of gene activation and silencing governing HF development and cycling are controlled by microRNAs (miRNAs; Yi and Fuchs, 2011; Botchkareva,

*Mohammed I. Ahmed and Majid Alam contributed equally to this paper.

Correspondence to Natalia V. Botchkareva: n.botchkareva@bradford.ac.uk

Abbreviations used in this paper: BIO, 6-bromoindirubin-3′-oxime; Dox, doxycycline; DTG, double transgenic K14-rtTA/miR-214-TRE; E, embryonic day; HF, hair follicle; P, postnatal day; PMEK, primary mouse epidermal keratinocyte; WT, wild type.

Supplemental Material can be found at:
/content/suppl/2014/11/20/jcb.201404001.DC1.html

The Rockefeller University Press $30.00
J. Cell Biol. Vol. 207 No. 4 549–567
www.jcb.org/cgi/doi/10.1083/jcb.201404001

Published November 24, 2014

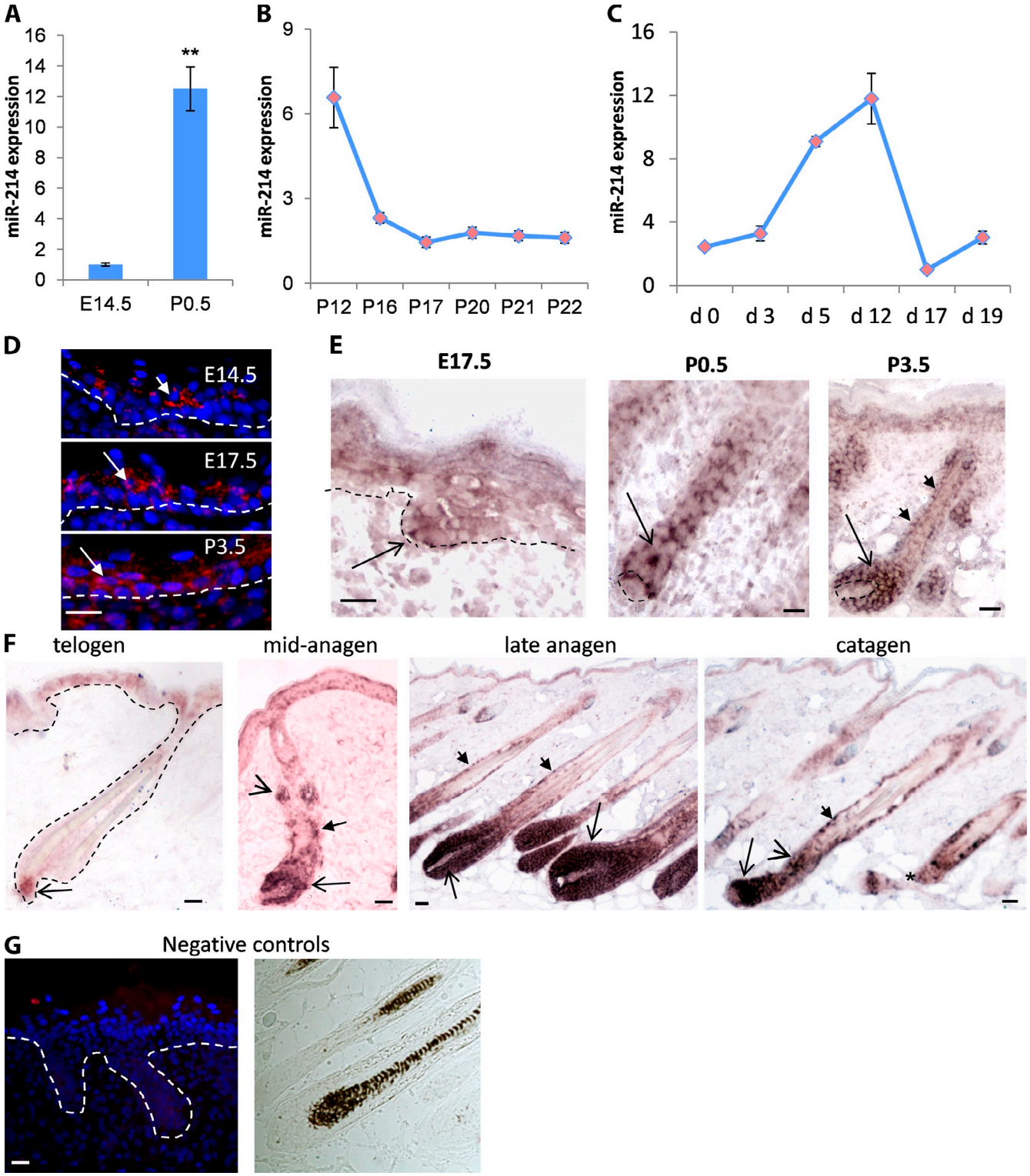

Figure 1. **Spatiotemporal expression of miR-214 during HF morphogenesis and cycling.** (A–C) TaqMan real-time RT-PCR analysis of miR-214 expression. (A) miR-214 levels in in the skin of newborn mice at P0.5 compared with embryonic skin at E14.5. *n* = 3 mice for each time point. Data are presented as mean ± SD (error bars); **, P < 0.01; Student's *t* test. (B) miR-214 levels in skin during the postnatal hair cycle: anagen-like stage (P12), catagen (P16–P17), and telogen (P20–P22). *n* = 2 mice for each time point. Data are presented as mean ± SEM (error bars). (C) miR-214 in depilation-induced hair cycle: telogen (day 0), anagen (days 3–12), and catagen (days 17–19). *n* = 2 mice for each time point. Data are presented as mean ± SEM (error bars). (D–G) miR-214 in situ hybridization. (D) miR-214 in the developing epidermis using Tyramide Signal Amplification for fluorescent detection. miR-214 expression was detected in the suprabasal epidermal layers at E14.5 (arrow); more prominent miR-214 signal is visible throughout the epidermis at E17.5 and P3.5 (arrows). The broken lines demarcate the epidermal–dermal border. (E) HF morphogenesis. miR-214 appears in the developing hair placodes at E17.5 (arrow). At P0.5, miR-214 is expressed throughout the epithelium of stage 3–6 HFs (arrow). In fully developed HFs (stage 8, P3.5), miR-214 expression increased in the developing hair matrix (arrow) and individual cells of the outer root sheath (arrowheads). (F) Hair cycle. miR-214 is expressed in telogen secondary germ (arrow), and appears in the hair matrix (arrow), outer root sheath (small arrow), and in the bulge area (arrowheads)

Published November 24, 2014

2012; Ning and Andl, 2013). miRNAs largely contribute to the regulation of gene expression by fine tuning and buffering the activity of signaling pathways. miRNAs interact with their target complimentary messenger RNAs by base-pairing between 5′ end sequences of miRNAs and mRNAs sequences located in the 3′ untranslated region (3′ UTR), which leads to either mRNA destabilization, the inhibition of translation initiation, or both (Lee et al., 1993; Ambros, 2001). In turn, the expression of miRNA can be controlled by cell type–specific transcription factors, and a major constituent of the miRNA processing machinery, Dicer, serves as a target gene of p63 and microphthalmia-associated transcription factor (MITF) in epithelial cells and melanocytes, respectively (Levy et al., 2010; Su et al., 2010). In addition, miRNAs can alter activities of the signaling pathways not only by targeting their genes, but also by acting as their downstream components (Ahmed et al., 2011). Therefore, miRNAs and their targets represent remarkably diverse regulatory networks, playing a key role in the execution of gene expression programs in stem cells and their progenies (Ambros, 2001; Inui et al., 2010).

Recent data demonstrated critical roles of miRNAs in controlling the activity of cutaneous stem cells and their lineage-committed progenies that drive skin development and regeneration (Yi and Fuchs, 2011; Botchkareva, 2012; Ning and Andl, 2013). Early studies by Andl et al. (2006) and Yi et al. (2006) have identified ∼70 miRNAs expressed in mouse embryonic skin. We have recently shown that expression levels of >200 miRNAs are changed during HF cyclic regeneration in mouse skin (Mardaryev et al., 2010). These findings suggest that miRNAs play a powerful role in the control of gene expression programs during skin development and hair cycle–associated tissue remodeling. Indeed, constitutive epidermal-specific deletion of the miRNA processors *Dicer* or *Dgcr8* results in the severe abnormalities in HF development characterized by the inability of the HFs to invaginate into the dermis (Andl et al., 2006; Yi et al., 2006). Inducible epidermal deletion of *Dicer* or *Drosha* in postnatal mouse skin has also demonstrated the crucial importance of miRNAs in the maintenance of the normal HF growth cycle (Teta et al., 2012).

Individual miRNAs are involved in controlling the expression of several key regulators of stem cell activity in the skin and HFs: miR-203 controls the proliferative potential of epithelial precursor cells by direct inhibition of p63 expression (Lena et al., 2008; Yi et al., 2008), and miR-125b serves as a rheostat that controls stem cell proliferation, fate commitment, and differentiation (Zhang et al., 2011), while miR-205 is indispensable for stem cell survival (Wang et al., 2013a). miR-31 is highly expressed in the HF during the anagen phase and controls hair cycle–associated tissue remodeling by regulating the expression of several important components of the Wnt, BMP, and FGF signaling pathways (Mardaryev et al., 2010).

Although substantial progress has been made in discovering the important players controlling skin and HF development and cycling, understanding the molecular mechanisms involved in the establishment of signaling/transcription networks in the keratinocytes still requires additional efforts. In this study, we aimed to explore a role of miR-214 in HF development and cycling. Yi et al. (2006) showed that miR-214 is one of the most abundant miRNAs expressed in the HFs of embryonic day 17.5 (E17.5) embryonic skin. Mouse miR-214 is encoded by a primary transcript Dynamin3-opposite strand (Dnm3os; Liu et al., 2010), deletion of which leads to skeletal abnormalities and a lethal phenotype (Watanabe et al., 2008). The expression of the miR-214 gene is developmentally regulated by Twist-1, a key transcriptional factor controlling epithelial–mesenchymal transitions (Lee et al., 2009), which is crucial for normal development and tissue repair. It has also been demonstrated that miR-214 plays an important role in controlling the development of the nervous system, teeth, the pancreas, and bone formation (Joglekar et al., 2007; Chen et al., 2010; Sehic et al., 2011; Wang et al., 2013b). However, its role in the control of skin and HF development and homeostasis is unknown.

In this study, we demonstrate that miR-214 show distinct expression patterns in the developing epidermis and HF. Keratinocyte-specific miR-214 overexpression causes a marked decrease in the number of HFs in developing skin, and a delay in anagen progression during postnatal development, which is associated with inhibition of cell proliferation in the epidermis and HFs. These effects are accompanied by dramatic changes in the gene expression and activity of different signaling pathways including Wnt, Shh, Eda, and Bmp, and are rescued by the administration of Wnt pathway activators. Furthermore, we identified β-catenin as a direct miR-214 target, which suggests that miR-214 is an important regulator of Wnt signaling pathway activity in developing and postnatal skin.

Results

miR-214 exhibits distinct expression patterns in the epidermis and HFs in developing and postnatal skin

To understand the role of miR-214 in the control of skin morphogenesis and HF cycling, miR-214 expression was examined in mouse back skin at different developmental stages, as well as during the first postnatal and depilation-induced hair cycles. Low levels of miR-214 expression were detected in embryonic skin at E14.5 during onset of the HF development, while its expression was dramatically elevated in the total skin of newborn mice containing HFs at different stages of development (Fig. 1 A). High miR-214 expression levels were maintained in the skin until P12, while its expression was decreased significantly during HF transition to the first regressing phase (catagen, P16-17)

in mid-anagen HF. In late anagen, prominent expression of miR-214 in the hair matrix (arrows) and in the outer root sheath (arrowheads) is seen. In catagen, miR-214 is expressed in the regressing hair matrix (arrow), outer root sheath (small arrow), and in the epithelial strand of the mid-catagen HF (arrowheads), whereas it disappears from the epithelial strand in the advanced catagen HFs (asterisk). (G) The scramble negative control using Tyramide (left) and chromogenic (right) detections. The broken line demarcates the epidermal–dermal border. Bars: (D) 25 µm; (E, left two panels) 25 µm; (E, right) 50 µm; (F) 50 µm; (G) 25 µm.

Published November 24, 2014

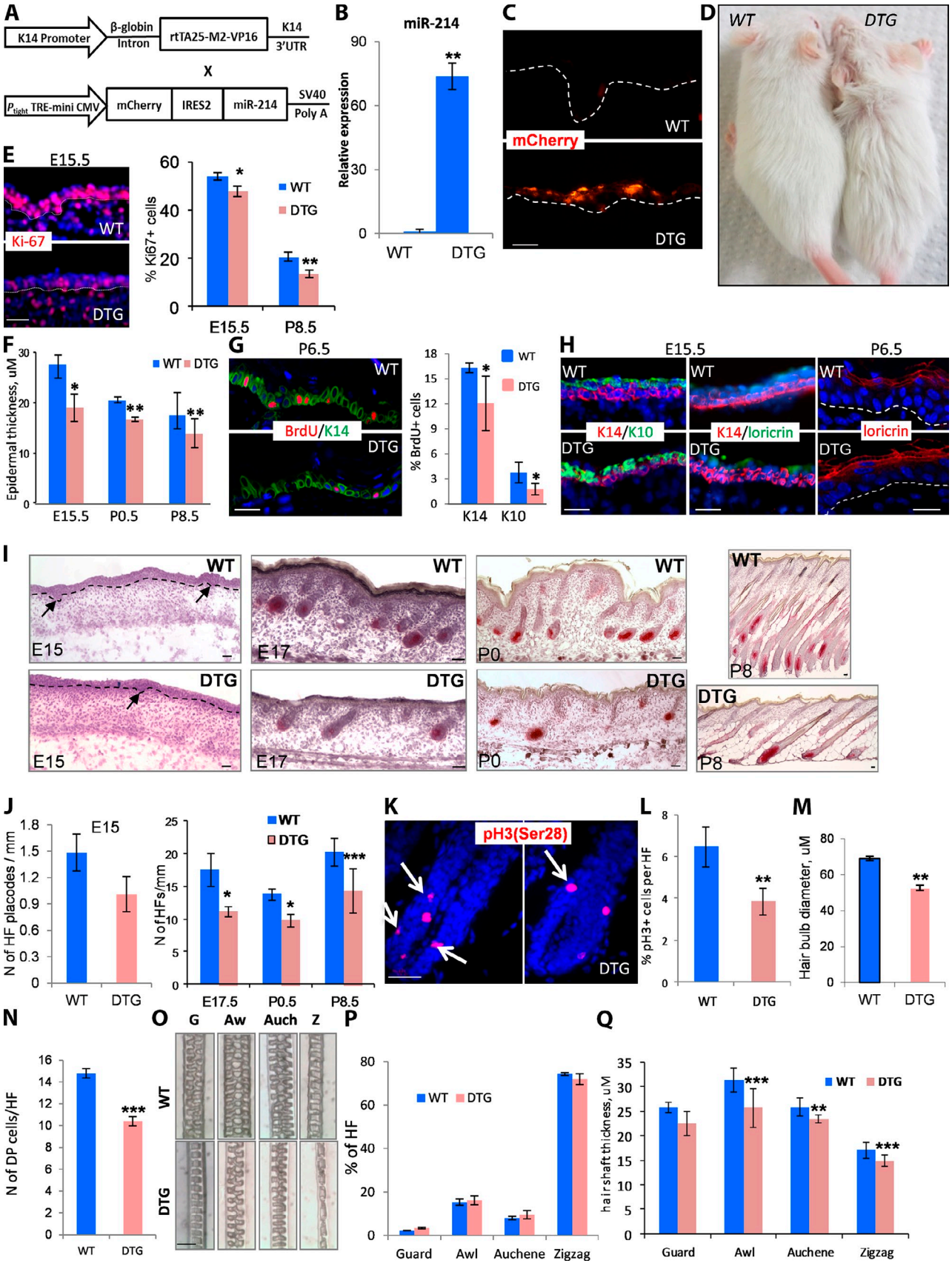

Figure 2. **Inhibitory effects of miR-214 on skin and HF morphogenesis.** (A) Schematic representation of the constructs for generation of K14-rtTA/miR-214-TRE (DTG) mice. (B) Real-time RT-PCR. There were increased levels of miR-214 in the skin of neonatal DTG mice at P0. *n* = 3 mice/genotype. (C) mCherry fluorescence in the epithelium of DTG mice at E15.5 after activation by Dox after E10.5. The broken lines demarcate the epidermal–dermal border.

Published November 24, 2014

and remained low during subsequent resting phase (telogen; P20-22; Fig. 1 B). Similar fluctuations in the miR-214 levels were observed in adult skin during depilation-induced hair cycle: miR-214 expression progressively increased during HF transition from telogen to anagen and was maximal during the late anagen stage of the hair cycle (day 12 after depilation) followed by rapid decrease during catagen (Fig. 1 C).

In situ hybridization analysis showed that in E14.5 and E17.5 skin, miR-214 expression was seen in the suprabasal epidermal layers, whereas in postnatal day 3.5 (P3.5) skin, relatively weak miR-214 expression was also seen in the basal epidermal layer (Fig. 1 D). miR-214 was abundantly expressed throughout the epithelium in the HF placodes and during more advanced stages of HF morphogenesis (E17.5–P0.5; Fig. 1 E; see Fig. 7 E). In fully developed HFs, miR-214 expression substantially increased in the developing hair matrix and individual cells of the outer root sheath (P3.5; Fig. 1 E).

During HF cycling, miR-214 expression was restricted to the secondary germ of the telogen HFs, while in early anagen HFs, miR-214 expression appeared in the growing hair matrix, the outer root sheath, and in the bulge area (Fig. 1 F). In fully developed anagen HFs, miR-214 was prominently expressed in the hair matrix, as well as in the distinct cells of the outer root sheath (Fig. 1 F; see Fig. 7 E). During catagen, miR-214 expression was seen in the regressing hair matrix, outer root sheath, and in the epithelial strand of the mid-catagen HF, whereas its expression disappeared from the epithelial strand at the advanced catagen stages (Fig. 1 F). These data suggest that miR-214 exhibits discrete expression patterns in selected epithelial compartments of the skin: it is predominantly localized in the suprabasal epidermal layers and in the epithelium of the developing HFs, as well as in the secondary germ of telogen HFs and hair matrix of anagen HFs.

Krt14-driven miR-214 overexpression results in alterations of epidermal and HF development

To amplify the miR-214 effects on the epithelial progenitor cell population located in the basal epidermal layer and HF outer root sheath, where miR-214 was relatively underexpressed compared with more the differentiated keratinocytes of the suprabasal epidermal layer and HF matrix keratinocytes (Fig. 1, D–F), mice overexpressing miR-214 under the control of doxycycline (Dox)-inducible Krt14-promoter (K14-rtTA/miR-214-TRE double transgenic [DTG]) were generated (Fig. 2 A). Induction of transgene by Dox starting from E10.5, which corresponds to the onset of Krt14 expression in the developing epidermis (Byrne et al., 1994), caused a dramatic increase in the level of miR-214 in the skin of DTG mice. This was confirmed by RT-qPCR (Fig. 2 B). Transgene expression was also confirmed by mCherry fluorescence in the basal epidermal layer of E15.5 skin (Fig. 2 C).

DTG mice were viable, fertile, and showed appearance of a "rough" fur coat postnatally (Fig. 2 D).

Between E15.5 and P8.5, DTG mice showed significantly decreased epidermal proliferation and thinner epidermis compared with wild type (WT) controls (Fig. 2, E and F). When P6 DTG and WT mice were pulsed with BrdU for 12 h followed by the costaining of BrdU and either K14 or K10, the majority of BrdU-positive cells were seen in the basal K14+ cells in both DTG and WT mice. However, it was a significant reduction in the number of BrdU+ cells in both basal and suprabasal epidermal layers of DTG mice compared with WT control (Fig. 2 G).

The expression of Keratin 14, Keratin 10, and Loricrin in basal or suprabasal epidermal layers, respectively, was quite similar in E15.5 DTG mice compared with WT mice (Fig. 2 H). However, Dox-treated epidermis of newborn DTG mice exhibited the increase of *Lor* transcript compared with the control (Fig. S1 A). Also, increased Loricrin protein expression was seen in the upper layers of the epidermis of the P6.5 DTG mice versus age-matched WT mice (Fig. 2 H). Therefore, decreased epidermal thickness in miR-214 DTG mice could be developed because of the reduced keratinocyte proliferation and accelerated terminal differentiation in the epidermis.

Interestingly, miR-214 overexpression caused a lack of ∼30% of HFs in the back skin (Fig. 2, I and J). The number of induced HFs was significantly decreased in DTG mice at E15.5, E17.5, P0.5, and P8.5 compared with WT controls (Fig. 2, I and J), which suggests that miR-214 overexpression alters the induction process in both primary and secondary HFs. The rate of HF development was not significantly different between DTG and WT mice; all HFs in DTG and WT mice reached the first anagen phase at P8.5 (Fig. 2 I). However, all transgenic HFs at P8.5 showed significantly reduced length, which was

(D) DTG and WT littermates were given Dox after E10.5 and photographed at P15. (E) Immunofluorescence of Ki-67 (red) in the epidermis of E15 skin with nuclear staining (DAPI, blue). There was a significant decrease of Ki-67+ cells at E15 and P8.5 in DTG epidermis. $n = 3$ mice/genotype for each time point. (F) Decrease in the epidermal thickness in DTG mice at E15, P0.5, and P8.5. $n = 3$ mice/genotype for each time point. (G) Immunofluorescence of BrdU (red) and K14 (green) in the epidermis of P6 skin with nuclear staining (DAPI, blue). There was a significant reduction in BrdU+ cells in both basal and suprabasal epidermal layers of DTG versus WT mice. $n = 3$ mice/genotype for each time point. (H) Immunofluorescence of K14 (red), K10 (green), and Loricrin (green) in the E15.5 epidermis and Loricrin (red) in the P6.5 epidermis with nuclear staining (DAPI, blue). There were no differences in the expression of K14, K10, and Loricirin between DTG and WT in E15 skin. There was increased Loricrin expression in DTG epidermis at P6.5. (I) Representative microphotographs of back skin histology of DTG and WT mice at different embryonic and postnatal days of skin and HF development. Arrows indicate HF placodes, and the broken lines demarcate the epidermal–dermal border. (J) Quantification of the total HF number per millimeter of skin in DTG versus WT littermate at E15, E17, P0.5, and P8.5. $n = 3$ mice/genotype for each time point. (K) Immunodetection of pH3(Ser28) (red) with nuclear staining (DAPI, blue) in the hair bulbs of DTG and WT mice at P8.5. (L) Quantification of a ratio of pH3(Ser28)+ to total cell number in the hair matrix at P8.5. $n = 3$ mice/genotype. (M) Significant reduction in hair bulb diameter in the DTG HFs at P8. $n = 3$ mice/genotype. (N) Quantification of the number of dermal papilla cells at P8.5. $n = 3$ mice/genotype. (O) Representative images of the different hair shaft types (guard, awl, auchene, and zigzag) plucked from telogen HFs of DTG and WT mice at P20. G, guard; Aw, awl; Ach, auchene; Z, zigzag. (P) Quantification of the number of different hair shaft types in DTG and WT mice. No difference between DTG and WT mice was detected. $n = 4$ mice/genotype. (Q) Significant decrease in the hair shaft thickness of the awl, auchene, and zigzag hairs in DTG versus WT mice. $n = 4$ mice/genotype. Data are presented as mean ± SD (error bars); *, $P < 0.05$; **, $P < 0.01$; ***, $P < 0.001$; Student's *t* test. Bars: (C, E, I, K, and O) 50 µm; (G and H) 25 µm.

Published November 24, 2014

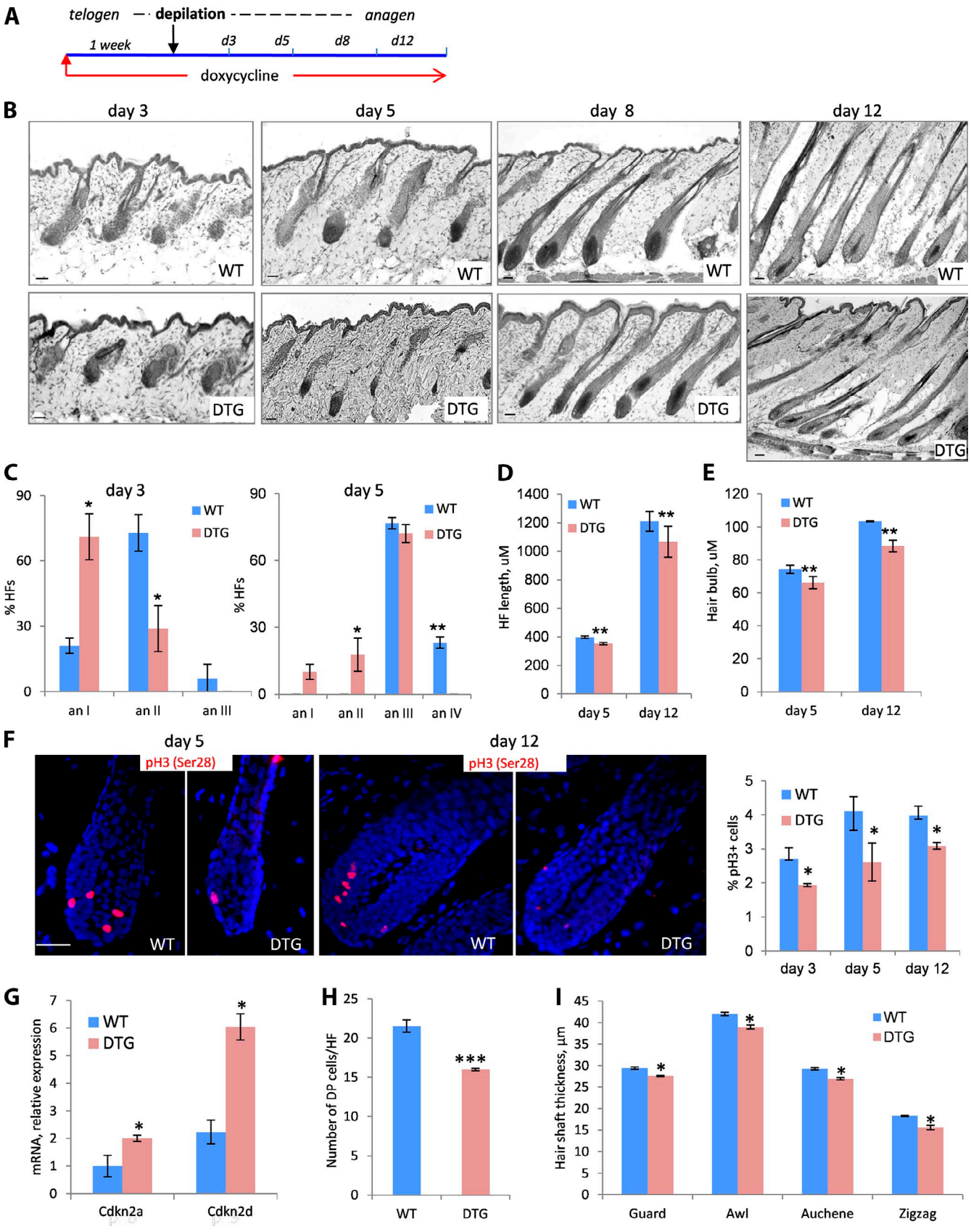

Figure 3. **Gain of miR-214 function inhibits hair cycle progression.** (A) Schematic illustration of the experimental design. (B) Representative microphotographs of back skin histology of DTG and WT mice at different days of a depilation-induced hair cycle. Bars, 50 µm. (C) Quantitative histomorphometry of HFs at different anagen substages at days 3 and 5 after depilation in DTG and WT mice. *n* = 5 mice/genotype for each time point. (D) Quantification of HF length at days 5 and 12 after depilation. *n* = 5 mice/genotype for each time point. (E) Quantification of hair bulb diameter in the HFs at day 5 and 12 after

Published November 24, 2014

accompanied by markedly reduced total skin thickness (Fig. S1, B and C). The hair bulb size and cell proliferation in the HF matrix were significantly reduced in all HFs of DTG mice versus the WT HFs (Fig. 2, I and K–M), whereas no apoptotic cells were detected in the HFs or interfollicular epidermis in DTG or WT mice (not depicted). In addition, a significant decrease in the number of dermal papilla cells was observed in transgenic HFs versus the corresponding controls (Fig. 2 N).

Despite the fact that the proportions of the guard, awl, auchen, and zigzag hair in DTG mice were similar to WT mice (Fig. 2, O and P), morphometric analyses of their hair shafts (P20; telogen HFs) revealed a significant decrease of their thickness but not the length in DTG versus WT mice (Fig. 2 Q and Fig. S1 D). Therefore, the changes in visual coat appearance in DTG mice were most likely caused by the reduced number of the HFs, as well as by the decreased thickness of the hair shafts induced by miR-214 overexpression.

Gain of miR-214 activity in postnatal skin alters HF cycling and HF size

To explore the effects of miR-214 on HF cycling, DTG mice were treated with Dox during telogen phase followed by the induction of the hair cycle by depilation (Fig. 3 A). Although telogen–anagen transition was initiated in DTG mice, they exhibited a significant delay in early anagen development compared with WT control (days 3 and 5 after depilation; Fig. 3, B and C). Anagen VI HFs were significantly shorter in DTG mice compared with WT mice (Fig. 3 D). On days 5–12 after depilation, the size of hair bulbs in DTG HFs was significantly reduced compared with WT controls (Fig. 3 E). These changes were associated with significantly decreased cell proliferation in the hair matrix and increased transcript levels of the cyclin-dependent kinase inhibitors *Cdkn2a (p16)* and *Cdkn2d (p19)* in DTG skin compared with WT mice (Fig. 3, F and G). Analysis of apoptosis by the detection of active caspase-3 did not reveal any differences between HFs in DTG and WT mice (Fig. S1 E). The number of dermal papilla cells in transgenic anagen VI HFs was significantly reduced (Fig. 3 H). Similar to HF morphogenesis, anagen DTG HFs produced significantly thinner hair shafts compared with WT controls (Fig. 3 I). These data suggest that miR-214 exerts its effects on HF development and cycling by modulation of keratinocyte proliferation and differentiation, as well as by regulating epithelial–mesenchymal interactions in the HF including the control of dermal papilla cell number.

miR-214 overexpression induces complex changes in gene expression programs in keratinocytes

To explore molecular mechanisms underlying the phenotype in miR-214 transgenic mice and identify potential targets of miR-214 in the keratinocytes, global mRNA expression profiling was performed in the back skin epithelium of neonatal DTG mice (P2.5), which received Dox for 48 h before skin collection (Fig. 4 A). The raw microarray expression profiles were background corrected and normalized with Bioconductor package limma (Smyth, 2005), and genes with more than twofold expression change in the epithelium of DTG mice compared with WT controls were identified as differentially expressed (Fig. 4 B). The in-house functional ontology database was used to categorize differentially expressed genes into the set of 12 distinct functional categories (Lewis et al., 2014). Bioinformatic analysis revealed twofold and higher changes in expression of 1,026 genes in skin epithelium of DTG versus WT mice (Fig. 4 B and Tables S1 and S2). Differentially expressed genes that belong to the "cell cycle" and "signaling" categories were further validated by RT-qPCR.

Using RT-qPCR, we confirmed that the transcript levels of *Ccnb1*, *Ccnd1*, *Ccnd2*, and *Cdk1* (cyclin B1, cyclin D1, cyclin D2, and cyclin-dependent kinase 1) were significantly lower in DTG mice compared with the WT littermates (Fig. 4 C). These data suggest that miR-214 indeed exerts inhibitory effects on cell proliferation, which were consistent with the epidermal and HF phenotypes seen in DTG mice (Figs. 2 and 3).

Interestingly, microarray analysis revealed changes in the expression of the genes encoding the components of several signaling pathways that are crucial for HF development and cycling, such as Wnt, Shh, Edar, and Bmp (Botchkarev and Paus, 2003; Schmidt-Ullrich et al., 2006; Blanpain and Fuchs, 2009). RT-qPCR confirmed significant down-regulation of the *Ctnnb1* and *Lef-1* expressions in the skin of DTG mice, which suggests inhibition of Wnt signaling activity induced by miR-214. Also, expressions of several genes that belong to Hedgehog signaling, such as *Shh* and its receptors *Smo* and *Ptch2*, were dramatically decreased in the epithelium of DTG versus WT mice. In addition, overexpression of miR-214 led to a significant decrease in the expression of *Edar* and the BMP inhibitor *Sostdc1* (Fig. 4 C). These data provide evidence that the effects of miR-214 on HF development and cycling are mediated, at least in part, by genes that control keratinocyte proliferation and mediate activity of key signaling pathways (Wnt, Hedgehog, Bmp, and Edar) known to be crucial for skin development and hair growth.

miR-214 overexpression in epithelial progenitor cells alters expression of key regulators of HF development and cycling

To further investigate the effects of gain of miR-214 functions on the activity of selected signaling pathways in skin, we analyzed the pattern of the expression of their different components in embryonic and postnatal skin of DTG and age-matched WT mice. Quantitative immunofluorescence analysis revealed the

depilation. *n* = 5 mice/genotype for each time point. (F) Immunodetection of pH3(Ser28) (red) in the hair bulbs of DTG and WT mice with nuclear staining (DAPI, blue). A significant reduction in the number of pH3(Ser28)+ cells in the HF of DTG mice at days 3, 5, and 12 after depilation was seen. *n* = 5 mice/genotype for each time point. Bar, 50 µm. (G) Real-time RT-PCR analysis of *Cdkn2a* and *Cdkn2d* expression at day 12 after depilation. *n* = 3 mice/genotype. (H) Quantification of the number of dermal papilla cells in anagen HFs at day 12 after depilation. *n* = 5 mice/genotype for each time point. (I) Quantification of the hair shaft thickness of the awl, auchene, and zigzag hairs in DTG versus WT mice plucked after the hair cycle completion at day 20 after depilation. *n* = 5 mice/genotype. Data are presented as mean ± SD (error bars); *, P < 0.05; **, P < 0.01; ***, P < 0.001; Student's *t* test.

Published November 24, 2014

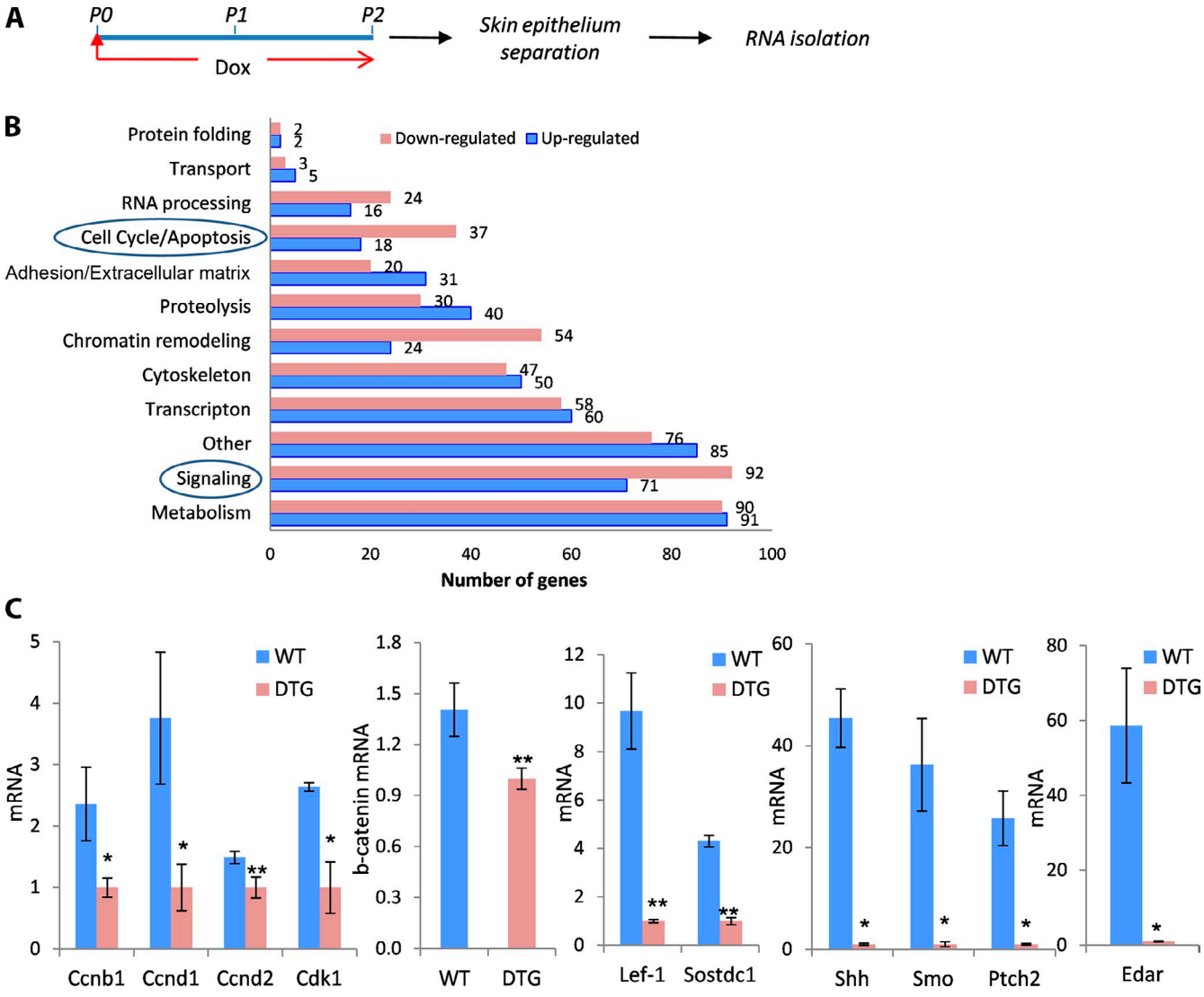

Figure 4. **Global gene expression profiling of the back skin epithelium of WT and K14-rtTA/miR-214-TRE mice.** (A) Schematic illustration of the experimental design. (B) Agilent microarray analysis of the back skin epithelium of DTG and WT mice. A bar chart depicts the ontology of the down- and up-regulated genes and the actual number of genes with more than twofold expression change in DTG and WT skin; (a full list of the genes is shown in Tables S1 and S2). (C) Validation of microarray. Real-time RT-PCR analysis of expression of the selected genes is shown. $n = 3$ mice/genotype. Data are presented as mean ± SD (error bars); *, $P < 0.05$; **, $P < 0.01$; Student's t test.

decreased levels of β-catenin, the downstream component of the Wnt pathway, in the HF placode epithelium of DTG mice (stages 1–2 of HF development; Fig. 5, A and H). Consistent with these data, a significant decrease of the β-catenin protein levels in the total skin of DTG mice was confirmed by Western blotting (Fig. 5 A). Lef-1 expression was also markedly decreased in the HF placode epithelium and in the developing dermal papilla (Fig. 5, B and H). In contrast, pSmad1/5/8 expression increased in the developing hair placodes and interfollicular epidermis of DTG mice versus WT controls, which suggests activation of BMP signaling driven by miR-214 overexpression (Fig. 5, C and H). Gain of miR-214 in the skin also resulted in the reduced expression of Shh (Fig. 5, D and I; and Fig. S1 F) and Edar (Fig. 5, D, E, and H). Analysis of Cyclin D1 and Cyclin D2 expression also revealed their decreased expression in the developing hair placodes (Fig. 5, F–H), as well as a reduced number of Cyclin D1–positive cells in the epidermis of DTG mice versus WT mice (Fig. S1 G). However, there were no changes in the expression of selected stem cell markers, such as Sox9 and Lhx2, between the hair placodes of DTG and WT mice (Fig. S1 H).

Similar to the HF development, elevation of miR-214 levels during hair cycle resulted in decreased expressions of β-catenin and Lef-1 in the hair matrix and the dermal papilla of DTG follicles, whereas Sox2 expression in the dermal papilla remained unchanged (Fig. 6, A, B, and G; and Fig. S1 I). Also, quantitative immunofluorescence analysis revealed increased expression of pSmad 1/5/8 in differentiating HF keratinocytes of DTG versus WT mice (Fig. 6, C and G). Shh expression was strongly decreased in the hair matrix of DTG HFs (Fig. 6, D and G). Consistent with microarray data, expression of cyclin D1 was also decreased in the hair matrix of DTG HFs (Fig. 6, E and G), and reduced expression of cyclin-dependent kinase 1 was also seen in the hair matrix of miR-214 transgenic mice (Fig. 6, F and G). In addition, expression of the

Published November 24, 2014

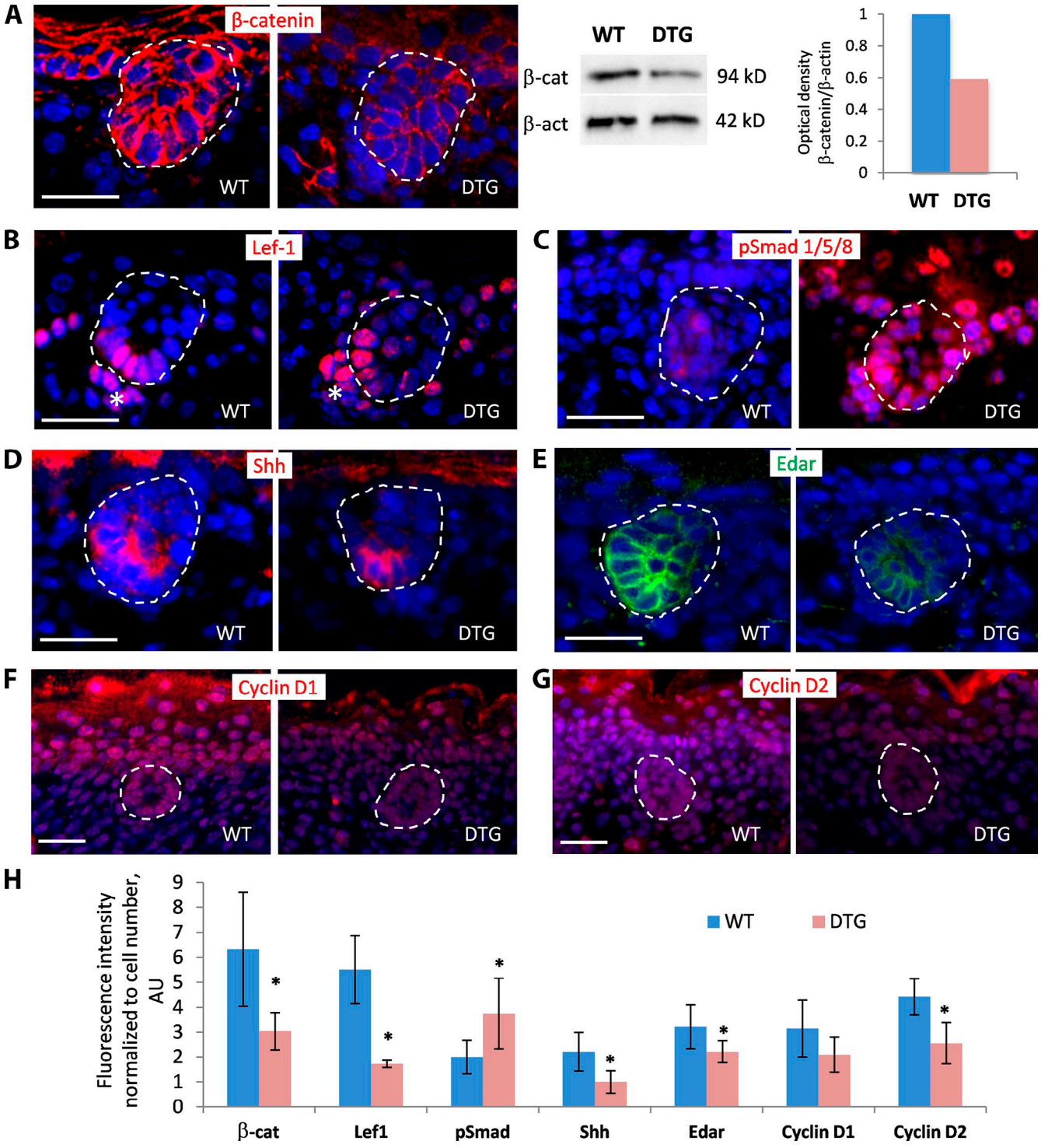

Figure 5. **Effect of miR-214 overexpression on the key regulators of HF morphogenesis.** (A, left) Immunofluorescence analysis of β-catenin (red) with nuclear staining (DAPI, blue). There was a marked decrease of β-catenin in hair placode epithelium of DTG mice at E17.5. (A, right) Western blot and its densitometry analysis. There were reduced levels of β-catenin protein in the skin of DTG mice at P0; data are shown as β-catenin band density normalized relative to β-actin. The data shown are from a single representative experiment out of three repeats. (B) Reduced expression of Lef-1 (red fluorescence) in hair placode epithelium and mesenchyme (asterisks) in the skin of DTG mice with nuclear staining (DAPI, blue). (C) More prominent expression of pSmad1/5/8 in DTG hair placodes and intrafollicular epidermis versus WT mice (red fluorescence; nuclear staining with DAPI, blue). (D and E) Decreased expressions of Shh (D) and Edar (E) in the HF placodes of DTG mice (red/green fluorescence; nuclear staining with DAPI, blue). (F and G) Reduced expression of Cyclin D1 (F) and Cyclin D2 (G) in the DTG hair placodes and the epidermis (red fluorescence; nuclear staining with DAPI, blue). (H) Quantitative immunofluorescence analysis. Immunofluorescence intensity was normalized to the number of DAPI+ cells in the selected areas. $n = 3$ mice/genotype. Data are presented as mean ± SD (error bars); *, $P < 0.05$; Student's *t* test. Broken lines demarcate the examples of the areas used for quantitative immunofluorescence analysis. Bars: (A–E) 25 µm; (F and G) 50 µm.

Published November 24, 2014

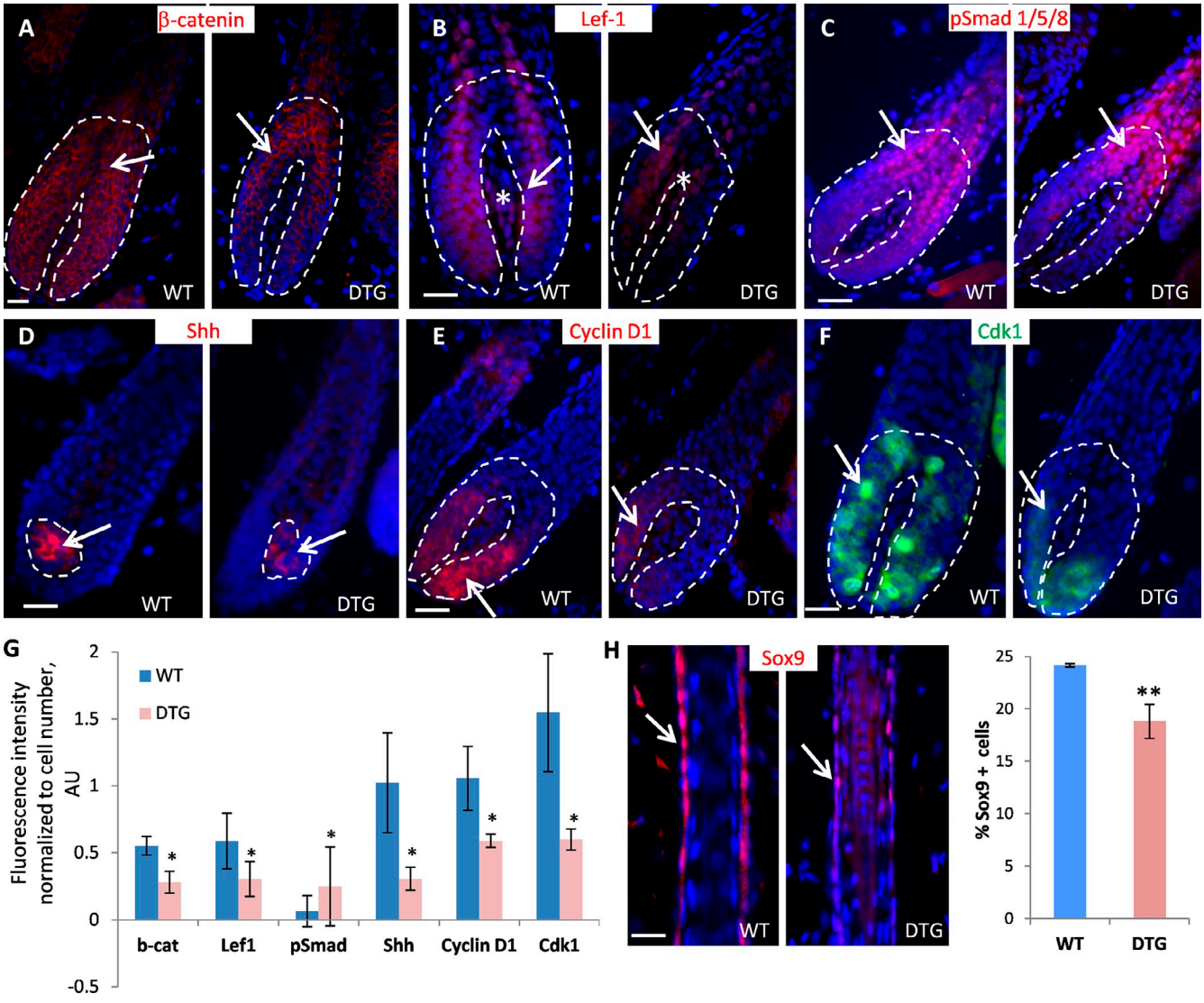

Figure 6. **Effect of miR-214 overexpression on the key regulators of HF cycling.** (A and B) Reduced expression of β-catenin and Lef-1 (red fluorescence) in the hair matrix (arrows) and dermal papilla (asterisks) of DTG follicles (nuclear staining with DAPI, blue). (C) Increased pSmad 1/5/8 expression in the postmitotic keratinocytes of the hair bulb and precortex in DTG mice (arrow; red fluorescence; nuclear staining with DAPI, blue). (D) Decrease in Shh expression in the hair matrix of DTG mice (arrow; red fluorescence; nuclear staining with DAPI, blue). (E and F) Decreased expression of cyclin D1 (red fluorescence) and cyclin-dependent kinase 1 (green fluorescence) in the hair matrix of DTG mice (arrows; nuclear staining with DAPI, blue). (G) Quantitative immunofluorescence analysis. Immunofluorescence intensity was normalized to the number of DAPI+ cells. *n* = 3 mice/genotype. The broken lines demarcate the areas of the examples used for quantitative immunofluorescence analysis. (H, left) Immunodetection of Sox9+ cells in the HF outer root sheath (red fluorescence). (H, right) Quantification of Sox9+ cells in the outer root sheath. *n* = 3 mice/genotype. Data are presented as mean ± SD (error bars); *, $P < 0.05$; **, $P < 0.01$; Student's *t* test. Bars: (A–F) 50 µm; (H) 25 µm.

Dlx3 transcription factor involved in the control of HF keratinocyte differentiation was less pronounced in transgenic HFs versus the controls (Fig. S1 J). Overexpression of miR-214 during the hair cycle was associated with a significant decrease in the number of Sox9-positive cells in the outer root sheath, which suggests a reduced supply of the progenitor cells from the bulge for the hair matrix of actively growing HFs upon miR-214 overexpression (Fig. 6 H).

These data suggest that miR-214 exerts inhibitory effects on HF development and cycling, at least in part, by regulating the activity of key signaling pathways (Wnt, Hedgehog, Bmp, and Edar) in keratinocytes, as well as by modulation of Wnt signaling in dermal papilla fibroblasts.

β-Catenin is a direct target of miR-214 in keratinocytes

To identify the direct targets of miR-214 in keratinocytes, gene expression profiling results obtained from the epithelium of neonatal DTG mice after 48 h of Dox activation were linked with four databases for prediction of miRNA targets, including PITA, miRanda, miRDB, and Targetscan (Rehmsmeier et al., 2004; Lewis et al., 2005; Kertesz et al., 2007; Wang and El Naqa, 2008; Fig. 7 A). The largest number of possible miR-214 target genes was predicted by PITA and miRanda (192 and 78, respectively), whereas TargetScan and miRDB showed only 18 and 11 possible targets, respectively. Intersections of PITA, miRanda, and miRDB predictions identified nine common

Published November 24, 2014

possible miR-214 targets, including *Ctnnb1* and *Shh* (Fig. S1 K). However, an overlap of all four databases revealed only three predicted target genes for miR-214, whose expression was altered in keratinocytes of DTG mice, including *Ctnnb1*, but not *Shh* (Fig. 7 A and Fig. S1 K).

To validate the results of bioinformatic analysis and explore whether *β-catenin* and *Shh* 3′ UTRs carry functional binding sites for miR-214 (Fig. 7 B and Fig. 1 L), the luciferase reporter assay was performed. Cotransfection of HaCaT cells with miR-214 mimic and the *β-catenin* 3′ UTR reporter construct caused significant reduction in luciferase activity, compared with the corresponding control, whereas this effect was not detected when *β-catenin* 3′ UTR was mutated (Fig. 7 C), thus confirming that *β-catenin* is a direct target of miR-214. However, the luciferase reporter assay did not confirm the direct interactions between miR-214 and 3′ UTR of *Shh*, which suggests that a decrease of its expression in the HFs after miR-214 overexpression is a secondary effect mediated by other factors (Fig. S1 M).

Next, the effect of miR-214 on the β-catenin/Tcf-dependent transcription activity was evaluated by using the TOPflash reporter assay. A significant induction in TOPflash reporter activity, without any effect on FOPflash activity (negative control), was detected in HaCaT cells treated with a synthetic Wnt agonist 6-bromoindirubin-3′-oxime (BIO; Meijer et al., 2003; Sato et al., 2004), whereas transfection of cells with miR-214 mimic significantly diminished TOPflash activity induced by BIO (Fig. 7 D).

Simultaneous in situ hybridization for miR-214 and immunofluorescence detection of β-catenin revealed a predominantly reciprocal expression pattern of miR-214 and β-catenin in the epidermis: miR-214 was seen in the suprabasal layer, whereas β-catenin was more strongly expressed in the basal cells (Fig. 7 E). A more complex pattern of miR-214 and β-catenin expressions was observed in the HFs: clear colocalization of miR-214 and β-catenin was seen in undifferentiated proliferating cells of the developing HFs and anagen hair matrix, whereas β-catenin was not coexpressed with miR-214 in the differentiating cells of the precortex (Fig. 7 E).

Furthermore, transfection of primary mouse epidermal keratinocytes (PMEKs) with either miR-214 mimic or its specific inhibitor resulted in the decrease and increase of the *β-catenin* mRNA expression, respectively (Fig. 7 F). Also, miR-214 mimic reduced levels of β-catenin protein in the keratinocytes (Fig. 7 G). miR-214 was also capable of interfering with the activity of Wnt signaling in keratinocytes induced by the GSK-3β inhibitor lithium chloride (LiCl; Klein and Melton, 1996; Fig. 7 H). Immunofluorescence analysis confirmed that miR-214 mimic decreases nuclear and cytoplasmic β-catenin protein levels compared with the control. Moreover, miR-214 abrogated LiCl-induced β-catenin expression: both nuclear and cytoplasmic β-catenin levels were significantly decreased in the keratinocytes synergistically treated with LiCl and miR-214 mimic compared with the cells treated with LiCl alone (Fig. 7 H). Consistent with this observation, Western blot analysis showed reduced levels of β-catenin in the keratinocytes cotreated with LiCl and miR-214 mimic compared with the cells treated with LiCl solo (Fig. S1 N).

Collectively, these data suggest that β-catenin is a genuine target of miR-214, and that miR-214 is involved in the control of the activity of the Wnt pathway in keratinocytes.

Activation of Wnt signaling rescues the skin phenotype in miR-214 transgenic mice

To further explore the functional links between miR-214 and β-catenin in vivo, miR-214 transgene was induced after E10.5, followed by the subcutaneous injections of Wnt agonist BIO on five consecutive days after birth. Although β-catenin mRNA levels were low in the skin of DTG mice treated with BIO, β-catenin protein expression was quite similar in the HFs of DTG and WT mice (Fig. 8, A and B). This suggests that the reduced levels of the β-catenin transcript were most likely compensated by β-catenin protein stabilization caused by the GSK-3 inhibition induced by BIO (Meijer et al., 2003). Pharmacological experiments revealed that BIO treatment lead to induction of new HFs in DTG mice postnatally, which resulted in the appearance of the HFs at early stages of morphogenesis (stages 2–3) in DTG mice followed by restoration of their total number, similar to the WT controls (Fig. 8, C–E). In addition, pharmacological Wnt activation resulted in a significant increase of the hair bulb diameter in the HFs at advanced stages (stages 6–7) of morphogenesis in DTG mice, whereas no increase of the hair bulb size was seen in WT mice treated with BIO (Fig. 8 F). These observations demonstrate that activation of Wnt signaling in DTG mice rescues the effects of miR-214 overexpression in vivo, confirming further that miR-214 does indeed interfere with Wnt pathway activity in the developing and postnatal skin.

Discussion

MicroRNA-dependent control of gene expression plays a fundamental role in the balancing and fine-tuning of lineage-specific differentiation programs in many organs, including skin (Andl et al., 2006; Yi et al., 2006). In this paper, we identify a novel role for miR-214 in the control of skin and HF development, and demonstrate that: (1) miR-214 shows spatial-temporal changes in the expression pattern in the skin during HF morphogenesis and cycling; (2) inducible overexpression of miR-214 in keratinocytes inhibits cell proliferation, and results in a formation of fewer HFs with decreased size of the hair bulb, which produce thinner hair; (3) miR-214 regulates the balance in the activities of multiple signaling pathways, including Wnt, Shh, Edar, and Bmp, in developing and postnatal skin; and (4) β-catenin serves as a direct miR-214 target in keratinocytes.

During skin development and postnatal growth, miR-214 expression predominates in differentiating populations of keratinocytes committed either to epidermal or HF cell fates (suprabasal epidermal or hair matrix keratinocytes, respectively), whereas its expression in the progenitor cell populations of the basal epidermal layer or HF outer root sheath appears to be considerably lower. K14-driven miR-214 overexpression in the progenitor cell populations of the epidermis and HF results in a reduced epidermal proliferation and accelerated differentiation,

Published November 24, 2014

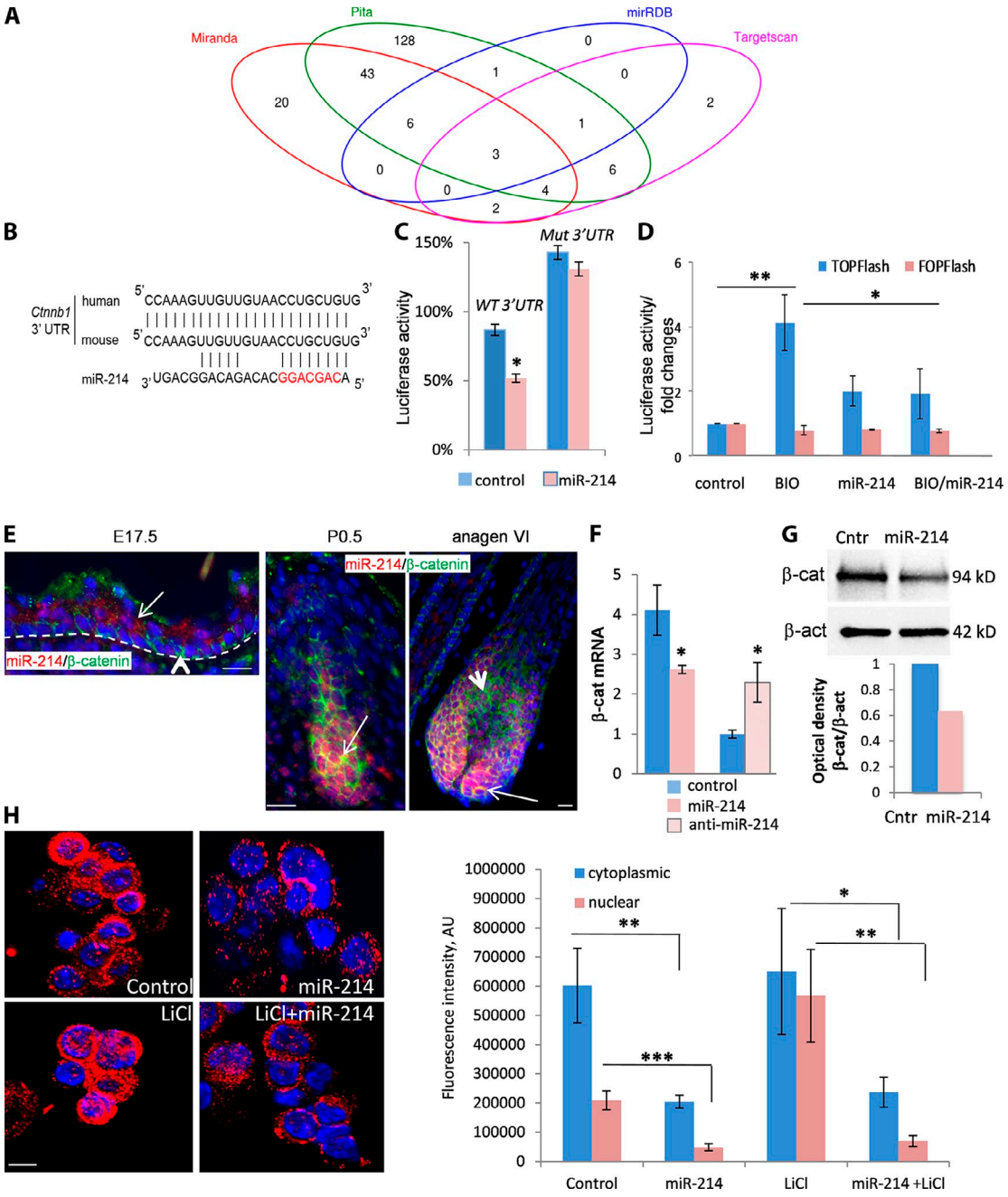

Figure 7. **miR-214 modulates the activity of Wnt signaling by targeting β-catenin.** (A) A Venn diagram depicting the overlap of four databases for prediction of miR-214 targets (PITA, miRanda, miRDB, and Targetscan) with gene expression profiling in the epithelium of neonatal DTG and WT mice after 48 h of Dox treatment. Only down-regulated genes (<1.5-fold) were included in the analysis. (B) Predicted interactions between miR-214 and *Ctnnb1*. Alignment of mouse and human sequences in the 3′ UTR of *Ctnnb1* mRNA is shown. (C) Significant reduction in luciferase activity in HaCaT cells due to cotransfection with miR-214 mimic and the *Ctnnb1* 3′ UTR construct encompassing the putative miR-214 target site. No changes in luciferase activity were detected when the miRNA binding site was mutated (mut-3′UTR). Each sample was normalized to Renilla luciferase activity. The data shown are from a single representative experiment out of three repeats. For the experiment shown, $n = 3$ for all experimental conditions. (D) TOPflash reporter assay. There was significant induction in TOPflash reporter activity in HaCaT cells by BIO, which was diminished by miR-214 mimic. There were no changes in FOPflash activity in any experimental groups. The data shown are from a single representative experiment out of three repeats. For the experiment shown, $n = 3$. (E) Dual fluorescent in situ hybridization for miR-214 (red) and immunofluorescence of β-catenin (green). β-Catenin is expressed in the basal layer (arrowhead), while more prominent miR-214 expression was seen in the suprabasal cells of the E17.5 epidermis (arrow). There was coexpression of miR-214 and β-catenin in the developing HF (stage 3 morphogenesis) and anagen VI hair matrix (arrows). There was also a lack of miR-214 in β-catenin+ differentiating cells of the precortex (arrowhead). The broken line demarcates the epidermal–dermal border. (F) Real-time RT-PCR. β-Catenin expression in primary epidermal keratinocytes transfected with either miR-214 mimic or miR-214 inhibitor is shown. The data shown are from a single representative experiment out of three repeats. For the experiment shown, $n = 3$. (G) Western blot and its densitometry analysis. There were reduced levels of β-catenin protein in primary epidermal keratinocytes transfected with miR-214 mimic. Data are shown as β-catenin band density normalized relative to β-actin. The data shown are from a single representative experiment out of three repeats. (H) Immunocytochemistry and quantitative immunofluorescence. There was prominent β-catenin staining (red) in primary epidermal keratinocytes treated with the GSK-3β inhibitor LiCl compared with the control, and decreased β-catenin staining in the nucleus of keratinocytes transfected with miR-214 mimic and synergistically exposed to miR-214 mimic and LiCl. The data shown are from a single representative experiment out of three repeats. For the experiment shown, $n = 3$. Data are presented as mean ± SD (error bars); *, $P < 0.05$; **, $P < 0.001$; ***, $P < 0.0001$; Student's *t* test. Bars: (E) 50 µm; (H) 5 µm.

Published November 24, 2014

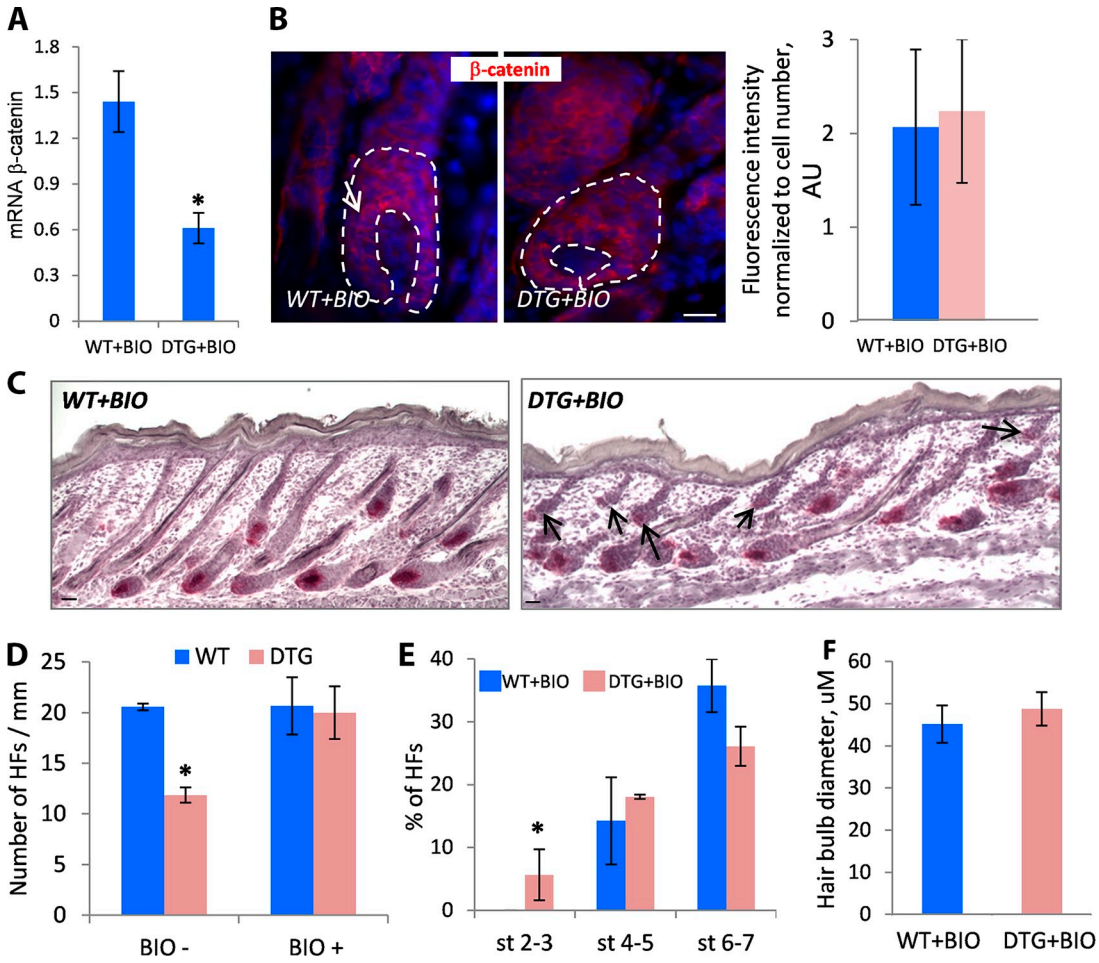

Figure 8. **Activation of Wnt signaling rescues the skin phenotype in miR-214 transgenic mice.** (A) Real-time RT-PCR. There were decreased levels of *β-catenin* transcript in the DTG skin treated with BIO versus BIO-treated WT mice. *n* = 3 mice/genotype. (B) Immunofluorescence analysis of β-catenin (red) in the HFs of WT and DTG mice treated with Wnt agonist BIO on 5 consecutive days (arrow). The broken lines demarcate the examples of the areas used for quantitative immunofluorescence analysis. Bar, 25 µm. (C) Representative microphotographs of back skin histology of WT and DTG mice after 5 d of BIO treatment at P5.5. Arrows show HF at 2–3 stages of morphogenesis. Bar, 100 µm. (D) There was a significant reduction in the number of HFs in DTG versus WT littermate at P5.5, while there was no difference in HF number between WT and DTG mice after 5 d of BIO treatment. Bar, 50 µm. *n* = 3 mice/genotype. (E) Quantitative analysis of HF at different stages of morphogenesis in the skin of WT and DTG mice after 5 d of BIO treatment. *n* = 3 mice/genotype. (F) Histomorphometric analysis of hair bulb diameter in DTG and WT skin treated with BIO as measured across the widest part. *n* = 3 mice/genotype. Data are presented as mean ± SD (error bars). *, $P < 0.05$; Student's *t* test.

as well as in formation of ∼30% fewer HFs with decreased hair bulb size and producing thinner hairs.

Skin and HF morphogenesis is controlled by coordinated activities of the Wnt, Hedgehog, Edar, Bmp, Fgf, Notch, and other signaling pathways (Millar, 2002; Schmidt-Ullrich and Paus, 2005; Blanpain and Fuchs, 2009). Among these pathways, Wnt signaling operates as the most powerful regulator of skin development. It controls cell proliferation in both epithelium (epidermis, HF matrix) and mesenchyme, and regulates differentiation of hair matrix keratinocytes and the morphogen-producing activity of dermal papilla cells (Zhou et al., 1995; Huelsken et al., 2001; Andl et al., 2002; Enshell-Seijffers et al., 2010; Choi et al., 2013; Fu and Hsu, 2013; Tsai et al., 2014). In the developing HFs, the Wnt signaling pathway operates as the activator of the placode formation, whereas BMP signaling inhibits this process and, together with Wnt inhibitors, Dkk1/2/4 promotes the interplacode cell fate in the epidermal progenitor cells (Botchkarev et al., 1999; Jiang et al., 1999; Andl et al., 2002; Sick et al., 2006). In turn, FGF and Edar pathways promote the placode cell fate, at least in part, by inhibiting the activity of BMP signaling (Eivers et al., 2008; Plouhinec et al., 2011), whereas Edar via the NF-kB pathway stimulates expression of the BMP antagonists, such as connective tissue growth factor (CTGF) and Follistatin (Mou et al., 2006). Edar serves as a downstream effector of Wnt signaling, which is initially activated in preplacodes independently of Edar/NF-κB activity, whereas later Edar signaling is required to refine the pattern of Wnt/β-catenin activity via stimulation of expression of the Wnt10b in the placode progenitor cells (Zhang et al., 2009). In addition, Edar signaling promotes HF placode formation by stimulation of Sonic hedgehog expression (Pummila et al., 2007), which operates as a potent stimulator of keratinocyte proliferation in the developing HF (St-Jacques et al., 1998; Chiang et al., 1999).

Recent data suggest that the activity of the Wnt signaling pathway varies considerably in distinct skin compartments:

Published November 24, 2014

low levels of activity are required for maintenance of epidermal proliferation, medium level signaling is required for maintenance of epithelial–mesenchymal interactions in the hair bulb to promote active hair growth phase, and high activity promotes hair shaft differentiation (Choi et al., 2013). Our data demonstrate that miR-214 contributes to the regulation of the activity of Wnt signaling in the developing and postnatal skin, at least in part, by targeting its key component β-catenin: (1) miR-214 and β-catenin exhibit reciprocal expression pattern in the epidermis, whereas miR-214 and β-catenin are colocalized in undifferentiated epithelial cells of the hair peg and in hair matrix keratinocytes; (2) β-catenin expression is markedly decreased in the epidermis, HF placodes, HF matrix, and dermal papilla after K14-driven miR-214 overexpression; (3) bioinformatic prediction analysis and experimental data confirms direct targeting of *β-catenin* 3′ UTR by miR-214 in keratinocytes; and (4) miR-214 is capable of interfering with the activity of Wnt signaling after its activation by the GSK-3β inhibitors both in vitro and in vivo.

Furthermore, the skin phenotype of miR-214 transgenic mice (decreased epidermal proliferation, proportional decrease in the number of all HF types, decrease of the size of hair bulbs, and formation of thinner hair versus the corresponding WT controls) is consistent with the skin phenotype of mice with conditional ablation of β-catenin either in keratinocytes or in the dermal papilla fibroblasts (Huelsken et al., 2001; Enshell-Seijffers et al., 2010; Tsai et al., 2014). Importantly, the key features of the skin phenotype in miR-214–overexpressing mice (decrease of the HF number and hair bulb size) are rescued by pharmacological activation of the Wnt pathway in vivo, thus further supporting the links between miR-214 and Wnt pathway activity in the skin. These data are also consistent with data published previously showing miR-214 targeting of β-catenin in hepatocellular carcinoma cells (Wang et al., 2012).

The Wnt signaling pathway is a potent regulator of cell proliferation, and many effects of miR-214 on skin and HF development are most likely associated with interference with cell cycle regulation: indeed, short-term activation of miR-214 (48 h) suppressed the expressions of several cyclins and cyclin-dependent kinases, including *cyclin B*, *cyclin D1*, *cyclin D2*, and *cdk1*. Consistent with these observations, substantial up-regulation in the cyclin-dependent kinase inhibitors p16 and p19 was still detected in fully developed follicles of the K14rtTA/TRE-miR-214 mice, which suggests the activation of the anti-proliferative program in response to increased levels of miR-214 in the keratinocytes. These data are in line with the results obtained in other models demonstrating that miR-214 expression is substantially decreased in cutaneous squamous cell carcinoma (Yamane et al., 2013) and that the anti-proliferative effects of miR-214 in the myoblast cell line are achieved by targeting Nras (Liu et al., 2010).

Reduced cell proliferation seen in the epidermis and HFs in K14rtTA/TRE-miR-214 mice could also be a result of altered activity of Shh signaling. Indeed, K14rtTA/TRE-miR-214 mice showed decreased expression of Shh and its signal tranducer Smo. Shh signaling is required for post-hair placode initiation growth by stimulating proliferation of HF epithelial cells via transcriptional activation of cyclin D1 and cyclin D2 (St-Jacques et al., 1998; Chiang et al., 1999; Mill et al., 2003; Schmidt-Ullrich et al., 2006). Shh also promotes epidermal proliferation (Zhou et al., 2006). In adult mice, Shh is essential for anagen onset and proper hair cycling (Sato et al., 1999; Wang et al., 2000). However, our experimental data validating the bioinformatic prediction suggested that *Shh* does not serve as a direct miR-214 target in the keratinocytes. Given that Wnt signaling operates as upstream of Edar and Shh pathways in the control of the HF placode formation (Schmidt-Ullrich et al., 2006; Zhang et al., 2009), these data suggest that down-regulation of Edar and Shh expression seen in the HF placodes of miR-214 DTG mice is, most likely, a result of the indirect effects linked to the miR-214–mediated decrease of Wnt signaling activity in keratinocytes.

Our data demonstrating that overexpression of miR-214 results in the development of smaller HFs producing thinner hair suggest miR-214 involvement in the control of HF size and its relevance to the mechanisms that contribute to HF miniaturization seen in androgenetic alopecia (Garza et al., 2011). However, additional studies are required to assess the role of miR-214 in the control of HF size in human skin, as well as the potential involvement of miR-214 in regulation of the activity of distinct HF stem cell populations residing in secondary hair germ and bulge during hair cycle (Hsu et al., 2011; Rompolas and Greco, 2014). Our data suggest that the decrease of HF size in K14rtTA/TRE-miR-214 mice could not only be associated with the decreased proliferation in the hair matrix, but also with miR-214 effects on the migration of the progenitor cells from the bulge alongside the outer root sheath toward the hair matrix.

Indeed, K14rtTA/miR-214 HFs contained significantly fewer Sox9+ cells in the outer root sheath. Sox9 is a transcriptional regulator that is expressed in the HF stem cells and their outer root sheath progenies, and is required for guiding stem cell progenies to the hair matrix (Vidal et al., 2005). Therefore, a reduced number of Sox9+ cells in the transgenic follicles suggests the inhibitory action of miR-214 on stem cells and their progenies, which contributes to the formation of the smaller hair bulbs. However, these effects could also be associated with decreased β-catenin expression, as β-catenin is acting as the upstream regulator of Sox9 expression in the intestinal epithelium and neural crest cells (Blache et al., 2004; Liu et al., 2013).

In addition to the changes seen in the HF epithelium, a significant reduction in the number of dermal papilla cells was observed in K14rtTA/miR-214 mice. This is consistent with previously published data demonstrating that a decrease of the hair bulb size is associated with reduced cellularity of the dermal papilla (Chi et al., 2013). Similar to mice with conditional ablation of β-catenin in the HF mesenchyme (Enshell-Seijffers et al., 2010), miR-214 overexpression results in the decrease of β-catenin, Lef1 expression, and lack of changes in Sox2 in the dermal papilla. Therefore, the effects seen in K14rtTA/miR-214 mice could be a result of the altered epithelial–mesenchymal interactions. Also, given that miRNAs are capable of exerting paracrine effects on distantly located cellular targets (Zhu and Fan, 2011), additional studies are required to clarify whether miR-214 overexpression in keratinocytes could directly influence

Published November 24, 2014

cell number and gene expression in dermal papilla fibroblasts, or if other paracrine factors released from keratinocytes affect traffic of the connective tissue progenitor cells to populate dermal papilla and/or their activity in the HFs in K14rtTA/miR-214 mice.

Additional studies are also required to define the upstream regulators that control miR-214 expression in the different cell types in the skin. For example, it has previously been shown that Twist1 transcriptionally regulates miR-214 expression in specific neural cell populations (Lee et al., 2009); however, a role of Twist1 in skin development and HF cycling remains unknown and needs to be carefully explored. Identification of the miR-214 upstream regulators in skin will help to recognize novel players in the miRNA-mediated gene regulatory circuits controlling keratinocyte proliferation and differentiation in the developing and postnatal skin.

In summary, our data reveal that miR-214 is a key determinant that controls the activity of the Wnt signaling pathway and β-catenin expression in the developing and postnatal skin and HFs. Because Wnt signaling plays a crucial role in the control of stem cell activity in many organs during development and regeneration, while its uncontrolled activation results in tumorigenesis (Chan et al., 1999; Malanchi et al., 2008), these data provide an important foundation for further analyses of the role of miR-214 as a regulator of Wnt pathway activity in many areas of research, including stem cell and cancer biology, regenerative medicine, and aging.

Materials and methods

Generation of transgenic mice

Animal studies were performed under protocols approved by Boston University and Home Office Project License (UK). K14-rtTA/TRE-miR-214 mice were generated on an FVB background. To generate TRE-miR-214 construct, a DNA fragment containing the precursor-mmu-miR-214 coding sequence was isolated from pCMV-miR-214 plasmid DNA (SC400919; OriGene) followed by blunt-end ligation into the pSTblue-1 vector (EMD Millipore). This fragment was then excised and ligated into BamHI–SalI sites of the pTRE2-Dual 2 plasmid (Takara Bio Inc.), which contains a pTight promoter consisting of a modified minimal CMV promoter, and seven direct repeats of a 36-bp regulatory sequence that contains the 19-bp tet-operator sequence, mCherry, and an internal ribosome entry site (IRES2). All cloning was verified by sequencing. A PspxI fragment from TRE-miR-214 construct was purified and pronuclear injections were performed in the Transgenic Core at the Boston University School of Medicine using FVB/NJ mice as a genetic background. Founders were identified by PCR using transgene promoter–specific DNA primers: forward, 5′-GTTCATGTACGGCTCCAAG-3′; and reverse, 5′-CGCAGCTTCACCTTGTAG-3′. To generate double-transgenic K14-rtTA/TRE-miR-214 mice, TRE-miR-214 mice were crossed with K14-rtTA according to standard protocols. To activate expression of tet/Dox-responsive transgenes, mice were fed chow containing 625 mg Dox/kg chow (Harlan Laboratories, Inc.). For activation of Wnt signaling, BIO (R&D Systems) was administered subcutaneously to back skin of neonatal mice in a concentration 2 µg/g (Gunn et al., 2011; Kwon et al., 2014) during five constitutive days starting from day 0 after birth.

Genotyping

Genotyping was performed using the following primers and PCR parameters. For K14rtTA mouse genotyping, primer sequences used were provided by The Jackson Laboratory, including forward primer oIMR7862, 5′-CACGATACACCTGACTAGCTGGGTG-3′; and reverse primer oIMR7863, 5′-CATCACCCACAGGCTAGCGCCAACT-3′ (PCR parameters: 94°C for 3 min [94°C for 30 s, 67°C for 60 s, 72°C for 60 s] for 35 cycles, 72°C for 2 min). For TRE-miR-214 mice, the forward primer, 5′-AGAACGTATGTCGAGGTAG-3′; and reverse primer, 5′-TTGGAGCCGTACATGAAC-3′ were used (PCR parameters: 94°C for 3 min [94°C for 30 s, 67°C for 60 s, 72°C for 60 s] for 35 cycles, 72°C for 2 min).

In situ hybridization, immunofluorescence, and histology

Skin cryosections (10 µm) were fixed in 4% paraformaldehyde for 10 min at room temperature. In brief, tissue sections were acetylated in triethanolamine buffer (4.5 mM triethanolamine, 6 M NCl, and 3 mM acetic anhydride) for 10 min and permeabilized (1% Triton X-100/1× DEPC-treated PBS) for 30 min, slides were hybridized with 2.5 pmol DIG-labeled miR-214 probe (Exiqon) diluted in hybridization buffer (50% formamide DI, 2× saline-sodium citrate (SCC), 1% dextran sulfate, and 0.4 mg/ml tRNA) for 16–18 h at 55°C overnight. Slides were subsequently washed twice in SCC (10 min, 4 times, 65°C), 0.1× SCC (60 min, 65°C), and 0.2× SCC (10 min, RT). Immunodetection of miR-214 was performed with sheep alkaline phosphatase–conjugated anti-DIG antibody (1:5,000; Roche) followed by a staining reaction with NBT/BCIP solution (Roche) for 16–18 h at RT. Alternatively, the signal was developed with the Tyramide Signal Amplification (TSA) system with FITC-conjugated reagent (PerkinElmer).

For immunofluorescence, the formalin-fixed cryosections or methanol-fixed cells were incubated with primary antisera listed in Table 1 overnight at 4°C, followed by application of corresponding Alexa Fluor 555 or Alexa Fluor 488 antibodies (1:200; Invitrogen) for 45 min at 37°C. Incubation steps were interspersed by washes with PBS. Sections were counterstained with DAPI.

For dual fluorescent in situ hybridization and immunofluorescence developed with the TSA system, in situ hybridization slides were processed for β-catenin immunofluorescence as described in the previous paragraph. For double immunofluorescence of Keratins and BrdU, the slides were treated with DNase I (20 µg/ml; Sigma-Aldrich) for 2 h at 37°C, then incubated with primary antibodies against BrdU (1:500; Abcam), followed by subsequent antibody costaining as described in the previous paragraph.

For detection of endogenous alkaline phosphatase, acetone-fixed cryosections (10 µm) were incubated in developing solution (100 mM NaCl, pH 8.3, 100 mM Tris, pH 9.5, 20 mM HCl, 0.05% Naphtol ASBI phosphate, 0.5% DMF, 25 mM sodium-nitrite, and 5% New fuchsin) for 15 min, followed by a quick wash in PBS and immersion of the slides in Vector Hematoxylin Nuclear counterstain solution (Vector Laboratories) for 30 s at RT (Botchkareva et al., 1999; Paus et al., 1999).

Microscopy and image analyses

Images were taken at RT using the fluorochromes DAPI, Alexa Fluor 488 (green), and Alexa Fluor 555 (red). Fluorescence images were acquired with a microscope (Eclipse50i) equipped with a Plan Fluor 20×/0.50 NA or 40×/0.75 NA objective lens (Nikon), a camera (EXi Aqua; QImaging), and Image-Pro Express software (version 6.3; Media Cybernetics). Brightfield microscopy was performed using a microscope (Eclipse 50i; Nikon) equipped with a Plan Fluor 20×/0.50 NA or 40×/0.75 NA objective lens (Nikon), a camera (VisiCam 3.0; VWR International), and Visi-Cam Image Analyzer software (VWR International). No imaging medium was used. For the illustration purposes, images of the skin cryosections were adjusted using the levels and brightness/contrast tools in Photoshop (CS6; Adobe); the same adjustments were applied to every pixel in each RGB channel.

Microarray and real-time PCR

Newborn K14-rtTA/TRE-miR-214 and WT mice were treated with Dox for 48 h to induce miR-214 followed by skin harvesting. Skins were treated with dispase at 37°C for 30 min to collect epidermis and HF epithelium. Total RNA was isolated by TRIzol (Sigma-Aldrich) and processed for microarray analysis by using 41K Whole Mouse Genome 60-mer oligo-microarray (Agilent Technologies). Expression of miR-214 was determined using TaqMan real-time PCR Assay (Applied Biosystems) under the following cycling conditions: 95°C for 10 min, followed by 40 cycles of 95°C for 15 s and 60°C for 60 s.

Differences between samples and controls were calculated based on the Ct ($^{\Delta\Delta}$Ct) method and normalized to the small nucleolar RNA 202 values (SnoRNA). Data were pooled, the means ± SD were calculated, and statistical analysis was performed using an unpaired Student's *t* test. Quantitative RT-PCR for mRNA was performed with iQ SYBR Green Supermix (Bio-Rad Laboratories), using 10 ng cDNA and 1 µM primers. PCR primers were designed with Beacon Designer software (Premier Biosoft International; Table 2). Amplification was performed at the following conditions: 95°C for 5 min, followed by 40 cycles of denaturation (95°C for 15 s), annealing (30 s at temperature experimentally determined for each primer pairs), and elongation (72°C for 15 s). Data analysis was performed as described above. Differences between samples and controls were calculated based on the Ct ($^{\Delta\Delta}$Ct) method and normalized to *β-actin*. Statistical analysis was performed using an unpaired Student's *t* test.

Published November 24, 2014

Table 1. **Primary antibodies and associated dilutions**

Antibody	Host	Dilution	Source
β-Catenin	Rabbit	1:2,000	Abcam
BrdU	Sheep	1:100	Abcam
CD34	Goat	1:200	BD
Cyclin D1	Rabbit	1:100	Abcam
Cyclin D2	Rabbit	1:100	Abcam
Cdk1	mouse	1:100	Abcam
Cytokeratin 10	Rabbit	1:500	Abcam
Cytokeratin 14	Guinea pig	1:500	Acris
Dlx3	Goat	1:500	Santa Cruz Biotechnology, Inc.
Edar	Goat	1:500	R&D Systems
Ki67	Rabbit	1:100	Abcam
Lef-1	Rabbit	1:100	Cell Signaling Technology
Lhx2	Goat	1:200	Santa Cruz Biotechnology, Inc.
Loricin	Rabbit	1:100	Abcam
Phospho-H3	Rabbit	1:100	Cell Signaling Technology
Phospho-Smad 1/5/8	Rabbit	1:500	Abcam
Sox 2	Goat	1:200	Santa Cruz Biotechnology, Inc.
Sox 9	Rabbit	1:250	Santa Cruz Biotechnology, Inc.
Shh	Rabbit	1:100	Santa Cruz Biotechnology, Inc.

Western blot analysis

5 µg of protein was extracted from snap-frozen skin samples or cultured cells with lysis buffer consisting of 50 mm Tris-HCl, 1% NP-40, 0.25% sodium deoxycholate, 150 mm NaCl, 1 mm EDTA, pH 7.4, and Complete Ultra protease inhibitor cocktail (Roche). Protein concentrations were determined using the Bradford assay. Proteins were resolved via SDS-PAGE. Membranes were incubated with primary antibodies against β-catenin (1:2,000) and β-actin (1:2,000; Table 1) overnight at 4°C. Horseradish peroxidase-tagged IgG antibody was used as a secondary antibody (1:5,000; Thermo Fisher Scientific). Antibody binding was visualized with an enhanced chemiluminescence system (SuperSignal West Pico kit; Thermo Fisher Scientific) and the Gel Doc XR+ system (Bio-Rad Laboratories). Densitometric analysis was performed using ImageJ software (National Institutes of Health).

Histomorphometry, quantitative immunofluorescence, and statistical analysis

For histomorphometry analysis, every tenth cryosection of dorsal skin from K14-rtTA/TRE-miR-214 and WT mice was used to exclude the repetitive evaluation of the same HF. The number of HFs per millimeter of epidermal length was calculated using sections from dorsal skin of K14-rtTA/TRE-miR-214 and WT samples at the different developmental points, including E17.5, P0.5, and P8.5.5 (n = 3 per each experimental group). Proliferation in the epidermis was assessed by the calculation of the ratio of the number of Ki67+ cells to DAPI+ cells in 50–60 microscopic fields. Proliferation in the HF was assessed by calculating the ratio of pH3(Ser28)+ to DAPI+ cells per hair bulb in 50–60 HFs of either K14-rtTA/TRE-miR-214 or WT mice. The hair bulb diameter was measured across the widest part of the bulb (Auber line). Altogether, HFs in 50–60 microscopic fields from distinct time points were analyzed and compared with a corresponding number of HF from the appropriate age-matched WT mice. Comparative analysis of Sox9+ cells was done by evaluating the ratio of the number Sox9+ to DAPI+ cells in the outer root sheath (from the distal end of the bulb to the sebaceous duct). In total, 50–60 follicles of either WT or K14-rtTA/TRE-miR-214 mice were included in the analysis. Data were pooled, the means ± SD were calculated, and statistical analysis was performed using an unpaired Student's t test.

For the assessment of the hair shaft length and width of the four HF types (guard, awl, auchene, and zigzag), hairs were plucked from the back skin of K14rtTA/TRE-miR-214 (n = 4) and WT mice (n = 4) in the telogen

Table 2. **List of primers used for RT-qPCR**

Gene		Accession	Sense sequence (5′-3′)	Anti-sense sequence (5′-3′)
Axin	Axin2	NM_015732	CACCTCTCCTCTGTTACCTTC	GTCAACGCTCTGCCCTAC
Actb	Actin, β	NM_007393	TTCCAGCCTTCCTTCTTG	GGAGCCAGAGCAGTAATC
Ctnnb1	Catenin, β1	NM_001165902	GCCACCAAACAGATACATAC	CCTCTCAGCAACTCTACAG
Cdkn2a	Cyclin-dependent kinase inhibitor 2A	NM_009877	GCTCTTTGTGTTCCGCTG	CTCTGCTCTTGGGATTGG
Cdkn2d	Cyclin-dependent kinase inhibitor 2D (p19)	NM_009878	GGCTCCTACAGGCAACAG	TAGATGGCTCACACTTCAGG
Ccnd1	Cyclin D1	NM_007631	GAGACCATTCCCTTGACTGC	GAAATGAACTTCACATCTGTGGC
Ccnd2	Cyclin D2	NM_009829	GGATGCTAGAGGTCTGTGAGG	CCAACACTACCAGTTCCCAC
Ccnb1	Cyclin B1	NM_172301	ATAATCCCTCTCCAAGCCCG	CTGCTCTTCCTCCAGTTGTC
Cdk1	Cyclin-dependent kinase 1	NM_007659	ATCAGACTTGAAAGCGAGGA	GGTGTAAGTAACTCTTAACGAGTG
Edar	Ectodysplasin-A receptor	NM_010100	GCCCCACCGAGTTGCCGTTT	CCAGCCGCTCGATCTGCACC
Krt10	Keratin 10	NM_010660	AGTCTGAAATCACTGAATTG	ATCTGGCTTTGAATCTGG
Lef-1	Lymphoid enhancer binding factor 1	NM_001276402	ACTCCAAGCAAGGCATGTC	GGGTGATCTGTCCAACGC
Lor	Loricrin	NM_008508	TTCCAAACCCTTCACATTTTAAG	GGGAGGTAGTCATTCAGAAAC
Ptch2	Patched homologue 2	NM_008958	TCCGCACCTCATATCCTAGC	CTGTCTCAATTACAGCCACTCG
Smo	Smoothened homologue	NM_176996	GCTGGAGTAGTCTGGTTCGT	GAGTCTCCATCTACCTGAGCC
Sostdc1	Sclerostin domain containing 1	NM_025312	CTTCCTCCTGCCATTCATCTC	GAACTCGACTGTTTCGATCCAG
Shh	Sonic hedgehog	NM_009170	GTTTATTCCCAACGTAGCCGA	CTTGTCTTTGCACCTCTGAGTC

phase of the hair cycle. The four hair types were distinguished on the basis of their hair length, number of kinks, and medulla width (Sharov et al., 2006). Hair shaft length and width of ~250 plucked hair shafts per animal were measured using ImageJ software. Data were pooled, the means ± SD were calculated, and statistical analysis was performed using an unpaired Student's *t* test.

The percentage of HFs in different anagen stages was assessed and calculated in K14-rtTA/TRE-miR-214 at days 3 and 5 after the depilation-induced hair cycle, respectively, as well as in their corresponding WT littermates. All evaluations were performed using accepted, well-defined morphological criteria of HFs at early, mid, and late anagen phase based on the changes in the shape and size of the hair matrix and the dermal papilla (Müller-Röver et al., 2001).

Immunofluorescence intensity was determined using ImageJ software, as described previously (Ramot et al., 2010). In brief, red or green fluorescent signal was collected from experimental tissues in RGB format using the same exposure conditions. To measure the fluorescence intensity at each pixel, the RGB images were converted to 8-bit grayscale format. Regions of interest of distinct size within the WT and DTG HFs were selected, and the mean values of intensity were calculated for each selected areas followed by the normalization relative to the number of DAPI+ cells.

Cell culture and transfections

PMEKs were prepared from newborn mice at P2–3. In brief, mouse skins were incubated in 0.25% trypsin at 4°C overnight. The epidermal portion was minced and filtered through a 70-µm cell strainer (BD Biosciences), which result in a single-cell suspension. PMEKs were grown in EMEM calcium-free medium (Lonza) supplemented with 0.05 mM calcium, at 33°C, 8% CO_2 (Scientific Laboratory Suppliers, Hessle, UK) until 60–70% confluent. PMEKs were transfected with 200 nM of synthetic miR-214 inhibitor (anti-miR-214), miR-214 mimic (pro-miR-214), or miRNA negative controls (GE Healthcare), using Lipofectamine RNAiMax (Invitrogen). Cells were harvested 24 h after transfection and used for further analyses. To induce Wnt signaling, PMEKs were treated with 10 mM lithium chloride (Klein and Melton, 1996). To examine the regulatory effects of miR-214 on Wnt/β-Catenin signaling, PMEKs were treated with 10 mM LiCl for 2 h, followed by transfection of cells with 200 nM pro-miR-214 or miRNA negative controls for 4 h at 33°C, 8% CO_2. Cells were then harvested 24 h after transfection.

miRNA binding predictions

MiR-214 binding was estimated as a consensus from four different prediction algorithms: TargetScan (http://www.targetscan.org/) predicts biological targets of miRNAs by searching for the presence of conserved sites that match the seed region of each miRNA; miRBase (http://microrna.sanger.ac.uk) uses the miRanda algorithm to predict miRNA-mRNA pairs; miRDB (http://mirdb.org/miRDB) uses the MirTarget2 algorithm, which was developed by analyzing thousands of genes impacted by miRNAs; and PITA (http://genie.weizmann.ac.il/pubs/mir07/mir07_data.html) confirms candidates predicted by the other three algorithms.

Luciferase reporter assay

HaCaT cells were grown in Dulbecco's modified Eagle's medium (Invitrogen) supplemented with heat-inactivated 10% FBS in an atmosphere of 5% CO_2 at 37°C, until 60–70% confluent. 3′ UTR fragments of *β-catenin* and *Shh* containing miR-214 putative target sites were amplified from mouse genomic DNA using forward and reverse primers containing XhoI and NotI restriction sequences, respectively. For 3′ UTR of *β-catenin* fragment, 5′-CGAGGAGTAACAATACAAATGG-3′ and 5′-CAGGTTCACTAGAACATAACAC-3′ forward and reverse primers, respectively, were used. To amplify a fragment of the 3′ UTR of *Shh*, 5′-ATGAACGGACCTTCAAGAGC-3′ and 5′-GCATAGCAGGAGAGGAATGC-3′ primers were used. The amplified fragments were cloned at XhoI and NotI sites downstream of CV40 promoter-driven Renilla luciferase cassette in pCHECK2 (Promega). Site-directed mutagenesis was performed using a QuikChange II XL Site-Directed Mutagenesis kit (Agilent Technologies) to mutate the β-catenin binding site according to the manufacturer's instructions. For the dual luciferase assay, these constructs (200 ng) were cotransfected with 200 nM miR-214 mimic or negative control mimic (GE Healthcare) into HaCaT cells using 0.5 µl Lipofectamine 2000 (Invitrogen) in 96-well plates. At 24 h after transfection, the relative luciferase activities were determined using Dual-Glo Luciferase Assay System (Promega). Assay was performed in triplicate for three independent trials.

TOPFlash and FOPFlash Wnt reporter assays

HaCaT cells were seeded onto 12-well dishes 24 h before transfection. At 80% confluence, a TOPFlash Wnt reporter plasmid (plasmid 12456; Addgene) were transfected into each well in combination with (1) control oligonucleotide (200 nM), (2) 10 µM of BIO (R&D Systems), (3) pro–miR-214 (200 nM), and (4) pro–miR-214 (200 nM) and 10 µM BIO (Sato et al., 1999). Transfection was done using Lipofectamine 2000 (Invitrogen). FOPFlash (TOPFlash mutant) reporter plasmid (plasmid 12457; Addgene) was used as a control. The cells were cultured for 24 h. The relative luciferase activities were determined using the Dual-Gloluciferase assay system (Promega) on a microplate reader (Infinite 2000; Tecan). All assays were performed in triplicate for three independent trials.

Online supplemental material

Fig. S1 shows additional details of the skin phenotype in K14-rtTA/miR-214-TRE mice during morphogenesis and the hair cycling, and the results of bioinformatic prediction of miR-214 targets in the keratinocytes and their validation. Tables S1 and S2 list the genes with down- and up-regulated expression in the skin epithelium of K14-rtTA/miR-214-TRE versus WT mice. Online supplemental material is available at http://www.jcb.org/cgi/content/full/jcb.201404001/DC1.

This study was supported by a grant from the Medical Research Council UK (MR/K011324/1) to N.V. Botchkareva.

The authors declare no competing financial interests.

Submitted: 1 April 2014
Accepted: 23 October 2014

References

Ahmed, M.I., A.N. Mardaryev, C.J. Lewis, A.A. Sharov, and N.V. Botchkareva. 2011. MicroRNA-21 is an important downstream component of BMP signalling in epidermal keratinocytes. *J. Cell Sci.* 124:3399–3404. http://dx.doi.org/10.1242/jcs.086710

Ambros, V. 2001. microRNAs: tiny regulators with great potential. *Cell*. 107: 823–826. http://dx.doi.org/10.1016/S0092-8674(01)00616-X

Andl, T., S.T. Reddy, T. Gaddapara, and S.E. Millar. 2002. WNT signals are required for the initiation of hair follicle development. *Dev. Cell*. 2:643–653. http://dx.doi.org/10.1016/S1534-5807(02)00167-3

Andl, T., E.P. Murchison, F. Liu, Y. Zhang, M. Yunta-Gonzalez, J.W. Tobias, C.D. Andl, J.T. Seykora, G.J. Hannon, and S.E. Millar. 2006. The miRNA-processing enzyme dicer is essential for the morphogenesis and maintenance of hair follicles. *Curr. Biol.* 16:1041–1049. http://dx.doi.org/10.1016/j.cub.2006.04.005

Blache, P., M. van de Wetering, I. Duluc, C. Domon, P. Berta, J.N. Freund, H. Clevers, and P. Jay. 2004. SOX9 is an intestine crypt transcription factor, is regulated by the Wnt pathway, and represses the CDX2 and MUC2 genes. *J. Cell Biol.* 166:37–47. http://dx.doi.org/10.1083/jcb.200311021

Blanpain, C., and E. Fuchs. 2009. Epidermal homeostasis: a balancing act of stem cells in the skin. *Nat. Rev. Mol. Cell Biol.* 10:207–217. http://dx.doi.org/10.1038/nrm2636

Botchkarev, V.A., and R. Paus. 2003. Molecular biology of hair morphogenesis: development and cycling. *J. Exp. Zoolog. B Mol. Dev. Evol.* 298B:164–180. http://dx.doi.org/10.1002/jez.b.33

Botchkarev, V.A., N.V. Botchkareva, W. Roth, M. Nakamura, L.H. Chen, W. Herzog, G. Lindner, J.A. McMahon, C. Peters, R. Lauster, et al. 1999. Noggin is a mesenchymally derived stimulator of hair-follicle induction. *Nat. Cell Biol.* 1:158–164. http://dx.doi.org/10.1038/11078

Botchkarev, V.A., M.R. Gdula, A.N. Mardaryev, A.A. Sharov, and M.Y. Fessing. 2012. Epigenetic regulation of gene expression in keratinocytes. *J. Invest. Dermatol.* 132:2505–2521. http://dx.doi.org/10.1038/jid.2012.182

Botchkareva, N.V. 2012. MicroRNA/mRNA regulatory networks in the control of skin development and regeneration. *Cell Cycle*. 11:468–474. http://dx.doi.org/10.4161/cc.11.3.19058

Botchkareva, N.V., V.A. Botchkarev, L.H. Chen, G. Lindner, and R. Paus. 1999. A role for p75 neurotrophin receptor in the control of hair follicle morphogenesis. *Dev. Biol.* 216:135–153. http://dx.doi.org/10.1006/dbio.1999.9464

Byrne, C., M. Tainsky, and E. Fuchs. 1994. Programming gene expression in developing epidermis. *Development*. 120:2369–2383.

Chan, E.F., U. Gat, J.M. McNiff, and E. Fuchs. 1999. A common human skin tumour is caused by activating mutations in β-catenin. *Nat. Genet.* 21:410–413. http://dx.doi.org/10.1038/7747

Chen, H., R. Shalom-Feuerstein, J. Riley, S.D. Zhang, P. Tucci, M. Agostini, D. Aberdam, R.A. Knight, G. Genchi, P. Nicotera, et al. 2010. miR-7 and miR-214 are specifically expressed during neuroblastoma differentiation, cortical development and embryonic stem cells differentiation, and control neurite outgrowth in vitro. *Biochem. Biophys. Res. Commun.* 394:921–927. http://dx.doi.org/10.1016/j.bbrc.2010.03.076

Chi, W., E. Wu, and B.A. Morgan. 2013. Dermal papilla cell number specifies hair size, shape and cycling and its reduction causes follicular decline. *Development*. 140:1676–1683. http://dx.doi.org/10.1242/dev.090662

Chiang, C., R.Z. Swan, M. Grachtchouk, M. Bolinger, Y. Litingtung, E.K. Robertson, M.K. Cooper, W. Gaffield, H. Westphal, P.A. Beachy, and A.A. Dlugosz. 1999. Essential role for Sonic hedgehog during hair follicle morphogenesis. *Dev. Biol.* 205:1–9. http://dx.doi.org/10.1006/dbio.1998.9103

Choi, Y.S., Y. Zhang, M. Xu, Y. Yang, M. Ito, T. Peng, Z. Cui, A. Nagy, A.K. Hadjantonakis, R.A. Lang, et al. 2013. Distinct functions for Wnt/β-catenin in hair follicle stem cell proliferation and survival and interfollicular epidermal homeostasis. *Cell Stem Cell*. 13:720–733. http://dx.doi.org/10.1016/j.stem.2013.10.003

Eivers, E., L.C. Fuentealba, and E.M. De Robertis. 2008. Integrating positional information at the level of Smad1/5/8. *Curr. Opin. Genet. Dev.* 18:304–310. http://dx.doi.org/10.1016/j.gde.2008.06.001

Enshell-Seijffers, D., C. Lindon, M. Kashiwagi, and B.A. Morgan. 2010. β-catenin activity in the dermal papilla regulates morphogenesis and regeneration of hair. *Dev. Cell*. 18:633–642. http://dx.doi.org/10.1016/j.devcel.2010.01.016

Frye, M., and S.A. Benitah. 2012. Chromatin regulators in mammalian epidermis. *Semin. Cell Dev. Biol.* 23:897–905. http://dx.doi.org/10.1016/j.semcdb.2012.08.009

Fu, J., and W. Hsu. 2013. Epidermal Wnt controls hair follicle induction by orchestrating dynamic signaling crosstalk between the epidermis and dermis. *J. Invest. Dermatol.* 133:890–898. http://dx.doi.org/10.1038/jid.2012.407

Garza, L.A., C.C. Yang, T. Zhao, H.B. Blatt, M. Lee, H. He, D.C. Stanton, L. Carrasco, J.H. Spiegel, J.W. Tobias, and G. Cotsarelis. 2011. Bald scalp in men with androgenetic alopecia retains hair follicle stem cells but lacks CD200-rich and CD34-positive hair follicle progenitor cells. *J. Clin. Invest.* 121:613–622. http://dx.doi.org/10.1172/JCI44478

Gunn, W.G., U. Krause, N. Lee, and C.A. Gregory. 2011. Pharmaceutical inhibition of glycogen synthetase kinase-3β reduces multiple myeloma-induced bone disease in a novel murine plasmacytoma xenograft model. *Blood*. 117:1641–1651. http://dx.doi.org/10.1182/blood-2010-09-308171

Hsu, Y.C., and E. Fuchs. 2012. A family business: stem cell progeny join the niche to regulate homeostasis. *Nat. Rev. Mol. Cell Biol.* 13:103–114. http://dx.doi.org/10.1038/nrm3272

Hsu, Y.C., H.A. Pasolli, and E. Fuchs. 2011. Dynamics between stem cells, niche, and progeny in the hair follicle. *Cell*. 144:92–105. http://dx.doi.org/10.1016/j.cell.2010.11.049

Huelsken, J., R. Vogel, B. Erdmann, G. Cotsarelis, and W. Birchmeier. 2001. β-Catenin controls hair follicle morphogenesis and stem cell differentiation in the skin. *Cell*. 105:533–545. http://dx.doi.org/10.1016/S0092-8674(01)00336-1

Inui, M., G. Martello, and S. Piccolo. 2010. MicroRNA control of signal transduction. *Nat. Rev. Mol. Cell Biol.* 11:252–263. http://dx.doi.org/10.1038/nrm2868

Jiang, T.X., Y.H. Liu, R.B. Widelitz, R.K. Kundu, R.E. Maxson, and C.M. Chuong. 1999. Epidermal dysplasia and abnormal hair follicles in transgenic mice overexpressing homeobox gene MSX-2. *J. Invest. Dermatol.* 113:230–237. http://dx.doi.org/10.1046/j.1523-1747.1999.00680.x

Joglekar, M.V., V.S. Parekh, and A.A. Hardikar. 2007. New pancreas from old: microregulators of pancreas regeneration. *Trends Endocrinol. Metab.* 18:393–400. http://dx.doi.org/10.1016/j.tem.2007.10.001

Kertesz, M., N. Iovino, U. Unnerstall, U. Gaul, and E. Segal. 2007. The role of site accessibility in microRNA target recognition. *Nat. Genet.* 39:1278–1284. http://dx.doi.org/10.1038/ng2135

Klein, P.S., and D.A. Melton. 1996. A molecular mechanism for the effect of lithium on development. *Proc. Natl. Acad. Sci. USA*. 93:8455–8459. http://dx.doi.org/10.1073/pnas.93.16.8455

Kwon, Y.J., C.H. Yoon, S.W. Lee, Y.B. Park, S.K. Lee, and M.C. Park. 2014. Inhibition of glycogen synthase kinase-3β suppresses inflammatory responses in rheumatoid arthritis fibroblast-like synoviocytes and collagen-induced arthritis. *Joint Bone Spine*. 81:240–246. http://dx.doi.org/10.1016/j.jbspin.2013.09.006

Lee, R.C., R.L. Feinbaum, and V. Ambros. 1993. The *C. elegans* heterochronic gene lin-4 encodes small RNAs with antisense complementarity to lin-14. *Cell*. 75:843–854. http://dx.doi.org/10.1016/0092-8674(93)90529-Y

Lee, Y.B., I. Bantounas, D.Y. Lee, L. Phylactou, M.A. Caldwell, and J.B. Uney. 2009. Twist-1 regulates the miR-199a/214 cluster during development. *Nucleic Acids Res.* 37:123–128. http://dx.doi.org/10.1093/nar/gkn920

Lena, A.M., R. Shalom-Feuerstein, P. Rivetti di Val Cervo, D. Aberdam, R.A. Knight, G. Melino, and E. Candi. 2008. miR-203 represses 'stemness' by repressing ΔNp63. *Cell Death Differ.* 15:1187–1195. http://dx.doi.org/10.1038/cdd.2008.69

Levy, C., M. Khaled, K.C. Robinson, R.A. Veguilla, P.H. Chen, S. Yokoyama, E. Makino, J. Lu, L. Larue, F. Beermann, et al. 2010. Lineage-specific transcriptional regulation of DICER by MITF in melanocytes. *Cell*. 141:994–1005. http://dx.doi.org/10.1016/j.cell.2010.05.004

Lewis, B.P., C.B. Burge, and D.P. Bartel. 2005. Conserved seed pairing, often flanked by adenosines, indicates that thousands of human genes are microRNA targets. *Cell*. 120:15–20. http://dx.doi.org/10.1016/j.cell.2004.12.035

Lewis, C.J., A.N. Mardaryev, K. Poterlowicz, T.Y. Sharova, A. Aziz, D.T. Sharpe, N.V. Botchkareva, and A.A. Sharov. 2014. Bone morphogenetic protein signaling suppresses wound-induced skin repair by inhibiting keratinocyte proliferation and migration. *J. Invest. Dermatol.* 134:827–837. http://dx.doi.org/10.1038/jid.2013.419

Liu, J., X.J. Luo, A.W. Xiong, Z.D. Zhang, S. Yue, M.S. Zhu, and S.Y. Cheng. 2010. MicroRNA-214 promotes myogenic differentiation by facilitating exit from mitosis via down-regulation of proto-oncogene N-ras. *J. Biol. Chem.* 285:26599–26607. http://dx.doi.org/10.1074/jbc.M110.115824

Liu, J.A., M.H. Wu, C.H. Yan, B.K. Chau, H. So, A. Ng, A. Chan, K.S. Cheah, J. Briscoe, and M. Cheung. 2013. Phosphorylation of Sox9 is required for neural crest delamination and is regulated downstream of BMP and canonical Wnt signaling. *Proc. Natl. Acad. Sci. USA*. 110:2882–2887. http://dx.doi.org/10.1073/pnas.1211747110

Malanchi, I., H. Peinado, D. Kassen, T. Hussenet, D. Metzger, P. Chambon, M. Huber, D. Hohl, A. Cano, W. Birchmeier, and J. Huelsken. 2008. Cutaneous cancer stem cell maintenance is dependent on β-catenin signalling. *Nature*. 452:650–653. http://dx.doi.org/10.1038/nature06835

Mardaryev, A.N., M.I. Ahmed, N.V. Vlahov, M.Y. Fessing, J.H. Gill, A.A. Sharov, and N.V. Botchkareva. 2010. Micro-RNA-31 controls hair cycle-associated changes in gene expression programs of the skin and hair follicle. *FASEB J.* 24:3869–3881. http://dx.doi.org/10.1096/fj.10-160663

Meijer, L., A.L. Skaltsounis, P. Magiatis, P. Polychronopoulos, M. Knockaert, M. Leost, X.P. Ryan, C.A. Vonica, A. Brivanlou, R. Dajani, et al. 2003. GSK-3-selective inhibitors derived from Tyrian purple indirubins. *Chem. Biol.* 10:1255–1266. http://dx.doi.org/10.1016/j.chembiol.2003.11.010

Mill, P., R. Mo, H. Fu, M. Grachtchouk, P.C. Kim, A.A. Dlugosz, and C.C. Hui. 2003. Sonic hedgehog-dependent activation of Gli2 is essential for embryonic hair follicle development. *Genes Dev.* 17:282–294. http://dx.doi.org/10.1101/gad.1038103

Millar, S.E. 2002. Molecular mechanisms regulating hair follicle development. *J. Invest. Dermatol.* 118:216–225. http://dx.doi.org/10.1046/j.0022-202x.2001.01670.x

Mou, C., B. Jackson, P. Schneider, P.A. Overbeek, and D.J. Headon. 2006. Generation of the primary hair follicle pattern. *Proc. Natl. Acad. Sci. USA*. 103:9075–9080. http://dx.doi.org/10.1073/pnas.0600825103

Müller-Röver, S., B. Handjiski, C. van der Veen, S. Eichmüller, K. Foitzik, I.A. McKay, K.S. Stenn, and R. Paus. 2001. A comprehensive guide for the accurate classification of murine hair follicles in distinct hair cycle stages. *J. Invest. Dermatol.* 117:3–15. http://dx.doi.org/10.1046/j.0022-202x.2001.01377.x

Ning, M.S., and T. Andl. 2013. Control by a hair's breadth: the role of microRNAs in the skin. *Cell. Mol. Life Sci.* 70:1149–1169. http://dx.doi.org/10.1007/s00018-012-1117-z

Paus, R., S. Müller-Röver, C. Van Der Veen, M. Maurer, S. Eichmüller, G. Ling, U. Hofmann, K. Foitzik, L. Mecklenburg, and B. Handjiski. 1999. A comprehensive guide for the recognition and classification of distinct stages of hair follicle morphogenesis. *J. Invest. Dermatol.* 113:523–532. http://dx.doi.org/10.1046/j.1523-1747.1999.00740.x

Plouhinec, J.L., L. Zakin, and E.M. De Robertis. 2011. Systems control of BMP morphogen flow in vertebrate embryos. *Curr. Opin. Genet. Dev.* 21:696–703. http://dx.doi.org/10.1016/j.gde.2011.09.001

Pummila, M., I. Fliniaux, R. Jaatinen, M.J. James, J. Laurikkala, P. Schneider, I. Thesleff, and M.L. Mikkola. 2007. Ectodysplasin has a dual role in ectodermal organogenesis: inhibition of Bmp activity and induction of Shh expression. *Development*. 134:117–125. http://dx.doi.org/10.1242/dev.02708

Ramot, Y., T. Bíró, S. Tiede, B.I. Tóth, E.A. Langan, K. Sugawara, K. Foitzik, A. Ingber, V. Goffin, L. Langbein, and R. Paus. 2010. Prolactin—a novel neuroendocrine regulator of human keratin expression in situ. *FASEB J.* 24:1768–1779. http://dx.doi.org/10.1096/fj.09-146415

Rehmsmeier, M., P. Steffen, M. Hochsmann, and R. Giegerich. 2004. Fast and effective prediction of microRNA/target duplexes. *RNA*. 10:1507–1517. http://dx.doi.org/10.1261/rna.5248604

Rompolas, P., and V. Greco. 2014. Stem cell dynamics in the hair follicle niche. *Semin. Cell Dev. Biol.* 25-26:34–42. http://dx.doi.org/10.1016/j.semcdb.2013.12.005

Sato, N., P.L. Leopold, and R.G. Crystal. 1999. Induction of the hair growth phase in postnatal mice by localized transient expression of Sonic hedgehog. *J. Clin. Invest.* 104:855–864. http://dx.doi.org/10.1172/JCI7691

Sato, N., L. Meijer, L. Skaltsounis, P. Greengard, and A.H. Brivanlou. 2004. Maintenance of pluripotency in human and mouse embryonic stem cells through activation of Wnt signaling by a pharmacological GSK-3-specific inhibitor. *Nat. Med.* 10:55–63. http://dx.doi.org/10.1038/nm979

Schmidt-Ullrich, R., and R. Paus. 2005. Molecular principles of hair follicle induction and morphogenesis. *BioEssays*. 27:247–261. http://dx.doi.org/10.1002/bies.20184

Schmidt-Ullrich, R., D.J. Tobin, D. Lenhard, P. Schneider, R. Paus, and C. Scheidereit. 2006. NF-κB transmits Eda A1/EdaR signalling to activate Shh and cyclin D1 expression, and controls post-initiation hair placode down growth. *Development*. 133:1045–1057. http://dx.doi.org/10.1242/dev.02278

Schneider, M.R., R. Schmidt-Ullrich, and R. Paus. 2009. The hair follicle as a dynamic miniorgan. *Curr. Biol.* 19:R132–R142. http://dx.doi.org/10.1016/j.cub.2008.12.005

Sehic, A., S. Risnes, C. Khuu, Q.E. Khan, and H. Osmundsen. 2011. Effects of in vivo transfection with anti-miR-214 on gene expression in murine molar tooth germ. *Physiol. Genomics*. 43:488–498. http://dx.doi.org/10.1152/physiolgenomics.00248.2010

Sharov, A.A., T.Y. Sharova, A.N. Mardaryev, A. Tommasi di Vignano, R. Atoyan, L. Weiner, S. Yang, J.L. Brissette, G.P. Dotto, and V.A. Botchkarev. 2006. Bone morphogenetic protein signaling regulates the size of hair follicles and modulates the expression of cell cycle-associated genes. *Proc. Natl. Acad. Sci. USA*. 103:18166–18171. http://dx.doi.org/10.1073/pnas.0608899103

Sick, S., S. Reinker, J. Timmer, and T. Schlake. 2006. WNT and DKK determine hair follicle spacing through a reaction-diffusion mechanism. *Science*. 314:1447–1450. http://dx.doi.org/10.1126/science.1130088

Smyth, G. 2005. Limma: linear models for microarray data. *In* Bioinformatics and Computational Biology Solutions using R and Bioconductor. V.C.R. Gentleman, S. Dudoit, R. Irizarry, and W. Huber, editors. Springer, New York. 397–420. http://dx.doi.org/10.1007/0-387-29362-0_23

St-Jacques, B., H.R. Dassule, I. Karavanova, V.A. Botchkarev, J. Li, P.S. Danielian, J.A. McMahon, P.M. Lewis, R. Paus, and A.P. McMahon. 1998. Sonic hedgehog signaling is essential for hair development. *Curr. Biol.* 8:1058–1069. http://dx.doi.org/10.1016/S0960-9822(98)70443-9

Stenn, K.S., and R. Paus. 2001. Controls of hair follicle cycling. *Physiol. Rev.* 81:449–494.

Su, X., D. Chakravarti, M.S. Cho, L. Liu, Y.J. Gi, Y.L. Lin, M.L. Leung, A. El-Naggar, C.J. Creighton, M.B. Suraokar, et al. 2010. TAp63 suppresses metastasis through coordinate regulation of Dicer and miRNAs. *Nature*. 467:986–990. http://dx.doi.org/10.1038/nature09459

Teta, M., Y.S. Choi, T. Okegbe, G. Wong, O.H. Tam, M.M. Chong, J.T. Seykora, A. Nagy, D.R. Littman, T. Andl, and S.E. Millar. 2012. Inducible deletion of epidermal Dicer and Drosha reveals multiple functions for miRNAs in postnatal skin. *Development*. 139:1405–1416. http://dx.doi.org/10.1242/dev.070920

Tsai, S.Y., R. Sennett, A. Rezza, C. Clavel, L. Grisanti, R. Zemla, S. Najam, and M. Rendl. 2014. Wnt/β-catenin signaling in dermal condensates is required for hair follicle formation. *Dev. Biol.* 385:179–188. http://dx.doi.org/10.1016/j.ydbio.2013.11.023

Vidal, V.P., M.C. Chaboissier, S. Lützkendorf, G. Cotsarelis, P. Mill, C.C. Hui, N. Ortonne, J.P. Ortonne, and A. Schedl. 2005. Sox9 is essential for outer root sheath differentiation and the formation of the hair stem cell compartment. *Curr. Biol.* 15:1340–1351. http://dx.doi.org/10.1016/j.cub.2005.06.064

Wang, X., and I.M. El Naqa. 2008. Prediction of both conserved and nonconserved microRNA targets in animals. *Bioinformatics*. 24:325–332. http://dx.doi.org/10.1093/bioinformatics/btm595

Wang, B., J.F. Fallon, and P.A. Beachy. 2000. Hedgehog-regulated processing of Gli3 produces an anterior/posterior repressor gradient in the developing vertebrate limb. *Cell*. 100:423–434. http://dx.doi.org/10.1016/S0092-8674(00)80678-9

Wang, X., J. Chen, F. Li, Y. Lin, X. Zhang, Z. Lv, and J. Jiang. 2012. MiR-214 inhibits cell growth in hepatocellular carcinoma through suppression of β-catenin. *Biochem. Biophys. Res. Commun.* 428:525–531. http://dx.doi.org/10.1016/j.bbrc.2012.10.039

Wang, D., Z. Zhang, E. O'Loughlin, L. Wang, X. Fan, E.C. Lai, and R. Yi. 2013a. MicroRNA-205 controls neonatal expansion of skin stem cells by modulating the PI(3)K pathway. *Nat. Cell Biol.* 15:1153–1163. http://dx.doi.org/10.1038/ncb2827

Wang, X., B. Guo, Q. Li, J. Peng, Z. Yang, A. Wang, D. Li, Z. Hou, K. Lv, G. Kan, et al. 2013b. miR-214 targets ATF4 to inhibit bone formation. *Nat. Med.* 19:93–100. http://dx.doi.org/10.1038/nm.3026

Watanabe, T., T. Sato, T. Amano, Y. Kawamura, N. Kawamura, H. Kawaguchi, N. Yamashita, H. Kurihara, and T. Nakaoka. 2008. Dnm3os, a non-coding RNA, is required for normal growth and skeletal development in mice. *Dev. Dyn.* 237:3738–3748. http://dx.doi.org/10.1002/dvdy.21787

Yamane, K., M. Jinnin, T. Etoh, Y. Kobayashi, N. Shimozono, S. Fukushima, S. Masuguchi, K. Maruo, Y. Inoue, T. Ishihara, et al. 2013. Down-regulation of miR-124/-214 in cutaneous squamous cell carcinoma mediates abnormal cell proliferation via the induction of ERK. *J. Mol. Med.* 91:69–81. http://dx.doi.org/10.1007/s00109-012-0935-7

Yi, R., and E. Fuchs. 2011. MicroRNAs and their roles in mammalian stem cells. *J. Cell Sci.* 124:1775–1783. http://dx.doi.org/10.1242/jcs.069104

Yi, R., D. O'Carroll, H.A. Pasolli, Z. Zhang, F.S. Dietrich, A. Tarakhovsky, and E. Fuchs. 2006. Morphogenesis in skin is governed by discrete sets of differentially expressed microRNAs. *Nat. Genet.* 38:356–362. http://dx.doi.org/10.1038/ng1744

Yi, R., M.N. Poy, M. Stoffel, and E. Fuchs. 2008. A skin microRNA promotes differentiation by repressing 'stemness'. *Nature*. 452:225–229. http://dx.doi.org/10.1038/nature06642

Zhang, Y., P. Tomann, T. Andl, N.M. Gallant, J. Huelsken, B. Jerchow, W. Birchmeier, R. Paus, S. Piccolo, M.L. Mikkola, et al. 2009. Reciprocal requirements for EDA/EDAR/NF-kappaB and Wnt/β-catenin signaling pathways in hair follicle induction. *Dev. Cell*. 17:49–61. http://dx.doi.org/10.1016/j.devcel.2009.05.011

Zhang, L., N. Stokes, L. Polak, and E. Fuchs. 2011. Specific microRNAs are preferentially expressed by skin stem cells to balance self-renewal and early lineage commitment. *Cell Stem Cell*. 8:294–308. http://dx.doi.org/10.1016/j.stem.2011.01.014

Zhou, P., C. Byrne, J. Jacobs, and E. Fuchs. 1995. Lymphoid enhancer factor 1 directs hair follicle patterning and epithelial cell fate. *Genes Dev.* 9:700–713. http://dx.doi.org/10.1101/gad.9.6.700

Zhou, J.X., L.W. Jia, W.M. Liu, C.L. Miao, S. Liu, Y.J. Cao, and E.K. Duan. 2006. Role of sonic hedgehog in maintaining a pool of proliferating stem cells in the human fetal epidermis. *Hum. Reprod.* 21:1698–1704. http://dx.doi.org/10.1093/humrep/del086

Zhu, H., and G.C. Fan. 2011. Extracellular/circulating microRNAs and their potential role in cardiovascular disease. *Am. J. Cardiovasc. Dis.* 1:138–149.

Ahmed et al., http://www.jcb.org/cgi/content/full/jcb.201404001/DC1

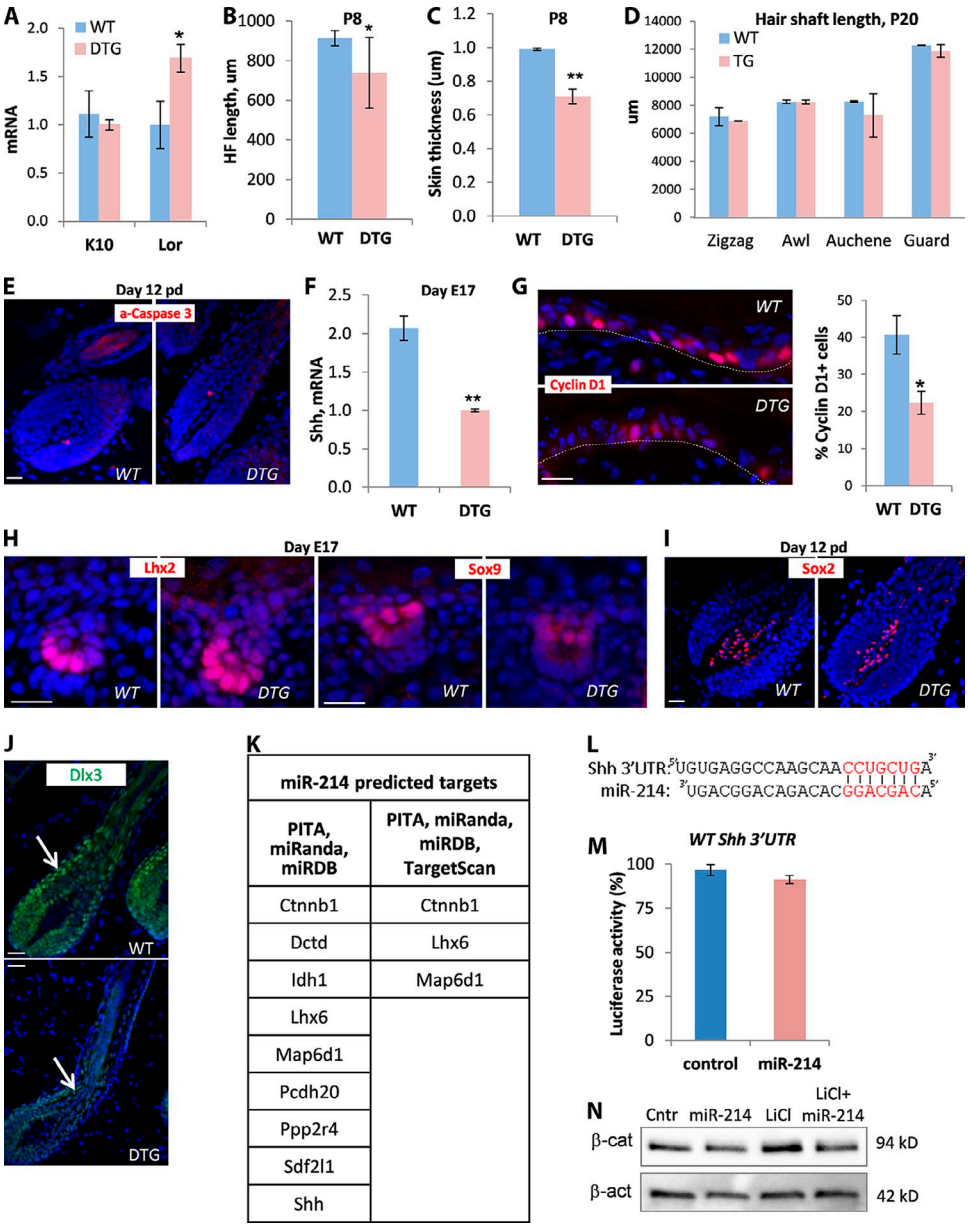

miR-214 predicted targets	
PITA, miRanda, miRDB	PITA, miRanda, miRDB, TargetScan
Ctnnb1	Ctnnb1
Dctd	Lhx6
Idh1	Map6d1
Lhx6	
Map6d1	
Pcdh20	
Ppp2r4	
Sdf2l1	
Shh	

Figure S1. **Characterization of the skin phenotype in K14-rtTA/miR-214-TRE mice and validation of miR-214 predicted targets in the keratinocytes.** (A) Real-time RT-PCR. There was a significant increase in *Lor* but not *K10* expression in the neonatal back skin epithelium of the DTG versus WT mice. $n = 3$ mice/genotype. (B–D) Induction of miR-214 transgene by Dox after E10. (B) A comparison of HF length in DTG and WT mice at P8. Significantly shorter HFs were seen in the DTG versus WT mice. $n = 3$ mice/genotype. (C) Significantly reduced total skin in DTG versus WT mice at P8. $n = 3$ mice/genotype. (D) Length of different hair shaft types (in micrometers) in DTG and WT mice plucked at P20, the time of the first telogen phase. No differences were found. $n = 4$ mice/genotype. (E) Immunofluorescence detection of active caspase-3 (red) with nuclear staining (DAPI, blue) in anagen HFs. No difference in a-caspase-3 between DTG and WT HFs was detected. (F) Real-time RT-PCR. A significant decrease in Shh transcript levels in skin of DTG versus WT mice was seen at E17 after miR-214 induction by Dox after E10. $n = 3$ mice/genotype. (G) Immunofluorescence analysis of Cyclin d1 expression in the epidermis. There was a significant decrease in the number of Cyclin D1+ cells in the DTG epidermis versus WT mice. (H) Immunofluorescence analysis of Lhx2 and Sox9 (red) with nuclear staining (DAPI, blue) in HF placodes of DTG and WT mice at E17. No difference in Lhx2 and Sox9 expression was detected. (I) Immunodetection of Sox2 (red) with nuclear staining (DAPI, blue) in the dermal papilla of anagen DTG and WT HFs after overexpression of miR-214 in telogen skin. No difference in Sox2 staining was observed. (J) Immunodetection of Dlx3 (green) with nuclear staining (DAPI, blue) in the anagen DTG and WT HFs after overexpression of miR-214 in telogen skin. There was a decrease in Dlx3 expression in the DTG HFs. (K) Bioinformatic analysis of predicted miR-214 target genes that are differentially expressed in DTG epithelium after 48 h of Dox activation. (L) Predicted interactions between miR-214 and *Shh*. The alignment of the mouse miR-214 sequence in the 3′ UTR of *Shh* mRNA is shown. (M) There were no changes in luciferase activity in HaCaT cells due to cotransfection with miR-214 mimic and the *Shh* 3′ UTR constructs encompassing the putative miR-214 target site. The data shown are from a single representative experiment out of three repeats. For the experiment shown, $n = 2$. (N) Western blot. There were reduced β-catenin levels in primary epidermal keratinocytes transfected with miR-214 compared with the control, as well as reduced β-catenin levels in the keratinocytes cotreated with LiCl and miR-214 mimic compared to the cells treated with LiCl alone. Data are presented as mean ± SD (error bars); *, $P < 0.05$; **$P < 0.001$; Student's *t* test. Bars: (E, G, and H) 25 µm; (I and J) 50 µm.

Table S1 - Genes that show 2-fold down-regulation in the keratinocytes of K14rtTA/TRE-miR-214 mice versus WT mice

Accession Number	Gene name	Symbol	Fold change
	Adhesion/Extracellular matrix		
NM_011302	retinoschisis (X-linked, juvenile) 1	Rs1	5.25
NM_178596	gap junction protein, delta 3	Gjd3	4.73
NM_010708	lectin, galactose binding, soluble 9, transcript variant 1	Lgals9	4.27
NM_010327	glycoprotein Ib, beta polypeptide, transcript variant 2	Gp1bb	3.93
NM_010577	integrin alpha 5	Itga5	3.73
NM_181277	collagen, type XIV, alpha 1	Col14a1	3.15
NM_001081249	versican, transcript variant 1	Vcan	2.90
NM_020486	basal cell adhesion molecule	Bcam	2.77
NM_021334	integrin alpha X	Itgax	2.72
NM_146007	collagen, type VI, alpha 2	Col6a2	2.68
NM_010386	histocompatibility 2, class II, locus DMa	H2-DMa	2.64
NM_013565	integrin alpha 3	Itga3	2.58
NM_011150	lectin, galactoside-binding, soluble, 3 binding protein	Lgals3bp	2.56
NM_023051	calsyntenin 1	Clstn1	2.50
NM_007992	fibulin 2, transcript variant 1	Fbln2	2.44
NM_178685	protocadherin 20	Pcdh20	2.43
NM_010181	fibrillin 2	Fbn2	2.35
NM_001082960	integrin alpha M, transcript variant 1	Itgam	2.32
NM_013552	hyaluronan mediated motility receptor (RHAMM)	Hmmr	2.18
NM_010180	fibulin 1	Fbln1	2.01
	Cell Cycle/Apoptosis		
NM_018754	stratifin	Sfn	3.34
NM_177372	DNA replication helicase 2 homolog	Dna2	3.28
NM_007631	cyclin D1*	Ccnd1	3.76
NM_008564	minichromosome maintenance deficient 2 mitotin	Mcm2	2.91
NM_028131	centromere protein N	Cenpn	2.88
NM_010059	DMC1 dosage suppressor of mck1 homolog, meiosis-specific homologous recombination	Dmc1	2.78
NM_028222	cyclin-dependent kinase inhibitor 3	Cdkn3	2.72
NM_008014	protein phosphatase 1G (formerly 2C), magnesium-dependent, gamma isoform	Ppm1g	2.65
NM_027263	apoptosis-inducing, TAF9-like domain 1	Apitd1	2.60
NM_001012273	baculoviral IAP repeat-containing 5, transcript variant 3	Birc5	2.51
NM_198654	NSL1, MIND kinetochore complex component, homolog	Nsl1	2.50
NM_011015	origin recognition complex, subunit 1, transcript variant A	Orc1	2.43
NM_027954	synaptonemal complex central element protein 2, transcript variant 2	Syce2	2.42
NM_019499	MAD2 mitotic arrest deficient-like 1	Mad2l1	2.33
NM_022654	leucine-rich and death domain containing	Lrdd	2.33
NM_008566	minichromosome maintenance deficient 5, cell division cycle 46	Mcm5	2.29
NM_026560	cell division cycle associated 8	Cdca8	2.28
NM_009828	cyclin A2	Ccna2	2.27
NM_198605	spindle and kinetochore associated complex subunit 3	Ska3	2.26
NM_001042421	kinetochore associated 1	Kntc1	2.25
NM_146235	excision repair cross-complementing rodent repair deficiency complementation group 6 like	Ercc6l	2.23
NM_001159930	centromere protein L , transcript variant 1	Cenpl	2.19

NM_007900	ect2 oncogene, transcript variant 1	Ect2	2.18
NM_007659	cyclin-dependent kinase 1*	Cdk1	2.64
NM_013929	SIVA1, apoptosis-inducing factor, transcript variant 1	Siva1	2.15
NM_011049	cyclin-dependent kinase 16	Cdk16	2.15
NM_172301	cyclin B1*	Ccnb1	2.36
NM_001014976	extra spindle poles-like 1	Espl1	2.15
NM_025995	F-box protein 5	Fbxo5	2.14
NM_011799	cell division cycle 6, transcript variant 1	Cdc6	2.07
NM_027290	minichromosome maintenance deficient 10	Mcm10	2.05
NM_025866	cell division cycle associated 7	Cdca7	2.05
NM_016681	checkpoint kinase 2	Chek2	2.04
NM_175554	claspin	Clspn	2.03
NM_008567	minichromosome maintenance deficient 6	Mcm6	2.03
NM_007630	cyclin B2	Ccnb2	2.02
NM_010790	maternal embryonic leucine zipper kinase	Melk	2.01
NM_009829	Cyclin D2*	Ccnd2	1.49
	Chromatin remodelling		
NM_178215	histone cluster 2, H3b	Hist2h3b	4.50
NM_007928	MAP/microtubule affinity-regulating kinase 2, transcript variant 1	Mark2	4.42
NM_175654	histone cluster 1, H4d	Hist1h4d	4.24
NM_178211	histone cluster 1, H4k	Hist1h4k	4.04
NM_178210	histone cluster 1, H4j	Hist1h4j	4.00
NM_178208	histone cluster 1, H4c	Hist1h4c	3.91
NM_175652	histone cluster 4, H4	Hist4h4	3.84
NM_001080819	AT rich interactive domain 1A	Arid1a	3.77
NM_030609	histone cluster 1, H1a	Hist1h1a	3.51
NM_026785	ubiquitin-conjugating enzyme E2C	Ube2c	3.39
NM_020034	histone cluster 1, H1b	Hist1h1b	3.39
NM_015787	histone cluster 1, H1e	Hist1h1e	3.28
NM_033596	histone cluster 2, H4	Hist2h4	3.17
NM_016957	high mobility group nucleosomal binding domain 2	Hmgn2	3.13
NM_001195421	histone cluster 1, H4m	Hist1h4m	3.01
NM_013548	histone cluster 1, H3f	Hist1h3f	2.90
NM_145073	histone cluster 1, H3g	Hist1h3g	2.84
NM_010931	ubiquitin-like, containing PHD and RING finger domains, 1, transcript variant 1	Uhrf1	2.72
NM_175653	histone cluster 1, H3c	Hist1h3c	2.66
NM_178856	GINS complex subunit 2 (Psf2 homolog)	Gins2	2.66
NM_012012	exonuclease 1	Exo1	2.62
NM_001204973	bromodomain containing 2 , transcript variant 2	Brd2	2.56
NM_021790	centromere protein K, transcript variant 1	Cenpk	2.55
NM_175663	histone cluster 1, H2ba	Hist1h2ba	2.54
NM_011234	RAD51 homolog	Rad51	2.53
NM_020022	replication factor C (activator 1) 2	Rfc2	2.51
NM_178183	histone cluster 1, H2ak	Hist1h2ak	2.46
NM_008210	H3 histone, family 3A	H3f3a	2.40
NM_011623	topoisomerase (DNA) II alpha	Top2a	2.38
NM_001163775	TAO kinase 2, transcript variant 2	Taok2	2.37
NM_181586	sirtuin 6 (silent mating type information regulation 2, homolog) 6 , transcript variant 1	Sirt6	2.35
NM_198160	SWI/SNF related, matrix associated, actin dependent regulator of chromatin, subfamily c, member 2, transcript variant 3	Smarcc2	2.35
NM_024184	ASF1 anti-silencing function 1 homolog B	Asf1b	2.33
NM_028039	establishment of cohesion 1 homolog 2	Esco2	2.33

NM_145946	Fanconi anemia, complementation group I	Fanci	2.31
NM_178200	histone cluster 1, H2bm	Hist1h2bm	2.24
NM_009030	retinoblastoma binding protein 4	Rbbp4	2.23
NM_008894	polymerase (DNA directed), delta 2, regulatory subunit	Pold2	2.20
NM_008228	histone deacetylase 1	Hdac1	2.20
NM_013883	sex comb on midleg homolog 1, transcript variant 1	Scmh1	2.18
NM_020004	K(lysine) acetyltransferase 2A, transcript variant 1	Kat2a	2.16
NM_011121	polo-like kinase 1	Plk1	2.16
NM_146208	nei like 3	Neil3	2.16
NM_134083	regulator of chromosome condensation and BTB (POZ) domain containing protein 2 , transcript variant 2	Rcbtb2	2.13
NM_008892	polymerase (DNA directed), alpha 1	Pola1	2.11
NM_029797	meiotic nuclear divisions 1 homolog	Mnd1	2.10
NM_013550	histone cluster 1, H3a	Hist1h3a	2.10
NM_010722	lamin B2	Lmnb2	2.09
NM_026632	replication protein A3	Rpa3	2.08
NM_153141	coactivator-associated arginine methyltransferase 1, transcript variant 2	Carm1	2.07
NM_023294	NDC80 homolog, kinetochore complex component	Ndc80	2.05
NM_172453	PIF1 5'-to-3' DNA helicase homolog	Pif1	2.05
NM_009013	RAD51 associated protein 1	Rad51ap1	2.03
NM_008017	structural maintenance of chromosomes 2	Smc2	1.98
	Cytoskeleton		
NM_011072	profilin 1	Pfn1	3.96
NM_010669	keratin 6B	Krt6b	3.94
NM_009451	tubulin, beta 4A class IVA	Tubb4a	3.93
NM_001163637	janus kinase and microtubule interacting protein 2	Jakmip2	3.39
NM_009449	tubulin, alpha 3B	Tuba3b	3.34
NM_008445	kinesin family member 3C	Kif3c	2.92
NM_130857	keratin associated protein 19-3	Krtap19-3	2.92
NM_183296	keratin associated protein 16-3	Krtap16-3	2.92
NM_016879	keratin 85	Krt85	2.90
NM_011526	transgelin	Tagln	2.88
NM_001163615	keratin associated protein 20-2	Krtap20-2	2.81
NM_130870	keratin associated protein 16-1	Krtap16-1	2.81
NM_175272	neuron navigator 2, transcript variant 1	Nav2	2.76
NM_001113406	keratin associated protein 11-1	Krtap11-1	2.70
NM_019445	formin 2	Fmn2	2.68
NM_148934	tubulin polyglutamylase complex subunit 1	Tpgs1	2.64
NM_010672	keratin associated protein 6-1	Krtap6-1	2.64
NM_028621	keratin associated protein 21-1	Krtap21-1	2.62
NM_019641	stathmin 1	Stmn1	2.60
NM_027771	keratin associated protein 7-1	Krtap7-1	2.58
NM_130873	keratin associated protein 19-4	Krtap19-4	2.57
NM_010626	kinesin family member 7	Kif7	2.50
NM_009931	collagen, type IV, alpha 1	Col4a1	2.42
NM_001024716	TRIO and F-actin binding protein, transcript variant 1	Triobp	2.41
NM_010662	keratin 13	Krt13	2.38
NM_026552	actin related protein 2/3 complex, subunit 4, transcript variant 1	Arpc4	2.37
NM_013928	schwannomin interacting protein 1, transcript variant 4	Schip1	2.34
NM_172946	keratin 222	Krt222	2.32
NM_011654	tubulin, alpha 1B	Tuba1b	2.29
NM_001166157	keratin 81	Krt81	2.29
NM_017470	dynein, axonemal, light chain 4	Dnalc4	2.29
NM_027800	keratin associated protein 2-4	Krtap2-4	2.28

NM_010676	keratin associated protein 19-5	Krtap19-5	2.27
NM_212483	keratin 42	Krt42	2.26
NM_198599	MAP6 domain containing 1	Map6d1	2.25
NM_197945	ProSAPiP1 protein	Prosapip1	2.24
NM_145575	caldesmon 1	Cald1	2.20
NM_017464	neural precursor cell expressed, developmentally down-regulated gene 9, transcript variant 2	Nedd9	2.19
NM_019670	diaphanous homolog 3	Diap3	2.18
NM_080728	myosin, heavy polypeptide 7, cardiac muscle, beta	Myh7	2.16
NM_134471	kinesin family member 2C	Kif2c	2.14
NM_009768	basigin, transcript variant 1	Bsg	2.14
NM_028390	anillin, actin binding protein	Anln	2.13
NM_001191018	keratin associated protein 22-2	Krtap22-2	2.11
NM_133851	nucleolar and spindle associated protein 1, transcript variant 1	Nusap1	2.05
NM_178926	vimentin-type intermediate filament associated coiled-coil protein, transcript variant 1	Vmac	2.01
NM_010675	keratin associated protein 8-1	Krtap8-1	1.98
	Metabolism		
NM_016956	hemoglobin, beta adult minor chain	Hbb-b2	14.97
NM_001080943	zinc finger, DHHC-type containing 22	Zdhhc22	13.25
NM_009653	aminolevulinic acid synthase 2, erythroid, transcript variant 1	Alas2	8.62
NM_008220	hemoglobin, beta adult major chain	Hbb-b1	8.30
NM_008218	hemoglobin alpha, adult chain 1	Hba-a1	6.67
NM_139142	solute carrier family 6 (neurotransmitter transporter), member 20A	Slc6a20a	5.09
NM_018763	carbohydrate sulfotransferase 2	Chst2	4.81
NM_001082975	short chain dehydrogenase/reductase family 39U, member 1	Sdr39u1	4.59
NM_009464	uncoupling protein 3 (mitochondrial, proton carrier)	Ucp3	4.46
NM_001033270	solute carrier family 4, sodium bicarbonate cotransporter, member 7	Slc4a7	4.43
NM_011671	uncoupling protein 2 (mitochondrial, proton carrier)	Ucp2	4.41
NM_027093	NADH dehydrogenase (ubiquinone) complex I, assembly factor 5	Ndufaf5	4.39
NM_001104531	cytochrome P450, family 2, subfamily d, polypeptide 11	Cyp2d11	4.17
NM_019698	aldehyde dehydrogenase 18 family, member A1, nuclear gene encoding mitochondrial protein, transcript variant 1	Aldh18a1	3.95
NM_010066	DNA methyltransferase (cytosine-5) 1 , transcript variant 2	Dnmt1	3.94
NM_001083955	hemoglobin alpha, adult chain 2	Hba-a2	3.58
NM_010596	potassium voltage-gated channel, shaker-related subfamily, member 7	Kcna7	3.47
NM_007817	cytochrome P450, family 2, subfamily f, polypeptide 2	Cyp2f2	3.46
NM_010359	glutathione S-transferase, mu 3	Gstm3	3.37
NM_175403	malectin	Mlec	3.34
NM_134118	trans-2,3-enoyl-CoA reductase , transcript variant 1	Tecr	3.31
NM_007807	cytochrome b-245, beta polypeptide	Cybb	3.31
NM_177186	solute carrier family 35, member E2	Slc35e2	3.26
NM_013784	phosphatidylinositol glycan anchor biosynthesis, class N	Pign	3.22
NM_009034	retinol binding protein 2, cellular	Rbp2	3.15
NM_011371	ST6 (alpha-N-acetyl-neuraminyl-2,3-beta-galactosyl-1,3)-N-acetylgalactosaminide alpha-2,6-sialyltransferase 1	St6galnac 1	3.15
NM_016966	3-phosphoglycerate dehydrogenase	Phgdh	3.09
NM_009181	ST8 alpha-N-acetyl-neuraminide alpha-2,8-sialyltransferase 2	St8sia2	3.03
NM_026969	Sec31 homolog A	Sec31a	2.98
NM_001243052	branched chain aminotransferase 2, mitochondrial, transcript variant 2	Bcat2	2.94
NM_027790	dehydrogenase/reductase member 2	Dhrs2	2.91

NM_133189	calcium channel, voltage-dependent, gamma subunit 7	Cacng7	2.85
NM_144845	UDP glycosyltransferases 3 family, polypeptide A2	Ugt3a2	2.84
NM_008525	aminolevulinate, delta-, dehydratase	Alad	2.84
NM_178788	dCMP deaminase (Dctd), transcript variant 1	Dctd	2.81
NM_011961	procollagen lysine, 2-oxoglutarate 5-dioxygenase 2, transcript variant 2	Plod2	2.79
NM_001033175	ceroid-lipofuscinosis, neuronal 6	Cln6	2.78
NM_213733	aminopeptidase-like 1	Npepl1	2.76
NM_030601	chloride channel calcium activated 2	Clca2	2.72
NM_207161	2'-deoxynucleoside 5'-phosphate N-hydrolase 1	Dnph1	2.69
NM_009437	thiosulfate sulfurtransferase, mitochondrial	Tst	2.68
NM_009723	ATPase, Ca++ transporting, plasma membrane 2, transcript variant 1	Atp2b2	2.67
NM_019435	NADH dehydrogenase (ubiquinone) 1 beta subcomplex, 11	Ndufb11	2.65
NM_009374	transglutaminase 3	Tgm3	2.62
NM_146198	solute carrier family 5 (sodium/glucose cotransporter), member 11	Slc5a11	2.59
NM_025412	pyrroline-5-carboxylate reductase-like	Pycrl	2.55
NM_033617	ATPase, H+ transporting, lysosomal V0 subunit B	Atp6v0b	2.53
NM_145603	carboxylesterase 2C	Ces2c	2.51
NM_008631	metallothionein 4	Mt4	2.46
NM_009272	spermidine synthase	Srm	2.41
NM_001044308	calcium channel, voltage-dependent, alpha 1I subunit	Cacna1i	2.40
NM_009662	arachidonate 5-lipoxygenase	Alox5	2.38
NM_009104	ribonucleotide reductase M2	Rrm2	2.38
NM_001163359	fidgetin-like 1, transcript variant 1	Fignl1	2.34
NM_009804	catalase	Cat	2.32
NM_010497	isocitrate dehydrogenase 1 (NADP+), soluble, transcript variant 2	Idh1	2.32
NM_008826	phosphofructokinase, liver, B-type	Pfkl	2.31
NM_009127	stearoyl-Coenzyme A desaturase 1	Scd1	2.28
NM_172371	solute carrier family 16 (monocarboxylic acid transporters), member 13	Slc16a13	2.28
NM_054094	acyl-CoA synthetase medium-chain family member 1	Acsm1	2.27
NM_025408	alkaline ceramidase 3	Acer3	2.26
NM_001271544	solute carrier family 4, sodium bicarbonate cotransporter, member 9, transcript variant 1	Slc4a9	2.26
NM_026764	glutathione S-transferase, mu 4 , transcript variant 1	Gstm4	2.25
NM_010274	glycerol phosphate dehydrogenase 2, mitochondrial (Gpd2), transcript variant 2	Gpd2	2.24
NM_010358	glutathione S-transferase, mu 1	Gstm1	2.22
NM_008278	hydroxyprostaglandin dehydrogenase 15	Hpgd	2.22
NM_020581	angiopoietin-like 4	Angptl4	2.21
NM_172117	ectonucleoside triphosphate diphosphohydrolase 6	Entpd6	2.15
NM_026678	biliverdin reductase A	Blvra	2.15
NM_080440	solute carrier family 8 (sodium/calcium exchanger), member 3, transcript variant 2	Slc8a3	2.15
NM_030262	protein O-fucosyltransferase 2	Pofut2	2.13
NM_172773	solute carrier family 17 (anion/sugar transporter), member 5	Slc17a5	2.12
NM_178696	solute carrier family 25, member 44, transcript variant 1	Slc25a44	2.11
NM_001040699	myotubularin related protein 7	Mtmr7	2.11
NM_177382	cytochrome P450, family 2, subfamily r, polypeptide 1	Cyp2r1	2.11
NM_007838	dolichyl-di-phosphooligosaccharide-protein glycotransferase	Ddost	2.10
NM_172609	translocase of outer mitochondrial membrane 22 homolog	Tomm22	2.08
NM_007621	carbonyl reductase 2	Cbr2	2.08
NM_013541	glutathione S-transferase, pi 1	Gstp1	2.07
NM_011962	procollagen-lysine, 2-oxoglutarate 5-dioxygenase 3	Plod3	2.07
NM_016666	aryl-hydrocarbon receptor-interacting protein	Aip	2.06

NM_007646	CD38 antigen	Cd38	2.05
NM_028638	glutamate decarboxylase-like 1	Gadl1	2.05
NM_007379	ATP-binding cassette, sub-family A, member 2	Abca2	2.04
NM_178086	fatty acid 2-hydroxylase	Fa2h	2.02
NM_019501	prenyl (solanesyl) diphosphate synthase, subunit 1	Pdss1	2.01
NM_008212	hydroxyacyl-Coenzyme A dehydrogenase	Hadh	2.01
NM_026947	enoyl-Coenzyme A delta isomerase 3	Eci3	2.00
NM_138665	sarcosine dehydrogenase	Sardh	2.00
NM_011977	solute carrier family 27 (fatty acid transporter), member 1	Slc27a1	2.00
	Others		
NM_001201391	hemoglobin subunit beta-1-like	Beta-s	29.45
NM_023900	pleckstrin homology domain containing, family J member 1	Plekhj1	5.60
NM_011174	proline rich protein HaeIII subfamily 1	Prh1	5.44
NM_021384	radical S-adenosyl methionine domain containing 2	Rsad2	4.67
NM_138602	PRA1 domain family 2	Praf2	4.14
NM_001042451	synuclein, alpha, transcript variant 1	Snca	4.05
NM_013877	calcium binding protein 5	Cabp5	3.98
NM_201518	fibronectin leucine rich transmembrane protein 2	Flrt2	3.83
NM_177994	R3H domain containing 4	R3hdm4	3.80
NM_001205102	leucine-rich repeat, immunoglobulin-like and transmembrane domains 3	Lrit3	3.76
NM_018803	synaptotagmin X	Syt10	3.74
NM_029000	GTPase, very large interferon inducible 1, transcript variant 1	Gvin1	3.73
NM_207105	histocompatibility 2, class II antigen A, beta 1	H2-Ab1	3.62
NM_080846	HIG1 domain family, member 1B	Higd1b	3.60
NM_001033478	family with sequence similarity 47, member E, transcript variant 1	Fam47e	3.53
NM_001081418	glioma tumor suppressor candidate region gene 1	Gltscr1	3.53
NM_145981	phytanoyl-CoA hydroxylase interacting protein	Phyhip	3.26
NM_021898	testis specific gene A8	Tsga8	3.11
NM_134122	nurim (nuclear envelope membrane protein)	Nrm	3.06
NM_001163614	achaete-scute complex homolog 4	Ascl4	3.04
NM_020583	interferon-stimulated protein, transcript variant 1	Isg20	2.98
NM_173862	family with sequence similarity 83, member A	Fam83a	2.94
NM_175427	family with sequence similarity 163, member B	Fam163b	2.91
NM_001082545	stefin A2	Stfa2	2.77
NM_183187	family with sequence similarity 107, member A	Fam107a	2.76
NM_001142642	fibrosin-like 1, transcript variant 1	Fbrsl1	2.76
NM_001199631	FK506 binding protein 8, transcript variant 3	Fkbp8	2.75
NM_172756	ankyrin repeat and LEM domain containing 1	Ankle1	2.75
NM_133859	olfactomedin-like 3	Olfml3	2.72
NM_001025576	coiled-coil domain containing 141	Ccdc141	2.71
NM_025620	RAB15 effector protein	Rep15	2.70
NM_010807	MARCKS-like 1	Marcksl1	2.63
NM_001081406	leucine rich repeat protein 1	Lrr1	2.51
NM_018884	PDZ domain containing RING finger 3	Pdzrn3	2.50
NM_183170	MPV17 mitochondrial membrane protein-like 2	Mpv17l2	2.44
NM_172116	Parkinson disease 7 domain containing 1	Pddc1	2.42
NM_133719	meteorin, glial cell differentiation regulator	Metrn	2.41
NM_030694	interferon induced transmembrane protein 2	Ifitm2	2.38
NM_145361	BTB (POZ) domain containing 2	Btbd2	2.37
NM_009185	Scl/Tal1 interrupting locus	Stil	2.37
NM_016737	stress-induced phosphoprotein 1	Stip1	2.35
NM_001163721	small integral membrane protein 1 , transcript variant 1	Smim1	2.35
NM_032543	ring finger protein 123	Rnf123	2.35

NM_018771	GIPC PDZ domain containing family, member 1	Gipc1	2.34
NM_025378	interferon induced transmembrane protein 3	Ifitm3	2.32
NM_029377	lin-37 homolog	Lin37	2.30
NM_001199337	apolipoprotein O, transcript variant 2	Apoo	2.29
NM_133831	glioma tumor suppressor candidate region gene 2	Gltscr2	2.27
NM_010219	FK506 binding protein 4	Fkbp4	2.27
NM_138682	leucine rich repeat containing 4	Lrrc4	2.26
NM_026457	spermatid associated, transcript variant 2	Spert	2.25
NM_013515	stomatin	Stom	2.24
NM_053113	eosinophil-associated, ribonuclease A family, member 11	Ear11	2.21
NM_177028	O-acyltransferase like	Oacyl	2.18
NM_011627	trophoblast glycoprotein, transcript variant 1	Tpbg	2.17
NM_146244	ribosomal protein S6 kinase-like 1	Rps6kl1	2.16
NM_133187	family with sequence similarity 198, member B	Fam198b	2.14
NM_001025610	membrane-spanning 4-domains, subfamily A, member 7, transcript variant 2	Ms4a7	2.13
NM_172488	laccase (multicopper oxidoreductase) domain containing 1	Lacc1	2.13
NM_175118	dual specificity phosphatase 28	Dusp28	2.12
NM_080595	EMI domain containing 1	Emid1	2.11
NM_144556	leucine-rich repeat LGI family, member 4	Lgi4	2.11
NM_019661	YKT6 homolog	Ykt6	2.10
NM_021294	diazepam binding inhibitor-like 5	Dbil5	2.09
NM_016663	synaptotagmin III, transcript variant 1	Syt3	2.08
NM_178919	lipase maturation factor 2	Lmf2	2.08
NM_011073	perforin 1 (pore forming protein)	Prf1	2.07
NM_145390	transportin 2 (importin 3, karyopherin beta 2b), transcript variant 1	Tnpo2	2.07
NM_009538	pleiomorphic adenoma gene-like 1	Plagl1	2.05
NM_026938	transmembrane protein 160	Tmem160	2.05
NM_010129	epithelial membrane protein 3, transcript variant 1	Emp3	2.04
NM_010590	ajuba LIM protein	Ajuba	2.03
NM_146156	PDLIM1 interacting kinase 1 like, transcript variant 1	Pdik1l	2.03
NM_001195088	transmembrane channel-like gene family 8, transcript variant A	Tmc8	2.03
NM_183194	gasdermin C3	Gsdmc3	2.01
NM_027984	epsin 3	Epn3	2.00
	Protein folding		
NM_024172	HSPA (heat shock 70kDa) binding protein, cytoplasmic cochaperone 1	Hspbp1	2.47
NM_175199	heat shock protein 12A	Hspa12a	2.03
	Proteolysis		
NM_023635	RAB27A, member RAS oncogene family	Rab27a	5.79
NM_009126	serine (or cysteine) peptidase inhibitor, clade B (ovalbumin), member 3A	Serpinb3a	5.55
NM_201363	serine (or cysteine) peptidase inhibitor, clade B, member 3C	Serpinb3c	4.67
NM_001169153	CD300 antigen like family member F, transcript variant 1	Cd300lf	4.17
NM_145578	ubiquitin-conjugating enzyme E2M, transcript variant 1	Ube2m	3.50
NM_025312	sclerostin domain containing 1*	Sostdc1	4.30
NM_025288	stefin A3	Stfa3	2.99
NM_173869	stefin A2 like 1	Stfa2l1	2.98
NM_001205070	Josephin domain containing 2, transcript variant 1	Josd2	2.94
NM_175188	membrane-associated ring finger (C3HC4) 1, transcript variant 3	March1	2.93
NM_010767	mannan-binding lectin serine peptidase 2, transcript variant 2	Masp2	2.91
NM_011187	proteasome (prosome, macropain) subunit, beta type 7	Psmb7	2.80

NM_145420	ubiquitin-conjugating enzyme E2D 1	Ube2d1	2.74
NM_008604	membrane metallo endopeptidase	Mme	2.65
NM_178738	protease, serine, 35	Prss35	2.60
NM_007649	CD48 antigen	Cd48	2.58
NM_019461	ubiquitin specific peptidase 27, X chromosome	Usp27x	2.53
NM_198680	serine (or cysteine) peptidase inhibitor, clade B (ovalbumin), member 3B	Serpinb3b	2.50
NM_010612	kinase insert domain protein receptor	Kdr	2.49
NM_010418	hect (homologous to the E6-AP (UBE3A) carboxyl terminus) domain and RCC1 (CHC1)-like domain (RLD) 2	Herc2	2.40
NM_015783	ISG15 ubiquitin-like modifier	Isg15	2.35
NM_133354	SMT3 suppressor of mif two 3 homolog 2	Sumo2	2.26
NM_011595	tissue inhibitor of metalloproteinase 3	Timp3	2.21
NM_001001650	protease, serine, 48	Prss48	2.20
NM_001082543	stefin A1	Stfa1	2.20
NM_023386	receptor transporter protein	Rtp4	2.15
NM_198028	serine (or cysteine) peptidase inhibitor, clade B (ovalbumin), member 10, transcript variant 1	Serpinb10	2.09
NM_008607	matrix metallopeptidase 13	Mmp13	2.09
NM_173754	ubiquitin specific peptidase 43	Usp43	2.04
NM_173052	serine (or cysteine) peptidase inhibitor, clade B, member 1b	Serpinb1b	2.01
	RNA processing		
NM_013932	DEAD (Asp-Glu-Ala-Asp) box polypeptide 25	Ddx25	12.54
NM_012011	eukaryotic translation initiation factor 2, subunit 3, structural gene Y-linked	Eif2s3y	6.25
NM_012008	DEAD (Asp-Glu-Ala-Asp) box polypeptide 3, Y-linked	Ddx3y	5.02
NM_153416	achalasia, adrenocortical insufficiency, alacrimia	Aaas	3.31
NM_011358	serine/arginine-rich splicing factor 2	Srsf2	2.99
NM_025500	mitochondrial ribosomal protein L37	Mrpl37	2.94
NM_018799	eukaryotic translation initiation factor 3, subunit I	Eif3i	2.70
NM_001008422	SR-related CTD-associated factor 1	Scaf1	2.54
NM_011431	elongation factor Tu GTP binding domain containing 2, transcript variant 1	Eftud2	2.42
NM_001166589	eukaryotic translation initiation factor 5A, transcript variant 1	Eif5a	2.41
NM_175001	mitochondrial ribosomal protein L22	Mrpl22	2.35
NM_026080	mitochondrial ribosomal protein S24	Mrps24	2.32
NM_023133	ribosomal protein S19	Rps19	2.26
NM_016805	heterogeneous nuclear ribonucleoprotein U	Hnrnpu	2.24
NM_175235	CUGBP, Elav-like family member 6	Celf6	2.22
NM_177367	gem (nuclear organelle) associated protein 4	Gemin4	2.20
NM_173757	mitochondrial ribosomal protein S27	Mrps27	2.19
NM_019484	Aly/REF export factor 2	Alyref2	2.15
NM_148917	poly(A) binding protein, cytoplasmic 4, transcript variant 2	Pabpc4	2.14
NM_009070	ribonucleic acid binding protein S1, transcript variant 1	Rnps1	2.12
NM_207523	ribosomal protein L23A	Rpl23a	2.12
NM_021288	thymidylate synthase, transcript variant 1	Tyms	2.09
NM_022313	Era (G-protein)-like 1	Eral1	2.08
NM_013507	eukaryotic translation initiation factor 4, gamma 2, transcript variant 1	Eif4g2	2.01
	Signalling		
NM_010100	ectodysplasin-A receptor*	Edar	58.69
NM_009170	sonic hedgehog*	Shh	45.41
NM_176996	smoothened homolog (Drosophila) (Smo)	Smo	36.25
NM_008958	patched homolog 2	Ptch2	25.72
NM_133249	peroxisome proliferative activated receptor, gamma,	Ppargc1b	16.21

	coactivator 1 beta		
NM_009987	chemokine (C-X3-C) receptor 1	Cx3cr1	9.75
ENSMUST00000029611	lymphoid enhancer binding factor 1*	Lef1	9.68
NM_001033960	RAB GTPase activating protein 1, transcript variant 2	Rabgap1	8.53
NM_007416	adrenergic receptor, alpha 1b	Adra1b	6.07
NM_001042605	CD74 antigen, transcript variant 1	Cd74	5.86
NM_199022	SHC (Src homology 2 domain containing) family, member 4	Shc4	4.08
NM_026864	RAS-like, family 11, member A	Rasl11a	3.99
NM_001272024	sema domain, transmembrane domain (TM), and cytoplasmic domain, (semaphorin) 6C , transcript variant 1	Sema6c	3.85
NM_009835	chemokine (C-C motif) receptor 6, transcript variant 1	Ccr6	3.73
NM_146862	olfactory receptor 763	Olfr763	3.59
NM_001081105	ras homolog gene family, member H	Rhoh	3.57
NM_022324	stromal cell-derived factor 2-like 1	Sdf2l1	3.57
NM_008973	pleiotrophin	Ptn	3.52
NM_011562	teratocarcinoma-derived growth factor 1	Tdgf1	3.47
NM_027242	protein phosphatase 1, regulatory subunit 35	Ppp1r35	3.44
NM_013834	secreted frizzled-related protein 1	Sfrp1	3.36
NM_146457	olfactory receptor 282	Olfr282	3.04
NM_011428	synaptosomal-associated protein 25	Snap25	2.85
NM_028808	purinergic receptor P2Y, G-protein coupled 13	P2ry13	2.84
NM_021885	tubby candidate gene	Tub	2.75
NM_007889	dishevelled 3, dsh homolog	Dvl3	2.71
NM_010275	glial cell line derived neurotrophic factor	Gdnf	2.68
NM_008975	protein tyrosine phosphatase 4a3, transcript variant 2	Ptp4a3	2.64
NM_008086	growth arrest specific 1	Gas1	2.61
NM_029408	IQ motif containing D	Iqcd	2.61
NM_183315	cortexin 1	Ctxn1	2.6
NM_207666	delta-like 2 homolog	Dlk2	2.6
NM_010733	leucine rich repeat protein 3, neuronal, transcript variant 2	Lrrn3	2.58
NM_029057	TBC1 domain family, member 30	Tbc1d30	2.58
NM_177740	RGM domain family, member A	Rgma	2.58
NM_013739	docking protein 3	Dok3	2.54
NM_010517	insulin-like growth factor binding protein 4	Igfbp4	2.52
NM_007479	ADP-ribosylation factor 4	Arf4	2.51
NM_009708	Rho family GTPase 2	Rnd2	2.48
NM_008342	insulin-like growth factor binding protein 2	Igfbp2	2.48
NM_022657	fibroblast growth factor 23	Fgf23	2.46
NM_028804	coiled-coil domain containing 3	Ccdc3	2.44
NM_026814	protein phosphatase 1, regulatory subunit 27	Ppp1r27	2.43
NM_198249	Rho guanine nucleotide exchange factor (GEF) 40 , transcript variant 1	Arhgef40	2.43
NM_008356	interleukin 13 receptor, alpha 2	Il13ra2	2.41
NM_011823	G protein-coupled receptor 34	Gpr34	2.41
NM_010572	insulin receptor substrate 4	Irs4	2.38
NM_145431	notchless homolog 1	Nle1	2.38
NM_145373	secreted and transmembrane 1A	Sectm1a	2.37
NM_027280	naked cuticle 1 homolog, transcript variant 1	Nkd1	2.37
NM_026840	platelet-derived growth factor receptor-like	Pdgfrl	2.34
NM_007955	protein tyrosine phosphatase, receptor type, V	Ptprv	2.31
NM_009750	nerve growth factor receptor (TNFRSF16) associated protein 1, transcript variant 1	Ngfrap1	2.26
NM_145379	MAS-related GPR, member F	Mrgprf	2.26
NM_016719	growth factor receptor bound protein 14	Grb14	2.25
NM_016802	ras homolog gene family, member A	Rhoa	2.25
NM_001033484	IQ motif containing GTPase activating protein 3	Iqgap3	2.25

NM_009109	ryanodine receptor 1, skeletal muscle	Ryr1	2.22
NM_008865	prolactin family 3, subfamily b, member 1	Prl3b1	2.22
NM_146216	Vac14 homolog	Vac14	2.22
NM_009314	tachykinin receptor 2	Tacr2	2.21
NM_016891	protein phosphatase 2 (formerly 2A), regulatory subunit A (PR 65), alpha isoform	Ppp2r1a	2.21
NM_016971	interleukin 22	Il22	2.2
NM_007486	Rho, GDP dissociation inhibitor (GDI) beta (Arhgdib)	Arhgdib	2.19
NM_021476	cysteinyl leukotriene receptor 1	Cysltr1	2.18
NM_011915	Wnt inhibitory factor 1	Wif1	2.18
NM_009216	somatostatin receptor 1	Sstr1	2.18
NM_001011850	olfactory receptor 1505	Olfr1505	2.17
NM_147030	olfactory receptor 1134	Olfr1134	2.14
NM_009028	RAS-like, family 2, locus 9	Rasl2-9	2.13
NM_026446	regulator of G-protein signaling 19	Rgs19	2.13
NM_010273	guanosine diphosphate (GDP) dissociation inhibitor 1	Gdi1	2.11
NM_146356	olfactory receptor 521	Olfr521	2.11
NM_020257	C-type lectin domain family 2, member i	Clec2i	2.1
NM_138748	protein phosphatase 2A, regulatory subunit B (PR 53)	Ppp2r4	2.09
NM_206975	interferon, alpha 14	Ifna14	2.08
NM_023209	PDZ binding kinase	Pbk	2.06
NM_008728	natriuretic peptide receptor 3	Npr3	2.04
NM_007865	delta-like 1	Dll1	2.04
NM_017472	sorting nexin 3	Snx3	2.03
NM_001198766	periostin, osteoblast specific factor, transcript variant 3	Postn	2.02
NM_031875	otoferlin, transcript variant 2	Otof	2.02
NM_175168	PTK7 protein tyrosine kinase 7	Ptk7	2.02
NM_028416	kringle containing transmembrane protein 2	Kremen2	2.02
NM_020259	Hedgehog-interacting protein	Hhip	2.01
NM_008113	Rho GDP dissociation inhibitor (GDI) gamma	Arhgdig	2.01
NM_001033851	copine VIII, transcript variant 2	Cpne8	2
NM_001038018	G protein-coupled receptor kinase 6, transcript variant 1	Grk6	2
NM_029646	interleukin 34, transcript variant 2	Il34	2
NM_001164724	interleukin 33, transcript variant 1	Il33	2
NM_001110320	CD72 antigen, transcript variant 1	Cd72	1.99
NM_027571	purinergic receptor P2Y, G-protein coupled 12	P2ry12	1.99
NM_001165902	beta-catenin*	Ctnnb1	1.4
	Transcription		
NM_172495	nuclear receptor coactivator 7, transcript variant 1	Ncoa7	11.61
NM_027395	brain abundant, membrane attached signal protein 1	Basp1	4.75
NM_011640	transformation related protein 53, transcript variant 1	Trp53	3.77
NM_008709	v-myc myelocytomatosis viral related oncogene, neuroblastoma derived	Mycn	3.65
NM_008688	nuclear factor I/C, transcript variant 1	Nfic	3.56
NM_009236	SRY-box containing gene 18	Sox18	3.55
NM_181319	T-box 22, transcript variant 2	Tbx22	3.54
NM_016662	Max dimerization protein 3	Mxd3	3.37
NM_010055	distal-less homeobox 3	Dlx3	3.30
NM_025788	nucleus accumbens associated 1, BEN and BTB (POZ) domain containing	Nacc1	3.02
NM_028016	Nanog homeobox	Nanog	2.94
NM_010466	homeobox C8	Hoxc8	2.87
NM_009089	polymerase (RNA) II (DNA directed) polypeptide A	Polr2a	2.81
NM_009331	transcription factor 7, T cell specific	Tcf7	2.76
NM_170759	zinc finger protein 628 (Zfp628)	Zfp628	2.73
NM_178757	interferon regulatory factor 2 binding protein 1	Irf2bp1	2.68
NM_026776	vacuolar protein sorting 25	Vps25	2.65

NM_026532	nuclear transport factor 2	Nutf2	2.64
NM_009235	SRY-box containing gene 15	Sox15	2.62
NM_146040	cell division cycle associated 7 like	Cdca7l	2.62
NM_008505	LIM domain only 2, transcript variant 1	Lmo2	2.58
NM_001037914	multiciliate cell differentiation	Mcin	2.50
NM_026192	calcium binding and coiled coil domain 1	Calcoco1	2.49
NM_011642	transformation related protein 73, transcript variant 1	Trp73	2.46
NM_001001980	LIM and calponin homology domains 1, transcript variant 1	Limch1	2.39
NM_010919	NK2 transcription factor related, locus 2, transcript variant 1	Nkx2-2	2.37
NM_178609	E2F transcription factor 7	E2f7	2.37
NM_027946	DDB1 and CUL4 associated factor 7	Dcaf7	2.36
NM_001033813	zinc finger protein 872	Zfp872	2.35
NM_011139	POU domain, class 2, transcription factor 3	Pou2f3	2.34
NM_011869	mediator complex subunit 24	Med24	2.33
NM_010835	homeobox, msh-like 1	Msx1	2.32
NM_008269	homeobox B6	Hoxb6	2.24
NM_026937	activating signal cointegrator 1 complex subunit 1 , transcript variant 2	Ascc1	2.23
NM_019574	POZ (BTB) and AT hook containing zinc finger 1, transcript variant 1	Patz1	2.22
NM_001109743	SKI family transcriptional corepressor 2	Skor2	2.22
NM_021501	protein inhibitor of activated STAT 4	Pias4	2.22
NM_001163763	transcription factor 19, transcript variant 1	Tcf19	2.21
NM_027658	hexamethylene bis-acetamide inducible 2 , transcript variant 1	Hexim2	2.17
NM_001034900	zinc finger protein 345	Zfp345	2.15
NM_019776	staphylococcal nuclease and tudor domain containing 1	Snd1	2.12
NM_029281	zinc finger protein 820	Zfp820	2.11
NM_008627	Meis homeobox 3	Meis3	2.09
NM_001168502	zinc finger protein 57, transcript variant 3	Zfp57	2.08
NM_194350	v-maf musculoaponeurotic fibrosarcoma oncogene family, protein A	Mafa	2.06
NM_145836	interferon regulatory factor 2 binding protein-like	Irf2bpl	2.06
NM_011249	retinoblastoma-like 1 (p107), transcript variant 1	Rbl1	2.06
NM_011377	single-minded homolog 2	Sim2	2.04
NM_025945	polymerase (RNA) III (DNA directed) polypeptide D, transcript variant 1	Polr3d	2.04
NM_027434	regulation of nuclear pre-mRNA domain containing 1B	Rprd1b	2.04
NM_008321	inhibitor of DNA binding 3	Id3	2.02
NM_010464	homeobox C13	Hoxc13	2.02
NM_009056	regulatory factor X, 2 (influences HLA class II expression), transcript variant 2	Rfx2	2.01
NM_001013368	E2F transcription factor 8	E2f8	2.01
NM_144799	LIM and cysteine-rich domains 1	Lmcd1	2.00
NM_022435	trans-acting transcription factor 5	Sp5	2.00
NM_008500	LIM homeobox protein 6, transcript variant 1	Lhx6	1.99
NM_007531	prohibitin 2	Phb2	1.99
	Transport		
NM_012037	vesicle amine transport protein 1 homolog	Vat1	2.04
NM_001164679	anoctamin 8	Ano8	2.23
NM_008226	hyperpolarization-activated, cyclic nucleotide-gated K+ 2	Hcn2	3.05

*genes validated by qPCR

Table S2. Genes that show 2-fold up-regulation in the epithelium of K14rtTA/TRE-miR-214 mice versus WT mice

Accession Number	Gene Name	Symbol	Fold Change
	Adhesion/Extracellular matrix		
NM_018857	mesothelin	Msln	43.81
NM_009856	CD83 antigen	Cd83	3.46
NM_139200	cytohesin 1 interacting protein	Cytip	3.39
NM_027852	retinoic acid receptor responder (tazarotene induced) 2	Rarres2	3.08
NM_001243008	collagen, type VI, alpha 3, transcript variant 1	Col6a3	2.98
NM_009903	claudin 4	Cldn4	2.96
NM_022032	PERP, TP53 apoptosis effector	Perp	2.76
NM_001008424	corneodesmosin	Cdsn	2.67
NM_010516	cysteine rich protein 61	Cyr61	2.56
NM_008013	fibrinogen-like protein 2	Fgl2	2.5
NM_053146	protocadherin beta 21	Pcdhb21	2.37
NM_021893	CD274 antigen	Cd274	2.31
NM_138672	stabilin 1	Stab1	2.3
NM_145158	elastin microfibril interfacer 2	Emilin2	2.25
NM_001093749	myelin protein zero-like 3, transcript variant 2	Mpzl3	2.19
NM_027893	poliovirus receptor-related 4 , transcript variant 1	Pvrl4	2.19
NM_033620	par-3 (partitioning defective 3) homolog, transcript variant 3	Pard3	2.18
NM_016919	collagen, type V, alpha 3	Col5a3	2.17
NM_010814	myelin oligodendrocyte glycoprotein	Mog	2.17
NM_008127	gap junction protein, beta 4	Gjb4	2.16
NM_010291	gap junction protein, beta 5	Gjb5	2.16
NM_011016	orosomucoid 2	Orm2	2.16
NM_001111058	CD33 antigen, transcript variant 1	Cd33	2.15
NM_080437	cadherin, EGF LAG seven-pass G-type receptor 3 (flamingo homolog, Drosophila)	Celsr3	2.13
NM_133743	Ly6/Plaur domain containing 3	Lypd3	2.13
NM_001113368	carcinoembryonic antigen-related cell adhesion molecule 2, transcript variant 1	Ceacam2	2.1
NM_008768	orosomucoid 1	Orm1	2.09
NM_028523	discoidin, CUB and LCCL domain containing 2	Dcbld2	2.08
NM_007993	fibrillin 1	Fbn1	2.08
NM_023420	collagen, type IV, alpha 3 binding protein, transcript variant 1	Col4a3bp	2.05
NM_001081053	integrin, alpha 10	Itga10	2
	Cell Cycle/Apoptosis		
NM_009397	tumor necrosis factor, alpha-induced protein 3, transcript variant 1	Tnfaip3	5.11
NM_007570	B cell translocation gene 2, anti-proliferative	Btg2	4.69
NM_011540	titin-cap	Tcap	4.31
NM_013642	dual specificity phosphatase 1	Dusp1	3.28
NM_207677	death effector domain-containing DNA binding protein 2	Dedd2	2.96
NM_009871	cyclin-dependent kinase 5, regulatory subunit 1 (p35)	Cdk5r1	2.63
NM_001162908	sestrin 1, transcript variant 1	Sesn1	2.61
NM_001081156	TMF1-regulated nuclear protein 1	Trnp1	2.61
NM_130886	caspase recruitment domain family, member 14	Card14	2.59
NM_009760	BCL2/adenovirus E1B interacting protein 3	Bnip3	2.46

NM_007609	caspase 4, apoptosis-related cysteine peptidase	Casp4	2.42
NM_008681	N-myc downstream regulated gene 1	Ndrg1	2.32
NM_013469	annexin A11	Anxa11	2.25
NM_025427	regulator of cell cycle	Rgcc	2.17
NM_001103182	lin-9 homolog, transcript variant 1	Lin9	2.14
NM_144899	ADAMTS-like 4	Adamtsl4	2.13
NM_001003920	BR serine/threonine kinase 1, transcript variant 1	Brsk1	2
NM_008795	cyclin-dependent kinase 18	Cdk18	2
	Chromatin remodeling		
NM_001097979	histone cluster 1, H2bq	Hist1h2bq	59.61
NM_178909	WD repeat domain 92	Wdr92	9.88
NM_178196	histone cluster 1, H2bg	Hist1h2bg	5.99
NM_015786	histone cluster 1, H1c	Hist1h1c	4.74
NM_023422	histone cluster 1, H2bc	Hist1h2bc	4.26
BC015270	histone cluster 2, H3c2	Hist2h3c2	3.7
BC059807	chromodomain helicase DNA binding protein 6	Chd6	3.64
NM_199299	PHD finger protein 15	Phf15	3.61
NM_013807	polo-like kinase 3	Plk3	3.51
NM_025519	charged multivesicular body protein 4C	Chmp4c	3.27
NM_001167884	suppressor of variegation 4-20 homolog 1 (Drosophila) , transcript variant 7	Suv420h1	2.69
NM_030082	histone cluster 3, H2ba	Hist3h2ba	2.58
NM_001081315	bromodomain and PHD finger containing, 3	Brpf3	2.49
NM_178218	histone cluster 3, H2a	Hist3h2a	2.4
NM_001109691	PHD finger protein 21A, transcript variant 3	Phf21a	2.34
NM_001128151	cat eye syndrome chromosome region, candidate 2	Cecr2	2.33
NM_001081269	Wolf-Hirschhorn syndrome candidate 1-like 1, transcript variant 2	Whsc1l1	2.24
NM_153421	polyhomeotic-like 3 (Drosophila) , transcript variant 2	Phc3	2.22
NM_010434	homeodomain interacting protein kinase 3, transcript variant 1	Hipk3	2.19
NM_027892	protein phosphatase 1, regulatory (inhibitor) subunit 12A	Ppp1r12a	2.16
NM_026110	PAX3 and PAX7 binding protein 1	Paxbp1	2.14
NM_001017426	KDM1 lysine (K)-specific demethylase 6B	Kdm6b	2.04
NM_001177374	ubiquitin protein ligase E3 component n-recognin 2, transcript variant 2	Ubr2	2.03
NM_011235	RAD51 homolog D	Rad51d	2.02
	Cytoskeleton		
NM_008508	loricrin	Lor	8.18
NM_025420	late cornified envelope 1M	Lce1m	5.51
NM_027762	trichohyalin-like 1	Tchhl1	4.5
NM_001099774	keratin associated protein 17-1	Krtap17-1	3.85
NM_029667	late cornified envelope 1I	Lce1i	3.83
NM_212487	keratin 78	Krt78	3.81
NM_027137	late cornified envelope 1D	Lce1d	3.62
NM_011472	small proline-rich protein 2F	Sprr2f	3.61
NM_001005510	spectrin repeat containing, nuclear envelope 2	Syne2	3.5
NM_013560	heat shock protein 1	Hspb1	3.49
NM_026394	late cornified envelope 1F	Lce1f	3.49
NM_011470	small proline-rich protein 2D	Sprr2d	3.49
NM_033373	keratin 23	Krt23	3.38
NM_011471	small proline-rich protein 2E	Sprr2e	3.23
NM_011619	troponin T2, cardiac, transcript variant 9	Tnnt2	3.19
NM_010664	keratin 18	Krt18	3.14
NM_001252372	myosin binding protein C, slow-type , transcript variant 1	Mybpc1	3.14

NM_008473	keratin 1	Krt1	3.06
NM_028622	late cornified envelope 1C (Lce1c)	Lce1c	2.97
NM_001039376	phosphodiesterase 4D interacting protein (myomegalin), transcript variant 1	Pde4dip	2.88
NM_026822	late cornified envelope 1B	Lce1b	2.84
NM_001271484	CAP-GLY domain containing linker protein family, member 4, transcript variant 4	Clip4	2.79
NM_028044	calponin 3, acidic	Cnn3	2.75
NM_007585	annexin A2	Anxa2	2.74
NM_033175	late cornified envelope 3C	Lce3c	2.72
NM_025501	late cornified envelope 3B	Lce3b	2.64
NM_001018079	late cornified envelope 3F	Lce3f	2.59
NM_026811	late cornified envelope 1E	Lce1e	2.57
NM_001270426	late cornified envelope 3D	Lce3d	2.55
NM_001039472	kinesin family member 21B	Kif21b	2.4
NM_018790	activity regulated cytoskeletal-associated protein	Arc	2.38
NM_028721	nephronophthisis 3 (adolescent), transcript variant 1	Nphp3	2.38
NM_025413	late cornified envelope 1G	Lce1g	2.33
NM_030203	TSPY-like 4	Tspyl4	2.33
NM_145070	huntingtin interacting protein 1 related	Hip1r	2.26
NM_010630	kinesin family member C2	Kifc2	2.24
NM_025984	late cornified envelope 1A1	Lce1a1	2.24
NM_019765	CAP-GLY domain containing linker protein 1	Clip1	2.19
NM_001039594	late cornified envelope 3A	Lce3a	2.18
NM_146120	gelsolin, transcript variant 1	Gsn	2.17
NM_001109657	growth arrest specific 7, transcript variant 2	Gas7	2.14
NM_133357	keratin 75	Krt75	2.11
NM_001254760	late cornified envelope 1K	Lce1k	2.11
NM_019809	PDZ and LIM domain 5, transcript variant 2	Pdlim5	2.08
NM_009450	tubulin, beta 2A class IIA	Tubb2a	2.07
NM_010660	keratin 10	Krt10	2.06
NM_175180	WD repeat domain 44	Wdr44	2.06
NM_178593	RCSD domain containing 1, transcript variant 1	Rcsd1	2.04
NM_198113	slingshot homolog 3	Ssh3	2.03
NM_001163664	troponin T3, skeletal, fast , transcript variant 1	Tnnt3	2.01
	Metabolism		
NM_013743	pyruvate dehydrogenase kinase, isoenzyme 4, nuclear gene encoding mitochondrial protein	Pdk4	5.79
NM_175650	ATPase type 13A5	Atp13a5	5.26
NM_027299	degenerative spermatocyte homolog 2 (Drosophila), lipid desaturase, transcript variant 1	Degs2	5.02
NM_011435	superoxide dismutase 3, extracellular	Sod3	4.95
NM_146118	solute carrier family 25 (mitochondrial carrier, phosphate carrier), member 25, transcript variant 1	Slc25a25	4.52
NM_001111331	Kv channel interacting protein 3, calsenilin , transcript variant 2	Kcnip3	4.38
NM_001199283	solute carrier family 43, member 2, transcript variant 1	Slc43a2	4.33
NM_007409	alcohol dehydrogenase 1 (class I)	Adh1	4.23
NM_001164613	ATPase type 13A4, transcript variant 3	Atp13a4	4.18
NM_001130194	bestrophin 2, transcript variant 1	Best2	4.18
NM_009593	ATP-binding cassette, sub-family G (WHITE), member 1	Abcg1	3.91
NM_026945	alcohol dehydrogenase 6A (class V)	Adh6a	3.68
NM_001177753	6-phosphofructo-2-kinase/fructose-2,6-biphosphatase 3, transcript variant 2	Pfkfb3	3.61
NM_194333	solute carrier family 23 (nucleobase transporters), member 3	Slc23a3	3.52
NM_001098789	NADH dehydrogenase (ubiquinone) 1 alpha subcomplex,	Ndufa4l2	3.45

	4-like 2		
NM_011031	procollagen-proline, 2-oxoglutarate 4-dioxygenase, alpha II polypeptide , transcript variant 2	P4ha2	3.45
NM_030696	solute carrier family 16 (monocarboxylic acid transporters), member 3	Slc16a3	3.28
NM_001042591	arrestin domain containing 3	Arrdc3	3.27
NM_028784	coagulation factor XIII, A1 subunit, transcript variant 1	F13a1	3.24
NM_028133	EGL nine homolog 3 (C. elegans)	Egln3	3.13
NM_183161	solute carrier family 17, member 9	Slc17a9	3.01
NM_033648	FXYD domain-containing ion transport regulator 4, transcript variant 1	Fxyd4	2.99
NM_001111111	autophagy related 16-like 2	Atg16l2	2.92
NM_001114084	diacylglycerol O-acyltransferase 2-like 6	Dgat2l6	2.88
NM_029415	solute carrier family 10 (sodium/bile acid cotransporter family), member 6	Slc10a6	2.84
NM_007421	adenylosuccinate synthetase like 1	Adssl1	2.74
NM_172883	major facilitator superfamily domain containing 7A	Mfsd7a	2.74
NM_013455	acrosin prepropeptide, transcript variant 1	Acr	2.71
NM_172837	lipase, family member K, transcript variant 2	Lipk	2.7
NM_030558	carbonic anhydrase 15	Car15	2.68
NM_153143	potassium channel tetramerisation domain containing 11	Kctd11	2.67
NM_001267707	solute carrier organic anion transporter family, member 1a5, transcript variant 1	Slco1a5	2.67
NM_007470	apolipoprotein D	Apod	2.66
NM_001195033	abhydrolase domain containing 12B	Abhd12b	2.65
NM_001079865	carboxylesterase 2F	Ces2f	2.65
NM_011198	prostaglandin-endoperoxide synthase 2	Ptgs2	2.65
NM_172524	NIPA-like domain containing 4	Nipal4	2.63
NM_177243	solute carrier family 26, member 9	Slc26a9	2.62
NM_153404	lipase, member H, transcript variant 2	Liph	2.58
NM_019664	potassium inwardly-rectifying channel, subfamily J, member 15 , transcript variant 2	Kcnj15	2.57
NM_001160165	neuraminidase 2, transcript variant 3	Neu2	2.56
NM_009695	apolipoprotein C-II	Apoc2	2.55
NM_011786	arachidonate lipoxygenase 3	Aloxe3	2.53
NM_001039176	elongation of very long chain fatty acids (FEN1/Elo2, SUR4/Elo3, yeast)-like 1, transcript variant 1	Elovl1	2.49
NM_175475	cytochrome P450, family 26, subfamily b, polypeptide 1, transcript variant 1	Cyp26b1	2.46
NM_001081349	solute carrier family 43, member 1, transcript variant 1	Slc43a1	2.41
NM_134006	retinol dehydrogenase 5	Rdh5	2.4
NM_001012434	potassium channel tetramerisation domain containing 14, transcript variant 2	Kctd14	2.39
NM_029688	sulfiredoxin 1 homolog	Srxn1	2.39
NM_001042719	DDHD domain containing 1, transcript variant 3	Ddhd1	2.36
NM_001081421	UDP-N-acetyl-alpha-D-galactosamine:polypeptide N-acetylgalactosaminyltransferase-like 1	Galntl1	2.36
NM_173785	IBA57, iron-sulfur cluster assembly homolog, transcript variant 1	Iba57	2.35
NM_027172	solute carrier protein family 52, member 3 , transcript variant 1	Slc52a3	2.35
NM_009022	aldehyde dehydrogenase family 1, subfamily A2	Aldh1a2	2.32
NM_027868	solute carrier family 41, member 3, transcript variant 1	Slc41a3	2.32
NM_145828	xylosyltransferase II	Xylt2	2.32
NM_021301	solute carrier family 15 (H+/peptide transporter), member 2, transcript variant 1	Slc15a2	2.28
BC047268	phospholipase D2	Pld2	2.27
NM_183220	1-aminocyclopropane-1-carboxylate synthase (non-functional)	Accs	2.24

NM_172692	glucosidase beta 2	Gba2	2.23
NM_053079	solute carrier family 15 (oligopeptide transporter), member 1	Slc15a1	2.23
NM_018830	N-acylsphingosine amidohydrolase 2	Asah2	2.22
NM_018881	flavin containing monooxygenase 2	Fmo2	2.22
NM_013509	enolase 2, gamma neuronal	Eno2	2.21
NM_001163689	patatin-like phospholipase domain containing 2, transcript variant 1	Pnpla2	2.21
NM_026784	phosphomevalonate kinase, transcript variant 1	Pmvk	2.18
NM_026644	1-acylglycerol-3-phosphate O-acyltransferase 4 (lysophosphatidic acid acyltransferase, delta)	Agpat4	2.17
NM_010239	ferritin heavy chain 1, transcript variant 1	Fth1	2.17
NM_008504	granzyme M (lymphocyte met-ase 1)	Gzmm	2.17
NM_145423	solute carrier family 5 (iodide transporter), member 8	Slc5a8	2.17
NM_052993	core 1 synthase, glycoprotein-N-acetylgalactosamine 3-beta-galactosyltransferase, 1	C1galt1	2.16
NM_019779	cytochrome P450, family 11, subfamily a, polypeptide 1	Cyp11a1	2.16
NM_175331	5'-nucleotidase domain containing 3	Nt5dc3	2.16
NM_008131	glutamate-ammonia ligase (glutamine synthetase)	Glul	2.15
NM_009177	ST3 beta-galactoside alpha-2,3-sialyltransferase 1	St3gal1	2.15
NM_001039710	coenzyme Q10 homolog B, transcript variant 1	Coq10b	2.14
NM_027340	lipase, family member N	Lipn	2.13
NM_147219	ATP-binding cassette, sub-family A , member 5	Abca5	2.09
NM_019807	acid phosphatase, prostate , transcript variant 2	Acpp	2.07
NM_172607	nicotinate phosphoribosyltransferase domain containing 1	Naprt1	2.07
NM_029810	5'-nucleotidase, cytosolic II , transcript variant 3	Nt5c2	2.07
NM_027406	aldehyde dehydrogenase 1 family, member L1	Aldh1l1	2.06
NM_153803	galactosidase, beta 1-like 2	Glb1l2	2.06
NM_001159864	potassium channel tetramerisation domain containing 18, transcript variant 1	Kctd18	2.05
NM_001161767	UDP-N-acetyl-alpha-D-galactosamine:polypeptide N-acetylgalactosaminyltransferase 6, transcript variant 1	Galnt6	2.04
NM_145447	major facilitator superfamily domain containing 7C	Mfsd7c	2.04
NM_013820	hexokinase 2	Hk2	2.03
NM_001161765	flavin containing monooxygenase 5, transcript variant 1	Fmo5	2.02
NM_025718	deoxyribonuclease 1-like 2	Dnase1l2	2.02
NM_013850	ATP-binding cassette, sub-family A, member 7	Abca7	2.01
NM_009721	ATPase, Na+/K+ transporting, beta 1 polypeptide	Atp1b1	2.01

Others

NM_172051	transmembrane and coiled coil domains 3, transcript variant 1	Tmcc3	7.29
NM_001163502	ELM2 and Myb/SANT-like domain containing 1, transcript variant 1	Elmsan1	6.84
NM_001166173	dermokine, transcript variant 3	Dmkn	5.26
NM_001204959	resistin , transcript variant 2	Retn	5.11
NM_175307	family with sequence similarity 46, member B	Fam46b	4.69
NM_001199210	eva-1 homolog C (C. elegans) , transcript variant 1	Eva1c	4.66
NM_197986	transmembrane protein 140	Tmem140	4
NM_172205	suprabasin, transcript variant 1	Sbsn	3.93
NM_001190436	Finkel-Biskis-Reilly murine sarcoma virus (FBR-MuSV) ubiquitously expressed, transcript variant 3	Fau	3.74
NM_028798	cysteine-rich C-terminal 1	Crct1	3.73
NM_001033411	predicted gene 826	Gm826	3.55
BC090258	interferon induced transmembrane protein 1	Ifitm1	3.24
NM_027511	histidine rich carboxyl terminus 1	Hrct1	3.19
NM_013473	annexin A8	Anxa8	3.16
NM_009778	complement component 3	C3	3.16

NM_145535	syndecan binding protein (syntenin) 2	Sdcbp2	2.91
NM_027585	cyclic nucleotide binding domain containing 2	Cnbd2	2.88
NM_001013749	transmembrane protein 151B	Tmem151b	2.87
NM_172801	otopetrin 2	Otop2	2.85
NM_001033410	predicted gene 757	Gm757	2.79
NM_181397	raftlin lipid raft linker 1	Rftn1	2.78
NM_001163572	transmembrane protein 170B	Tmem170b	2.73
NM_001025572	ankyrin repeat domain 12	Ankrd12	2.58
NM_010220	FK506 binding protein 5	Fkbp5	2.57
NM_173415	nyctalopin	Nyx	2.57
NM_175407	sine oculis-binding protein homolog (Drosophila)	Sobp	2.56
NM_176860	ubiquitin associated and SH3 domain containing, B	Ubash3b	2.56
NM_010732	leucine rich repeat protein 2, neuronal	Lrrn2	2.52
NM_031195	macrophage scavenger receptor 1, transcript variant 1	Msr1	2.52
NM_020578	EH-domain containing 3	Ehd3	2.48
NM_011573	testis expressed gene 264, transcript variant 1	Tex264	2.48
NM_013562	interferon-related developmental regulator 1	Ifrd1	2.4
NM_019576	thrombospondin, type I, domain 1, transcript variant 1	Thsd1	2.39
NM_170684	copine VII	Cpne7	2.38
NM_029116	kelch repeat and BTB (POZ) domain containing 11	Kbtbd11	2.38
NM_010706	lectin, galactose binding, soluble 4	Lgals4	2.37
NM_176834	ring finger protein 208	Rnf208	2.37
NM_011029	ribosomal protein SA	Rpsa	2.36
NM_026146	EPS8-like 1	Eps8l1	2.34
NM_178884	obscurin-like 1	Obsl1	2.33
NM_146008	t-complex 11 (mouse) like 2	Tcp11l2	2.32
NM_026835	membrane-spanning 4-domains, subfamily A, member 6D	Ms4a6d	2.31
NM_001085507	zinc finger and BTB domain containing 34	Zbtb34	2.31
NM_133898	NEDD4 binding protein 2-like 1	N4bp2l1	2.3
NM_001081652	NAC alpha domain containing	Nacad	2.3
NM_001162974	leucine rich repeat containing 51, transcript variant 3	Lrrc51	2.29
NM_001038592	glutaredoxin 2 , transcript variant 1	Glrx2	2.28
NM_001205353	GRAM domain containing 4, transcript variant 2	Gramd4	2.28
NM_144797	meteorin, glial cell differentiation regulator-like	Metrnl	2.28
NM_001159577	ligand of numb-protein X 1, transcript variant 1	Lnx1	2.24
NM_027898	GRAM domain containing 1A	Gramd1a	2.23
NM_001136259	target of myb1 homolog, transcript variant 2	Tom1	2.22
NM_009150	selenium binding protein 1	Selenbp1	2.2
NM_001164557	PDZK1 interacting protein 1 , transcript variant 1	Pdzk1ip1	2.18
NM_145853	two pore channel 1	Tpcn1	2.17
NM_053167	tripartite motif-containing 9 , transcript variant 1	Trim9	2.17
NM_027166	yippee-like 5	Ypel5	2.17
NM_011157	serglycin	Srgn	2.16
NM_026588	syntaxin 19	Stx19	2.16
NM_001168514	mitogen-activated protein kinase 14, transcript variant 4	Mapk14	2.15
NM_178242	trinucleotide repeat containing 18, transcript variant B	Tnrc18	2.14
NM_009441	tetratricopeptide repeat domain 3	Ttc3	2.14
NM_153507	copine II	Cpne2	2.13
NM_013532	leukocyte immunoglobulin-like receptor, subfamily B, member 4	Lilrb4	2.13
NM_001081235	meningioma 1	Mn1	2.13
NM_001024134	tripartite motif-containing 15, transcript variant 2	Trim15	2.13
NM_011123	proteolipid protein (myelin) 1	Plp1	2.12
NM_053166	tripartite motif-containing 7	Trim7	2.12
NM_181073	pleckstrin homology domain containing, family H (with MyTH4 domain) member 1	Plekhh1	2.11

NM_133774	StAR-related lipid transfer (START) domain containing 4	Stard4	2.11
NM_001146022	WD repeat and FYVE domain containing 4	Wdfy4	2.11
NM_001008233	pleckstrin homology domain containing, family N member 1	Plekhn1	2.1
NM_177775	extended synaptotagmin-like protein 3	Esyt3	2.07
NM_026235	La ribonucleoprotein domain family, member 6	Larp6	2.07
NM_019814	HIG1 domain family, member 1A	Higd1a	2.06
NM_177185	ubinuclein 2	Ubn2	2.06
NM_001256057	predicted gene 11570	Gm11570	2.05
NM_172694	multiple EGF-like-domains 9	Megf9	2.05
NM_177632	family with sequence similarity 43, member A	Fam43a	2.04
NM_001146043	G elongation factor, mitochondrial 2, transcript variant 2	Gfm2	2.04
NM_027116	NTPase, KAP family P-loop domain containing 1	Nkpd1	2.04
NM_028950	NOL1/NOP2/Sun domain family member 6, transcript variant 2	Nsun6	2.04
NM_001271727	tripartite motif-containing 2, transcript variant 3	Trim2	2.02
NM_016714	nucleoporin 50	Nup50	2.01
NM_001045483	mitogen-activated protein kinase 1 interacting protein 1, transcript variant 1	Mapk1ip1	2
	Protein folding		
NM_028430	peptidylprolyl isomerase (cyclophilin)-like 6	Ppil6	2.25
NM_018808	DnaJ (Hsp40) homolog, subfamily B, member 1	Dnajb1	2.23
	Proteolysis		
NM_013459	complement factor D (adipsin)	Cfd	11.31
NM_177322	angiotensin II receptor, type 1a	Agtr1a	8.65
NM_011414	secretory leukocyte peptidase inhibitor	Slpi	7.4
NM_008871	serine (or cysteine) peptidase inhibitor, clade E, member 1	Serpine1	6.57
NM_001252569	serine (or cysteine) peptidase inhibitor, clade A, member 1A, transcript variant 2	Serpina1a	3.91
NM_133753	ERBB receptor feedback inhibitor 1	Errfi1	3.83
NM_001199940	serine (or cysteine) peptidase inhibitor, clade A, member 3I	Serpina3i	3.72
NM_015790	icos ligand	Icosl	3.69
NM_010511	interferon gamma receptor 1	Ifngr1	3.56
NM_009247	serine (or cysteine) peptidase inhibitor, clade A, member 1E	Serpina1e	3.47
NM_028660	kallikrein related-peptidase 9	Klk9	3.39
NM_009245	serine (or cysteine) peptidase inhibitor, clade A, member 1C	Serpina1c	3.31
NM_024406	fatty acid binding protein 4, adipocyte	Fabp4	3.12
NM_009776	serine (or cysteine) peptidase inhibitor, clade G, member 1	Serping1	3.09
NM_011113	plasminogen activator, urokinase receptor	Plaur	2.99
NM_009543	ring finger protein 103	Rnf103	2.98
NM_007796	cytotoxic T lymphocyte-associated protein 2 alpha, transcript variant 1	Ctla2a	2.87
NM_009246	serine (or cysteine) peptidase inhibitor, clade A, member 1D	Serpina1d	2.87
NM_027997	serine (or cysteine) peptidase inhibitor, clade A, member 9	Serpina9	2.83
NM_007781	colony stimulating factor 2 receptor, beta 2, low-affinity	Csf2rb2	2.79
NM_178691	YOD1 OTU deubiquitinating enzyme 1 homologue	Yod1	2.71
NM_001025439	calcium/calmodulin-dependent protein kinase II, delta, transcript variant 1	Camk2d	2.62
NM_016845	proacrosin binding protein, transcript variant 1	Acrbp	2.61
NM_026414	aspartic peptidase, retroviral-like 1	Asprv1	2.61
NM_019932	platelet factor 4	Pf4	2.47
NM_001039042	kallikrein related-peptidase 13	Klk13	2.42
NM_007797	cytotoxic T lymphocyte-associated protein 2 beta, transcript variant 1	Ctla2b	2.41

NM_008906	cathepsin A , transcript variant 1	Ctsa	2.41
NM_173749	peptidase domain containing associated with muscle regeneration 1	Pamr1	2.4
NM_001040106	AP2 associated kinase 1, transcript variant 1	Aak1	2.26
NM_178730	transmembrane protease, serine 11f	Tmprss11f	2.23
NM_028894	LON peptidase N-terminal domain and ring finger 3	Lonrf3	2.21
NM_011177	kallikrein related-peptidase 6, transcript variant 1	Klk6	2.2
NM_183284	serine peptidase inhibitor, Kazal type 2	Spink2	2.17
NM_001081115	non-specific cytotoxic cell receptor protein 1 homolog (zebrafish)	Nccrp1	2.13
NM_052976	oligophrenin 1	Ophn1	2.12
NM_178694	zyg-11 related, cell cycle regulator	Zer1	2.11
NM_139147	Rab40b, member RAS oncogene family	Rab40b	2.06
NM_007899	extracellular matrix protein 1, transcript variant 1	Ecm1	2.05
NM_001001803	serine peptidase inhibitor, Kazal type 7 (putative)	Spink7	2.04
	RNA processing		
NM_011756	zinc finger protein 36	Zfp36	4.91
NM_007475	ribosomal protein, large, P0	Rplp0	2.95
BC096413	ribosomal protein L37a	Rpl37a	2.82
NM_001114079	poly(A) binding protein, cytoplasmic 1-like	Pabpc1l	2.8
NM_133819	protein phosphatase 1, regulatory (inhibitor) subunit 15b	Ppp1r15b	2.79
NM_009095	ribosomal protein S5	Rps5	2.62
NM_033541	2'-5' oligoadenylate synthetase 1C	Oas1c	2.43
NM_025963	ribosomal protein S10	Rps10	2.42
NM_026020	ribosomal protein, large P2	Rplp2	2.22
NM_016680	CLK4-associating serine/arginine rich protein, transcript variant L	Clasrp	2.14
NM_053255	elaC homolog 1	Elac1	2.1
NM_025919	ribosomal protein L11	Rpl11	2.1
NM_175937	cytoplasmic polyadenylation element binding protein 2 , transcript variant 1	Cpeb2	2.09
NM_175529	leukocyte receptor cluster (LRC) member 9	Leng9	2.07
NM_011287	ribosomal protein L10A	Rpl10a	2.03
NM_001024837	adenosine deaminase, RNA-specific, B1, transcript variant 2	Adarb1	2.02
	Signalling		
NM_011314	serum amyloid A 2	Saa2	40.51
NM_008176	chemokine (C-X-C motif) ligand 1	Cxcl1	23.24
NM_009117	serum amyloid A 1	Saa1	12.21
NM_011333	chemokine (C-C motif) ligand 2	Ccl2	9.04
NM_008361	interleukin 1 beta	Il1b	8.5
NM_009627	adrenomedullin	Adm	7.04
NM_007707	suppressor of cytokine signaling 3	Socs3	4.9
NM_007913	early growth response 1	Egr1	4.62
NM_015811	regulator of G-protein signaling 1	Rgs1	4.39
NM_011338	chemokine (C-C motif) ligand 9	Ccl9	4.29
NM_177868	forkhead-associated (FHA) phosphopeptide binding domain 1	Fhad1	3.93
NM_013652	chemokine (C-C motif) ligand 4	Ccl4	3.8
NM_015776	microfibrillar associated protein 5	Mfap5	3.58
NM_026577	ADP-ribosylation factor-like 13B	Arl13b	3.55
NM_029083	DNA-damage-inducible transcript 4	Ddit4	3.51
NM_008344	insulin-like growth factor binding protein 6	Igfbp6	3.38
NM_011817	growth arrest and DNA-damage-inducible 45 gamma	Gadd45g	3.37
NM_009615	a disintegrin and metallopeptidase domain 17	Adam17	3.33

NM_009061	regulator of G-protein signaling 2	Rgs2	3.28
NM_017466	chemokine (C-C motif) receptor-like 2	Ccrl2	3.27
NM_020622	family with sequence similarity 3, member B	Fam3b	3.19
NM_009841	CD14 antigen	Cd14	3.17
NM_146491	olfactory receptor 1410	Olfr1410	3.14
NM_011905	toll-like receptor 2	Tlr2	3.14
NM_177137	guanine nucleotide binding protein, alpha stimulating, olfactory type, transcript variant 2	Gnal	3.07
NM_145857	nucleotide-binding oligomerization domain containing 2	Nod2	2.99
NM_172718	small G protein signaling modulator 1, transcript variant 1	Sgsm1	2.99
NM_009017	retinoic acid early transcript beta	Raet1b	2.95
NM_023463	lymphocyte antigen 6 complex, locus G6C	Ly6g6c	2.84
NM_001163262	c-Maf inducing protein, transcript variant 1	Cmip	2.8
NM_027106	arginine vasopressin-induced 1	Avpi1	2.77
NM_010276	GTP binding protein	Gem	2.76
NM_008855	protein kinase C, beta	Prkcb	2.62
NM_021274	chemokine (C-X-C motif) ligand 10	Cxcl10	2.61
NM_001163634	wingless-related MMTV integration site 7B, transcript variant 2	Wnt7b	2.59
NM_178256	RALBP1 associated Eps domain containing protein 2	Reps2	2.58
NM_007706	suppressor of cytokine signaling 2, transcript variant 1	Socs2	2.57
NM_013693	tumor necrosis factor	Tnf	2.52
NM_025540	sarcolipin	Sln	2.46
NM_001081155	Rap1 GTPase-activating protein , transcript variant 1	Rap1gap	2.45
NM_009184	PTK6 protein tyrosine kinase 6	Ptk6	2.44
NM_010592	Jun proto-oncogene related gene d	Jund	2.43
NM_011058	platelet derived growth factor receptor, alpha polypeptide , transcript variant 1	Pdgfra	2.42
NM_010831	salt inducible kinase 1	Sik1	2.39
NM_008773	purinergic receptor P2Y, G-protein coupled 2	P2ry2	2.37
NM_025404	ADP-ribosylation factor-like 4D	Arl4d	2.36
NM_022019	dual specificity phosphatase 10	Dusp10	2.36
NM_008343	insulin-like growth factor binding protein 3	Igfbp3	2.33
NM_001130409	PTK2 protein tyrosine kinase 2, transcript variant 2	Ptk2	2.32
NM_001081212	insulin receptor substrate 2	Irs2	2.31
NM_178111	transformation related protein 53 inducible nuclear protein 2	Trp53inp2	2.3
NM_178258	interleukin 22 receptor, alpha 2	Il22ra2	2.28
NM_013584	leukemia inhibitory factor receptor, transcript variant 1	Lifr	2.28
NM_198703	WNK lysine deficient protein kinase 1, transcript variant 1	Wnk1	2.28
NM_001035533	A kinase (PRKA) anchor protein 2, transcript variant 1	Akap2	2.25
NM_018883	calcium/calmodulin-dependent protein kinase kinase 1, alpha	Camkk1	2.24
NM_021306	endothelin converting enzyme-like 1	Ecel1	2.24
NM_010559	interleukin 6 receptor, alpha	Il6ra	2.22
NM_175445	Ras association (RalGDS/AF-6) domain family member 2	Rassf2	2.22
NM_011530	transporter 2, ATP-binding cassette, sub-family B (MDR/TAP)	Tap2	2.16
NM_139307	vasorin	Vasn	2.16
NM_010950	numb-like	Numbl	2.15
NM_133924	sorting nexin family member 21	Snx21	2.12
NM_001025250	vascular endothelial growth factor A, transcript variant 1	Vegfa	2.1
NM_007557	bone morphogenetic protein 7	Bmp7	2.09
NM_001002842	PML-RAR alpha-regulated adaptor molecule 1 (Pram1), transcript variant 1	Pram1	2.09
BC122879	nebulette	Nebl	2.05
NM_080843	suppressor of cytokine signaling 4	Socs4	2.02

NM_146322	olfactory receptor 187	Olfr187	2.01
NM_178710	salt inducible kinase 2	Sik2	2.01
NM_001081412	breakpoint cluster region	Bcr	2
	Transcription		
NM_001077364	TSC22 domain family, member 3, transcript variant 1	Tsc22d3	13.68
NM_007498	activating transcription factor 3	Atf3	7.41
NM_008036	FBJ osteosarcoma oncogene B	Fosb	7.34
NM_010444	nuclear receptor subfamily 4, group A, member 1	Nr4a1	7.12
NM_010234	FBJ osteosarcoma oncogene	Fos	6.58
NM_010828	Cbp/p300-interacting transactivator, with Glu/Asp-rich carboxy-terminal domain, 2	Cited2	6.21
NM_007679	CCAAT/enhancer binding protein (C/EBP), delta	Cebpd	5.67
NM_153287	cysteine-serine-rich nuclear protein 1	Csrnp1	4.92
NM_001033324	zinc finger and BTB domain containing 16	Zbtb16	4.28
NM_010591	Jun oncogene	Jun	4.23
NM_016868	hypoxia inducible factor 3, alpha subunit , transcript variant 2	Hif3a	4.01
NM_007914	ets homologous factor	Ehf	3.86
NM_008390	interferon regulatory factor 1, transcript variant 1	Irf1	3.81
NM_001113333	cryptochrome 2 (photolyase-like) , transcript variant 2	Cry2	3.67
NM_010638	Kruppel-like factor 9	Klf9	3.46
NM_010907	nuclear factor of kappa light polypeptide gene enhancer in B cells inhibitor, alpha	Nfkbia	3.39
NM_021897	transformation related protein 53 inducible nuclear protein 1, transcript variant 1	Trp53inp1	3.39
NM_010755	v-maf musculoaponeurotic fibrosarcoma oncogene family, protein F	Maff	3.33
NM_008452	Kruppel-like factor 2	Klf2	3.14
NM_027477	zinc finger protein 398 , transcript variant 1	Zfp398	3.06
NM_013874	D4, zinc and double PHD fingers family 1	Dpf1	3
NM_010235	fos-like antigen 1	Fosl1	2.99
NM_009821	runt related transcription factor 1, transcript variant 4	Runx1	2.97
NM_017373	nuclear factor, interleukin 3, regulated	Nfil3	2.94
NM_030612	nuclear factor of kappa light polypeptide gene enhancer in B cells inhibitor, zeta , transcript variant 1	Nfkbiz	2.88
NM_010056	distal-less homeobox 5, transcript variant 1	Dlx5	2.79
NM_009565	zinc finger and BTB domain containing 7B	Zbtb7b	2.71
NM_011276	ring finger protein, LIM domain interacting	Rlim	2.7
NM_010499	immediate early response 2	Ier2	2.63
NM_023755	transcription factor CP2-like 1	Tfcp2l1	2.58
NM_027947	zinc finger and BTB domain containing 43, transcript variant 1	Zbtb43	2.57
NM_011498	basic helix-loop-helix family, member e40	Bhlhe40	2.48
NM_009637	AE binding protein 2, transcript variant 3	Aebp2	2.47
NM_153599	cyclin-dependent kinase 8	Cdk8	2.47
NM_020610	nuclear receptor interacting protein 3	Nrip3	2.46
NM_023184	Kruppel-like factor 15	Klf15	2.42
NM_183208	zinc finger, MIZ-type containing 1	Zmiz1	2.4
NM_013519	forkhead box C2	Foxc2	2.39
NM_001029929	zinc finger, MYND-type containing 15	Zmynd15	2.38
NM_010137	endothelial PAS domain protein 1	Epas1	2.37
NM_021397	zinc finger and BTB domain containing 32	Zbtb32	2.37
NM_027264	zinc finger protein 715	Zfp715	2.34
NM_011803	Kruppel-like factor 6	Klf6	2.3
NM_175606	HOP homeobox, transcript variant 1	Hopx	2.29
NM_011753	zinc finger protein 26	Zfp26	2.29

NM_177993	high mobility group box transcription factor 1, transcript variant 2	Hbp1	2.25
NM_011066	period circadian clock 2	Per2	2.22
NM_001100460	zinc finger and BTB domain containing 42	Zbtb42	2.22
NM_009744	B cell leukemia/lymphoma 6	Bcl6	2.19
NM_008554	achaete-scute complex homolog 2 (Drosophila)	Ascl2	2.15
NM_001025577	avian musculoaponeurotic fibrosarcoma (v-maf) AS42 oncogene homolog	Maf	2.15
NM_177660	zinc finger and BTB domain containing 10	Zbtb10	2.15
NM_009884	CCAAT/enhancer binding protein (C/EBP), gamma	Cebpg	2.06
NM_010658	v-maf musculoaponeurotic fibrosarcoma oncogene family, protein B	Mafb	2.04
NM_008270	homeobox B9	Hoxb9	2.03
NM_001009935	thioredoxin interacting protein, transcript variant 1	Txnip	2.03
NM_177790	zinc finger protein 385C	Zfp385c	2.01
NM_001029838	Pbx/knotted 1 homeobox 2 , transcript variant 2	Pknox2	2.01
NM_172643	zinc finger and BTB domain containing 41 homolog	Zbtb41	2.01
NM_031391	general transcription factor II A, 1, transcript variant 1	Gtf2a1	2
	Transport		
NM_008432	potassium channel, subfamily U, member 1	Kcnu1	2.48
NM_020506	exportin 4	Xpo4	2.09
NM_029491	trafficking protein particle complex 8, transcript variant 2	Trappc8	2.04
NM_011324	sodium channel, nonvoltage-gated 1 alpha	Scnn1a	2.03
NM_172476	transmembrane channel-like gene family 7	Tmc7	2.01

*genes validated by qPCR